STUDY AND INVESTIGATION OF A UHF-VHF ANTENNA

FINAL REPORT
January 1963 through January 1965

Contract AF 33(657)-10607
Project 6278, Task 627801
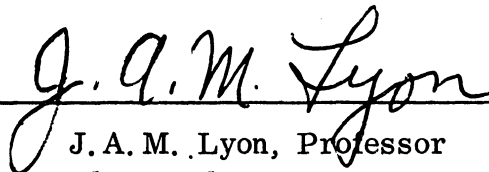O. E. Horton, Project Monitor

Technical Report AFAL-TR-65-64
April 1965

Prepared by

J. A. M. Lyon   G. G. Rassweiler, D. M. Grimes, S. B. Rhee
J. E. Herman and A. I. Simanyi

Approved by _____

J. A. M. Lyon, Professor
Electrical Engineering

Air Force Avionics Laboratory AVWE
Research and Technology Division, AFSC
Wright-Patterson Air Force Base, Ohio 45433

FOREWORD

TABLE OF CONTENTS

ABSTRACT

The results of a program for the miniaturization of antennas through the use of ferrite materials is described. The antennas include the log conical spirals, both within and outside a cavity, the cavity-backed log spiral, a helix, a zigzag, and the cavity-backed slot antenna. Generally speaking, linear reductions of the order of 2 or 3:1 were achieved for the wideband antennas, and above 6:1 for the slot antenna. An experimental study of ferrite material vs temperature and frequency is included as well as a theoretical review of the current status and basic limitations of ferrite materials.

This technical report has been reviewed and is approved.

RONALD G. STIMMEL
Acting Chief
Electronic Warfare Division

I

INTRODUCTION

Many attempts at miniaturizing antennas have been made, usually by loading the antennas with dielectric or ferrite materials or with circuit elements. In the present investigation we have limited our attention to ferrite loading. With cavity or waveguide antennas, the advantage of loading with high μ or ϵ materials is quite obvious; the cutoff size of the cavity or waveguide is smaller due to a change in wavelength. For free-standing antennas, the advantage of loading antennas is less obvious. Repeated attempts, reported in the literature, to load a dipole antenna with material have resulted only in changes in the resonant frequency and radiation resistance; however, the resonant frequency could be shifted by circuit elements, and the increase in radiation resistance was usually due to the losses in the ferrite.

The result of loading loop antennas, of course, has been much more productive. Great gains in the effective receiving aperture have been achieved, and ferrite loaded antennas in low frequency radios are common. More recently, the loading of broadband antennas, as has been done on this project, has resulted in size reduction due, apparently, to a change in the phase velocity of the wave along the antenna, and thus a shift of the 'active regions' to a smaller part of the antenna.

The use of ferrite at the higher frequencies of 50-700Mc has caused losses in antenna efficiency due to basic ferrite limitations and materials manufacturing problems. These have not been entirely overcome on this project; however, size reduction has been achieved with less loss than encountered in the use of either attenuators (to lower the VSWR) or absorption of the waves at the low frequency end of the antenna (to preserve the axial radiation mode and a good VSWR). Further improvement of ferrite materials in the future may be expected.

In Section II, the studies of ferrite loaded broadband antennas are reported. In Section III the investigation of the effects of magnetic tuning of a ferrite loaded

cavity backed slot antenna is discussed and in Section IV is presented a survey of ferrite material characteristics and some results of an experimental study of ferrite characteristics vs temperature and frequency. In Section V some brief recommendations for future work are made.

II
BROADBAND ANTENNAS WITH FERRITE LOADING

A major objective on broadband antennas has been to utilize the benefits of ferrite loading and still retain the broadband characteristic of a given form of antenna. Some placement of ferrite may change the radiation characteristics of a given antenna type. However, it is believed that certain basic types of broadband antennas such as equiangular spirals, the log conical spiral, the helical antenna, and the zigzag antenna, and the zigzag antenna can be modified in such a way as to provide a miniature type of antenna and yet each type will retain its basic characteristics. Results to date have indicated very favorable results in regard to the retention of the radiation pattern. In addition, ferrite loading makes possible the retention of the desired radiation pattern through a greater range of frequency than was heretofore possible without ferrite loading, due to a lowering of the low frequency limit of an antenna. The desired upper frequency characteristics of the antenna must be retained by not loading the upper frequency active regions, since the present ferrite[+] is very lossy above 500 Mc and future ferrites (discussed in Section IV) are high frequency limited. The ferrite-loaded spiral antenna will be discussed first (Section 2.1), followed by the ferrite-loaded helix and log conical sprial antennas.

──────────────

[+]Type "A" with composition, $Ni_{.9696}Zn_{.0404}Co_{.03}Fe_{1.84}Al_{.04}O_4$

2.1 Ferrite-Loaded Spiral Antenna

2.1.1 Experimental Loading

The VSWR of the cavity-backed equiangular spiral shown in Fig. 1(a) was measured with and without ferrite loading. The feed shown in Fig. 1(b) is of the 'infinite balun' type. Standard 50 ohm coaxial cable was used for the feed construction.

The VSWR for the simplest loading condition is shown in Fig. 2. The cavity was fully loaded with the ferrite powder. A thin layer of ferrite powder was also placed on top of the spiral. The fully loaded case produced a reduction of the lower cutoff frequency (or alternatively, of size) by a factor of approximately 2. The narrow-banding effect, due to the magnetic Q becoming small above 700 Mc, is a function of the type of material and loading used, and is not a basic limitation. Figure 3 shows that approximately the same result can be obtained by loading only one arm of the spiral. This method has the advantage of using less ferrite material.

Figure 4 shows the response of the bidirectional spiral without a cavity in both the loaded and unloaded conditions. The curves have the same general shape as the cavity backed spiral. Thus the cavity introduces little basic deterioration of the antenna response. Preliminary efficiency measurements for the loaded spiral without cavity indicate an efficiency of about 80 per cent. Efficiencies of unloaded spirals are typically greater than 90 per cent.

Additional experiments were performed on an equiangular spiral which was mounted on the apex of a Styrofoam cone. This mounting allowed the equiangular spiral antenna to be centered in a cylindrical cavity flush with the flanges of the cavity. The space between the Styrofoam cone and the wall of the metal cavity was, in the ferrite loading situation, filled with powdered ferrite as shown in the insert of Fig. 5, which depicts VSWR with and without ferrite loading. Figure 6 shows radiation patterns for the equiangular spiral, as depicted in Fig. 5, with and without

ferrite loading over a range of 300 - 900 Mc, showing that the patterns of the loaded

antenna are at least as good as those of the unloaded antenna.
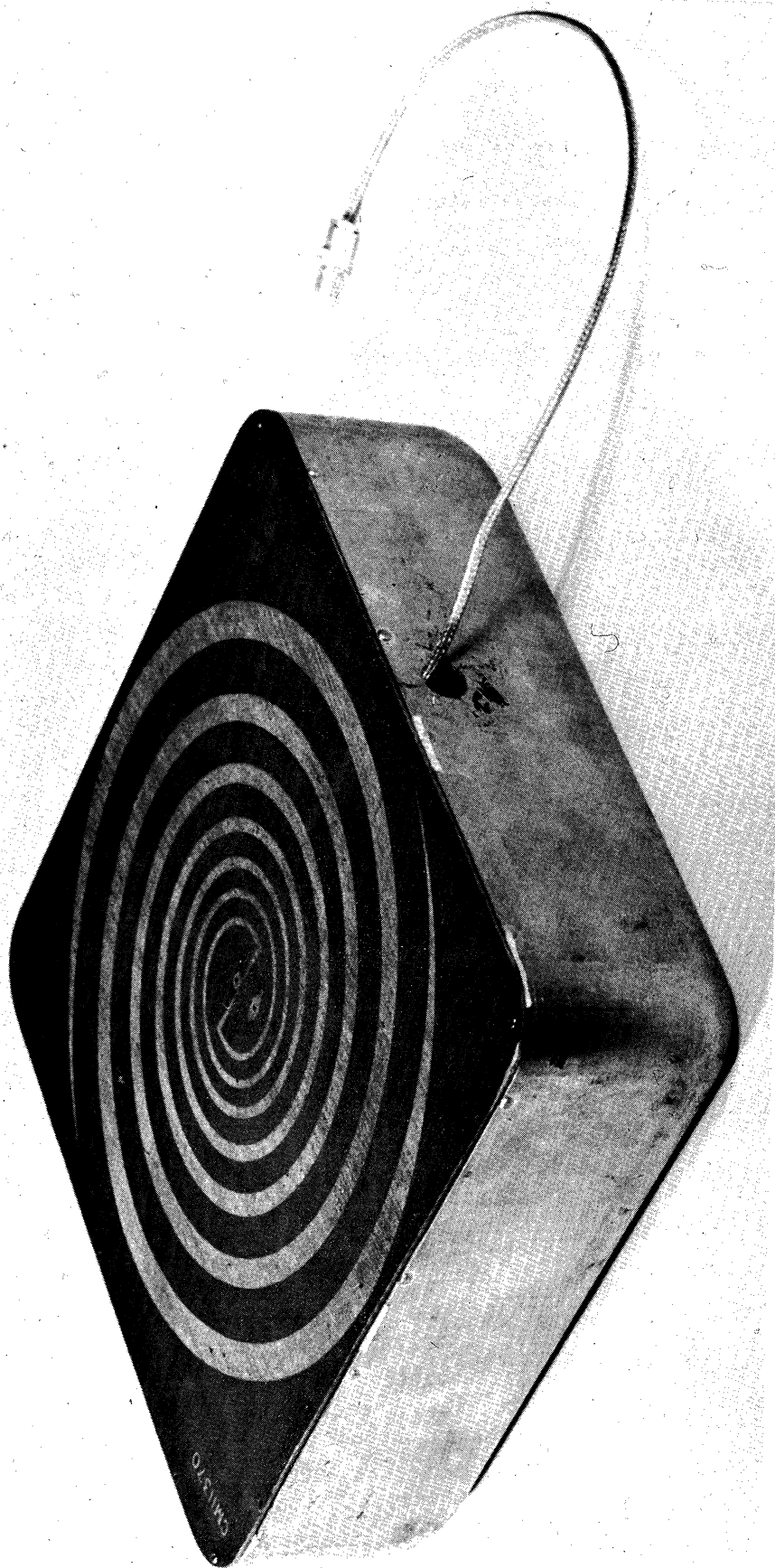
FIG 1a: EQUIANGULAR SPIRAL
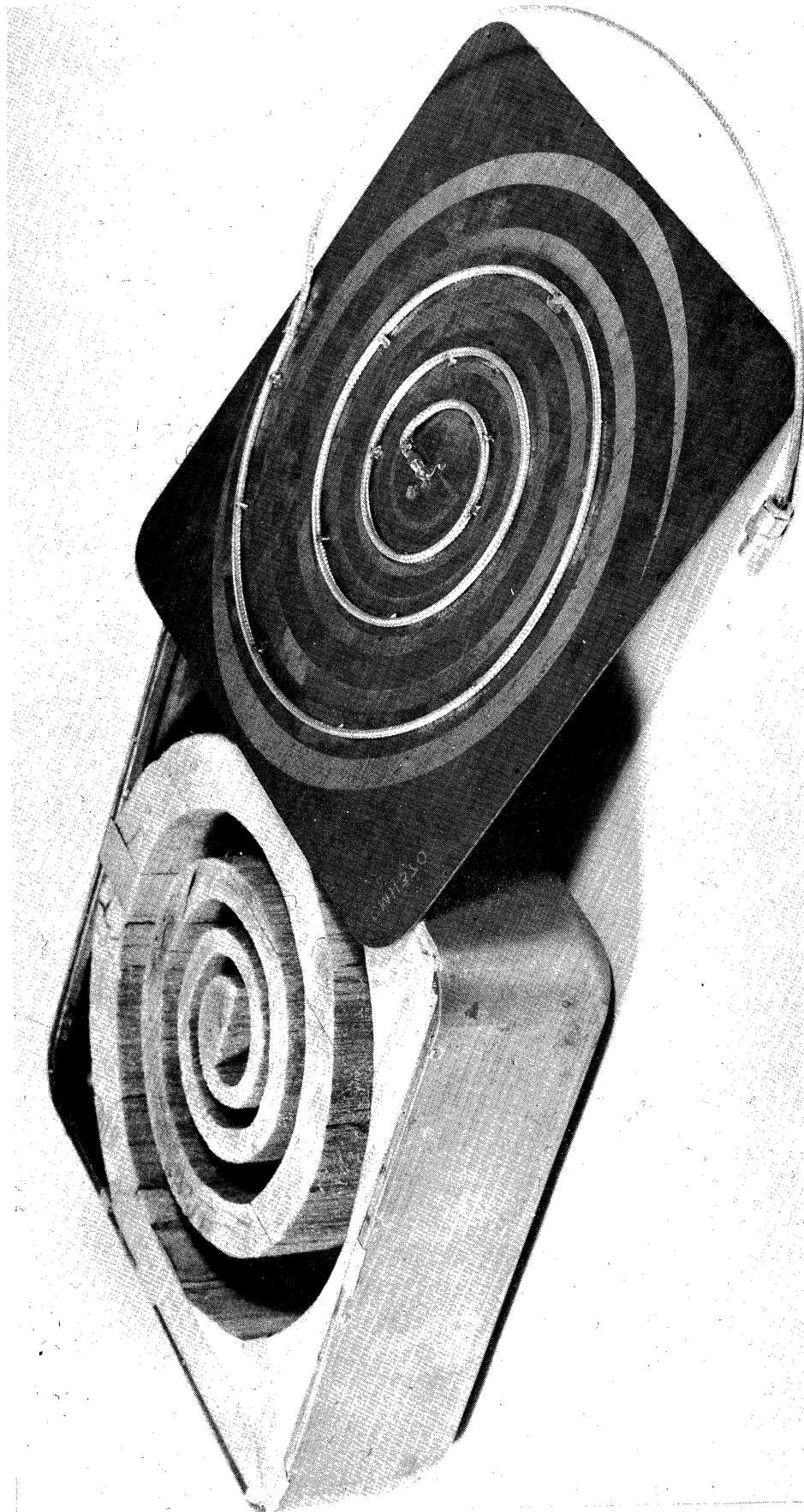
FIG. 1b: CONSTRUCTION SHOWING FEED AND A SINGLE FILAR LOADING

Air case

Ferrite loaded cavity

Loaded cavity; 1/4" ferrite on top

Cavity depth 2-3/16"
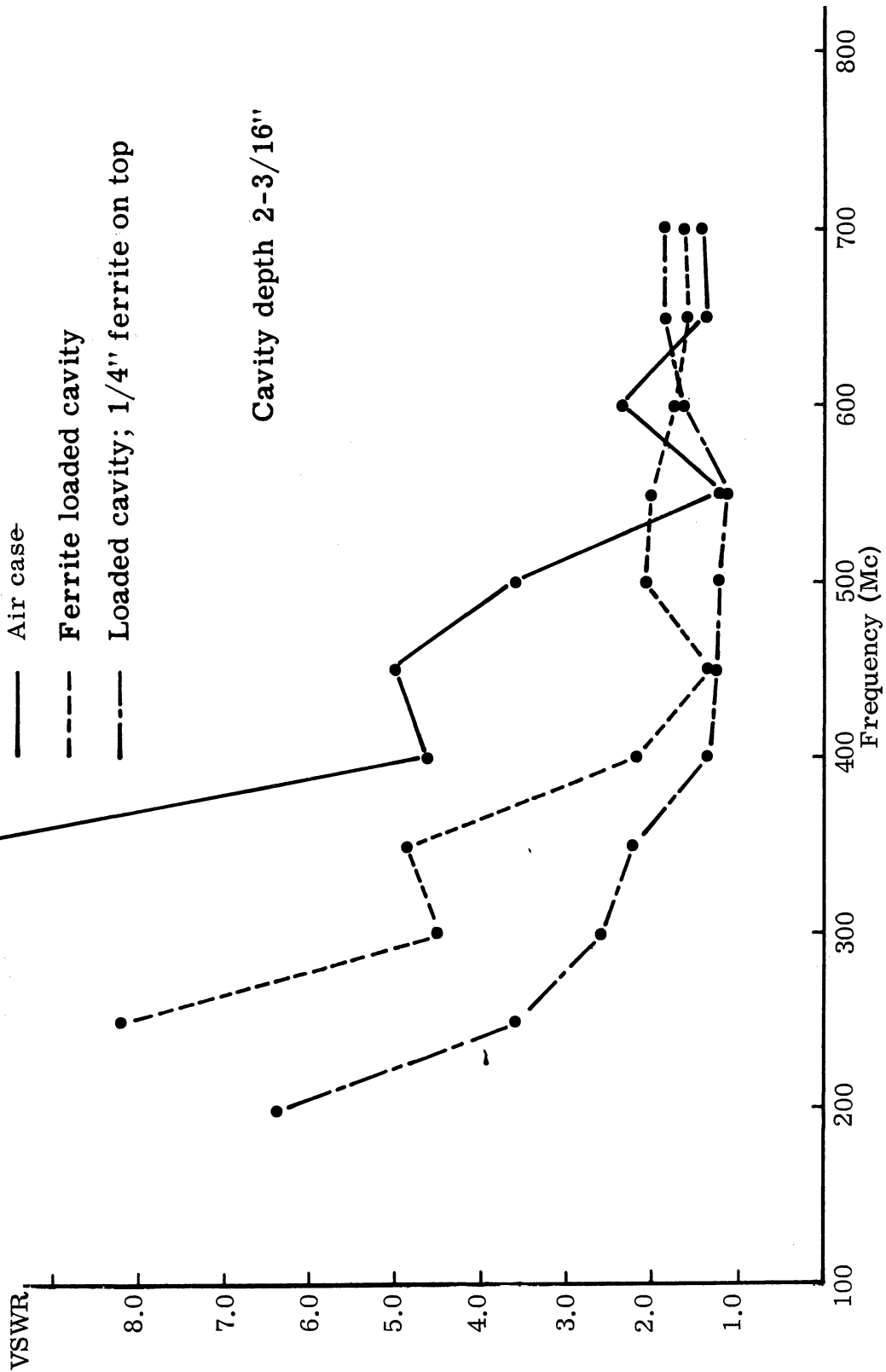
FIG. 2: VSWR FOR FULLY LOADED SPIRAL

Frequency (Mc)

VSWR

Air case-

Coax fed arm loaded from cavity side, 2-3/16"deep

Coax fed arm loaded from both sides, 2-3/16" deep

Cavity depth 2-3/16"
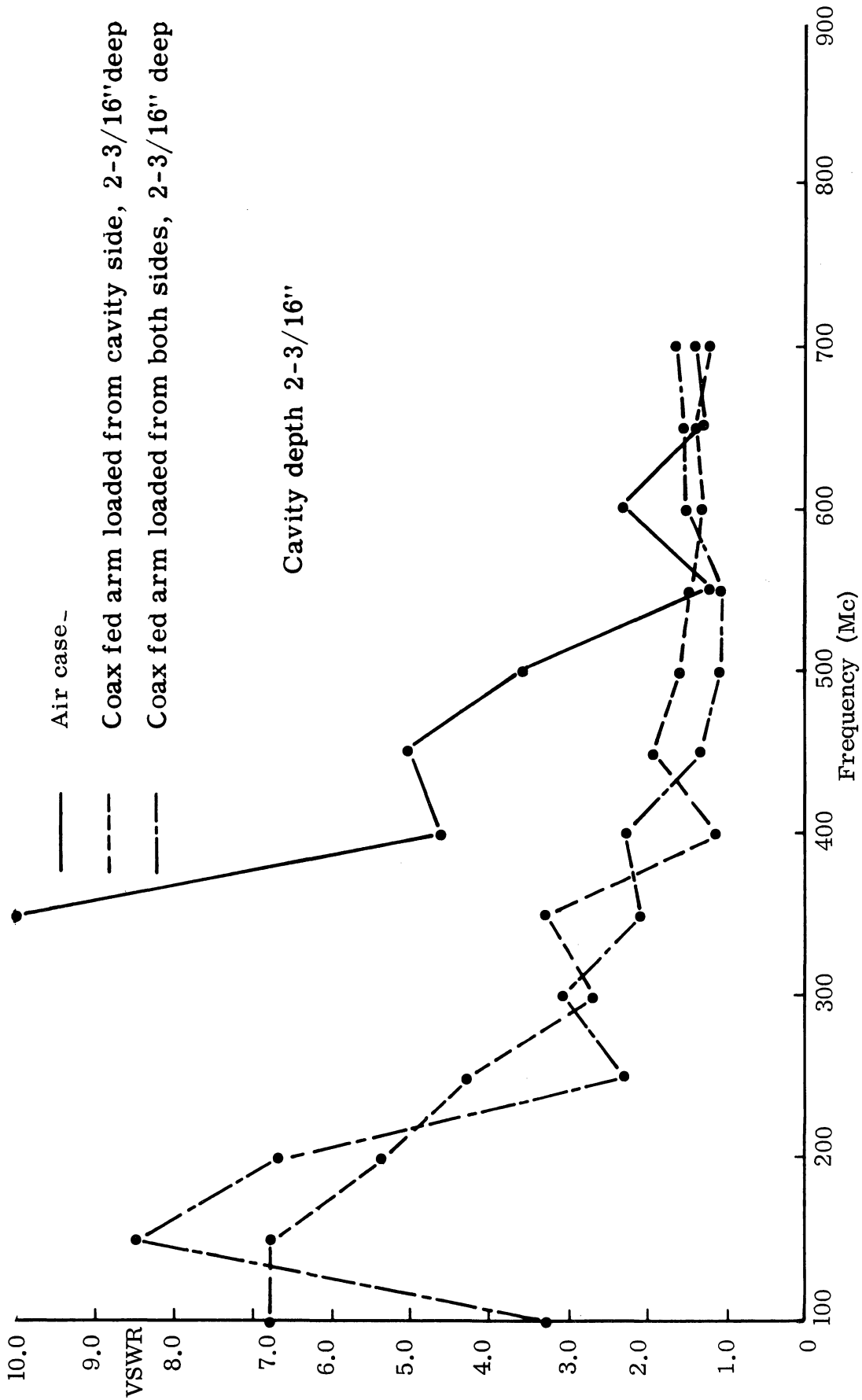
FIG. 3: VSWR FOR SINGLE FILAR LOADING

Frequency (Mc)
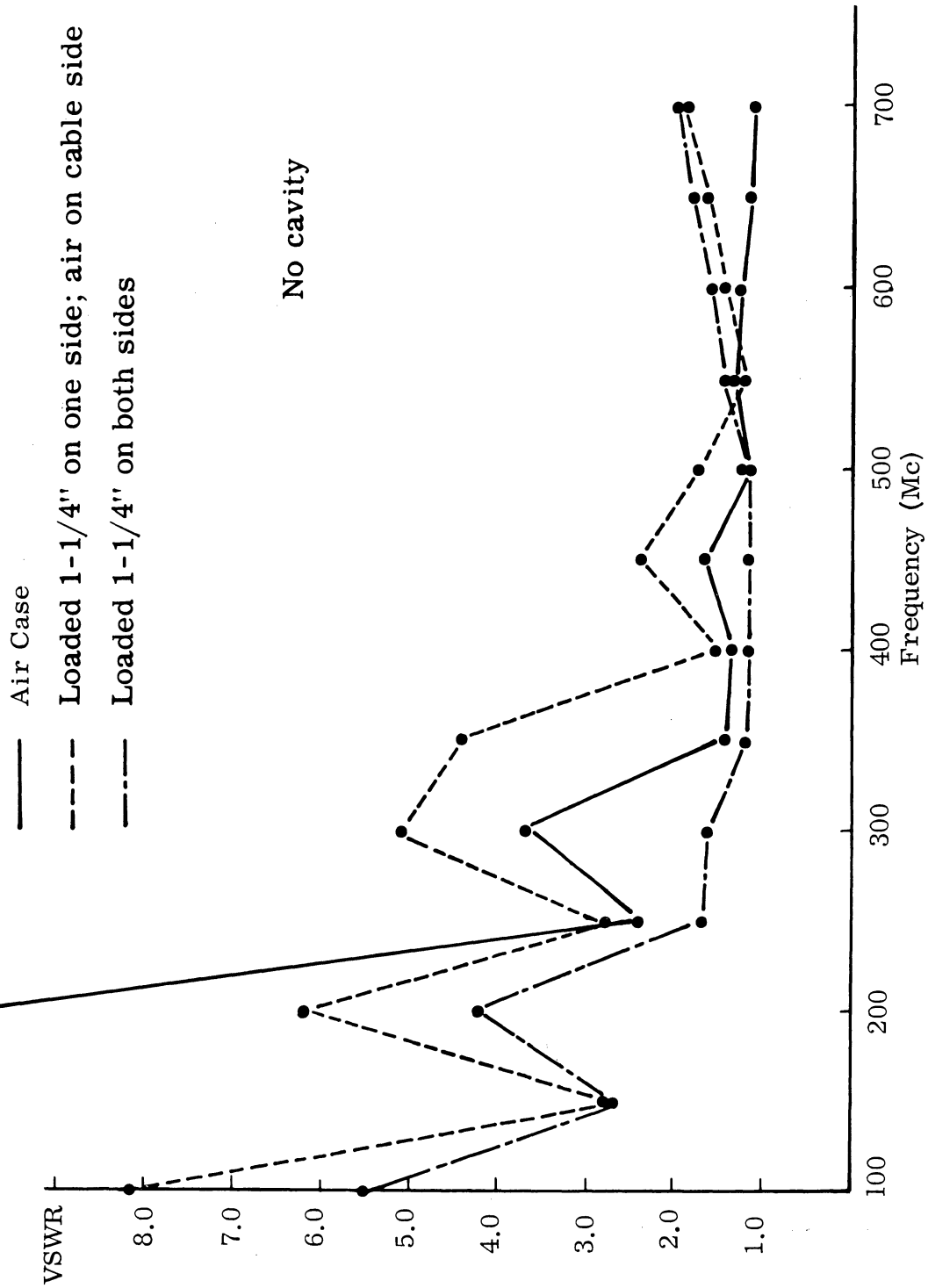
VSWR

FIG. 4. VSWR FOR LOADED SPIRAL WITH NO CAVITY
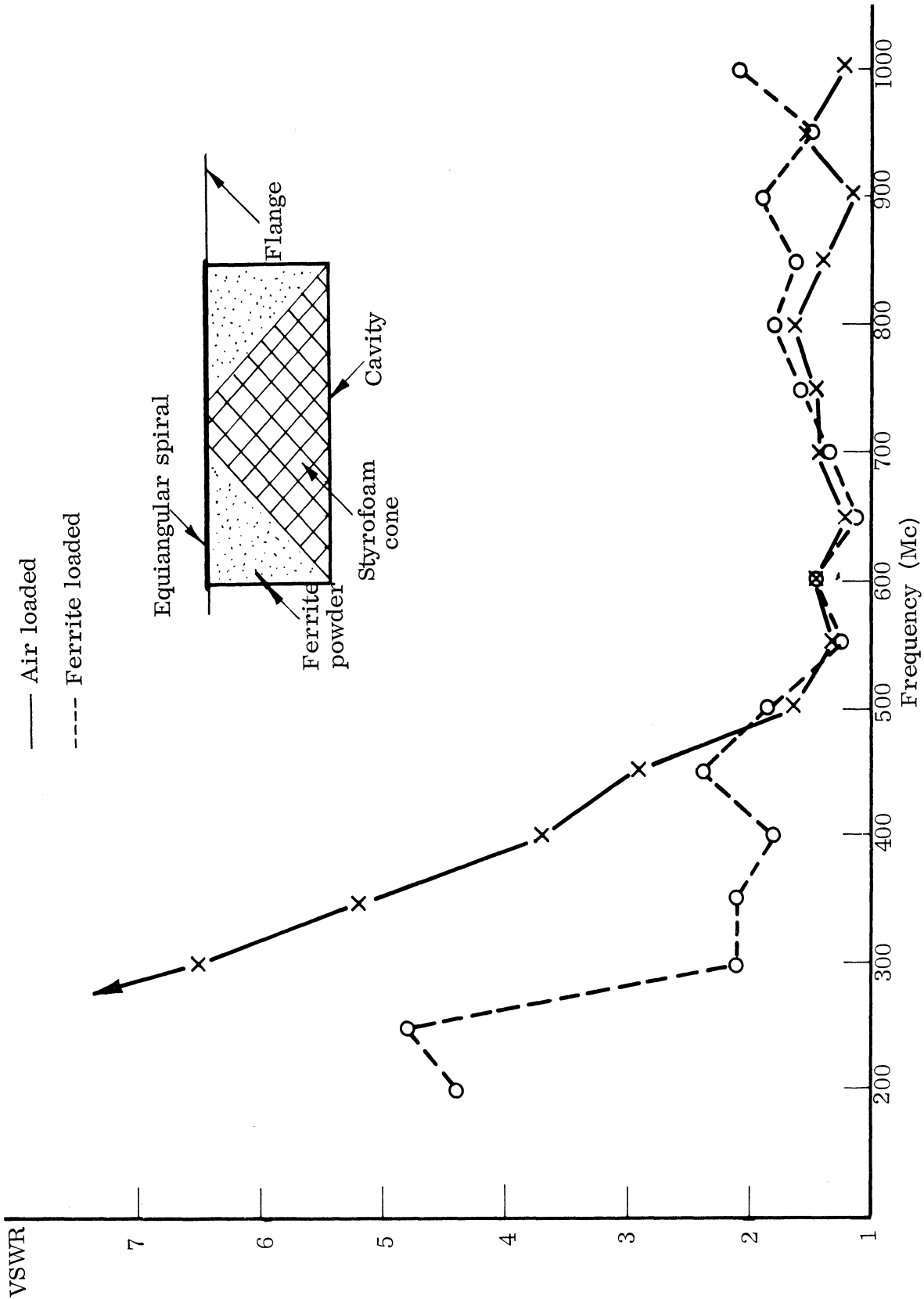
FIG. 5: UNIDIRECTIONAL EQUIANGULAR SPIRAL (No. 301) WITH TAPERED FERRITE LOADING.

E_ϕ

300 Mc

E_θ

300 Mc
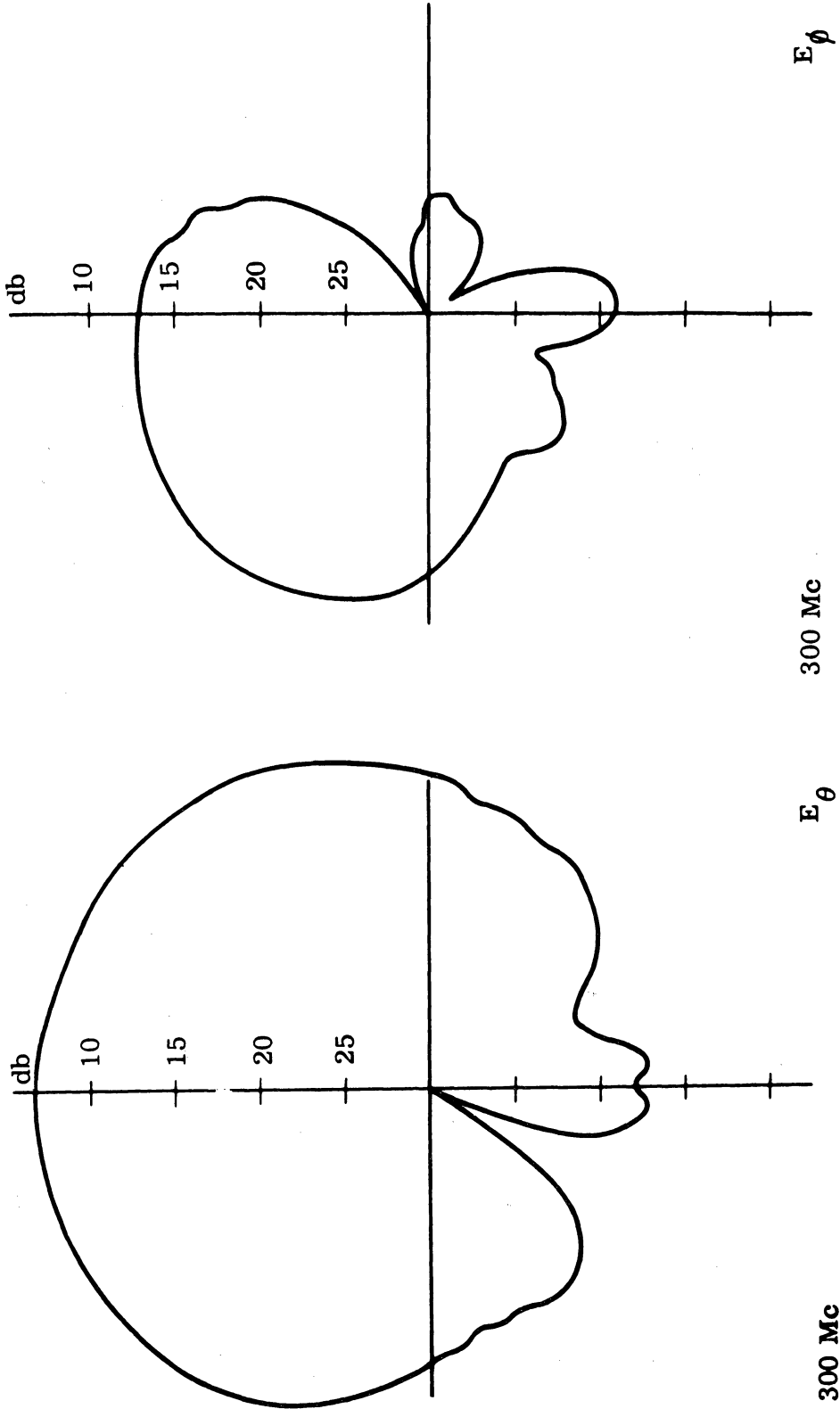
FIG. 6a: NO. 301 AIR LOADED
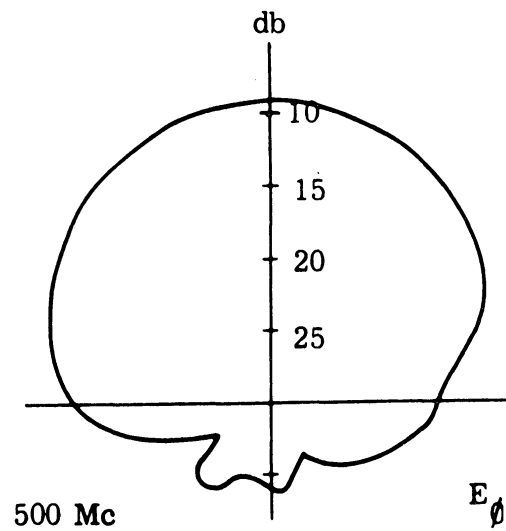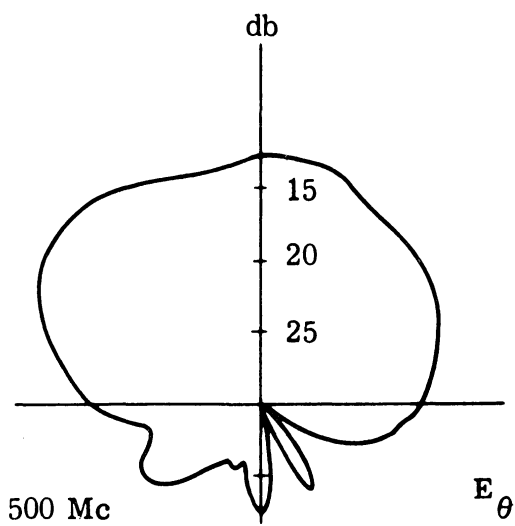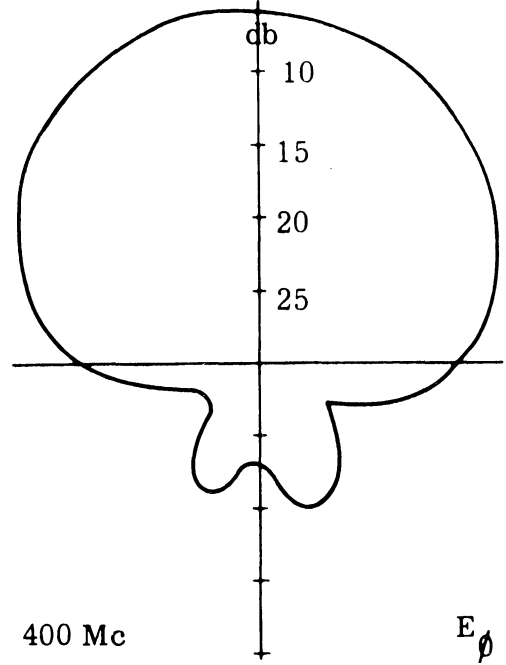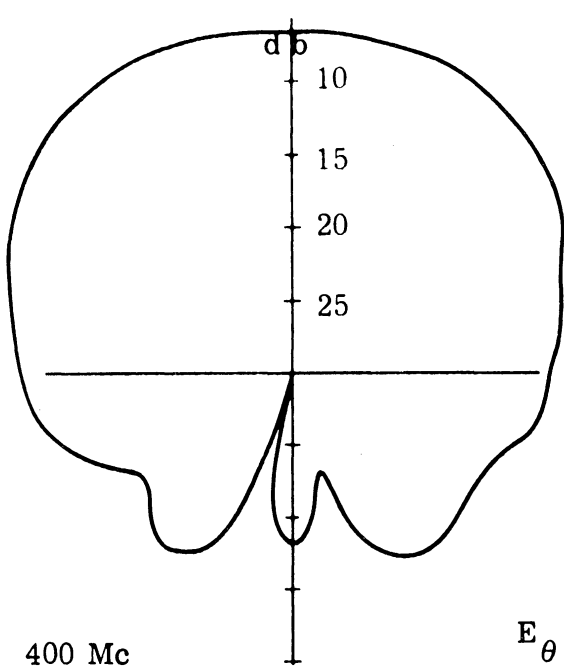
FIG. 6b: NO. 301 AIR LOADED

FIG. 6c: NO. 301 AIR LOADED

800 Mc — E_θ

800 Mc — E_ϕ

900 Mc — E_θ

900 Mc — E_ϕ
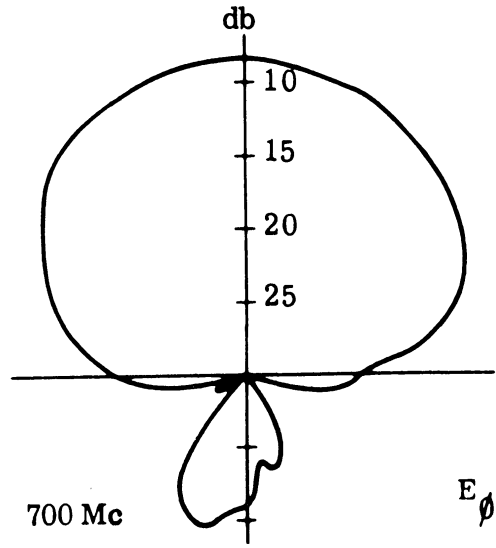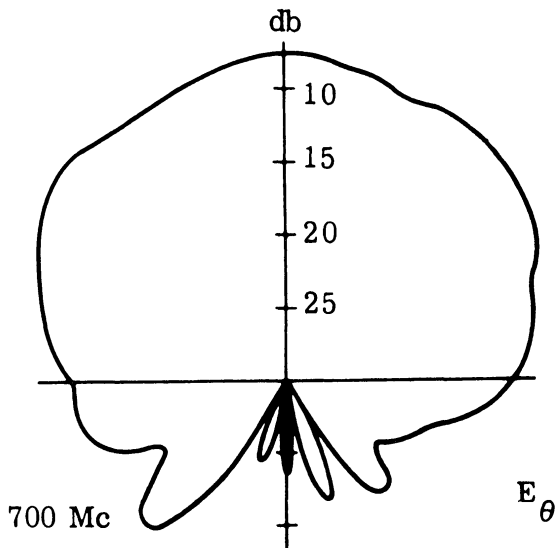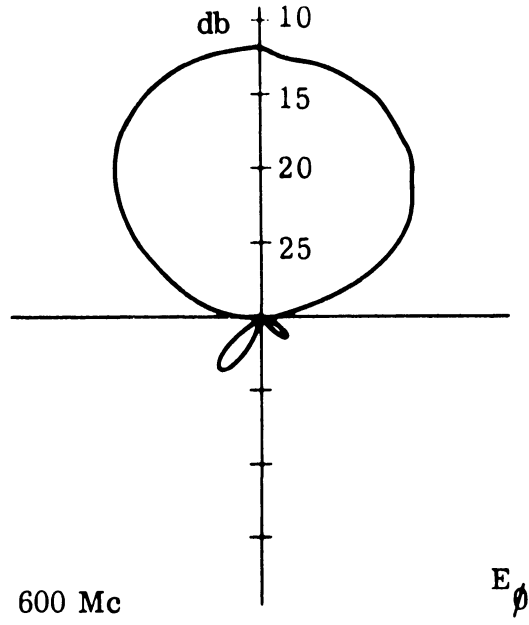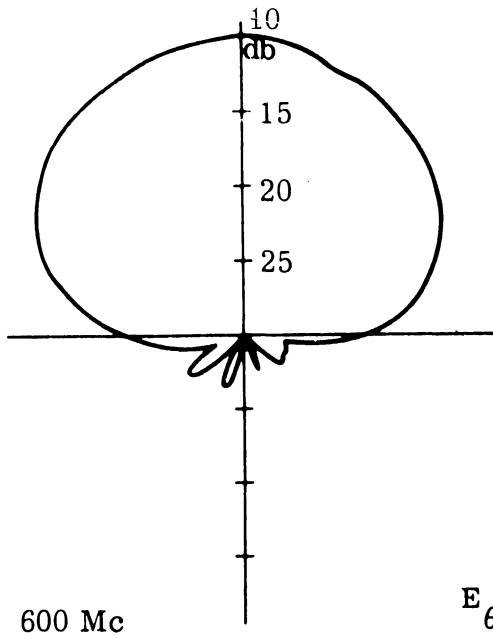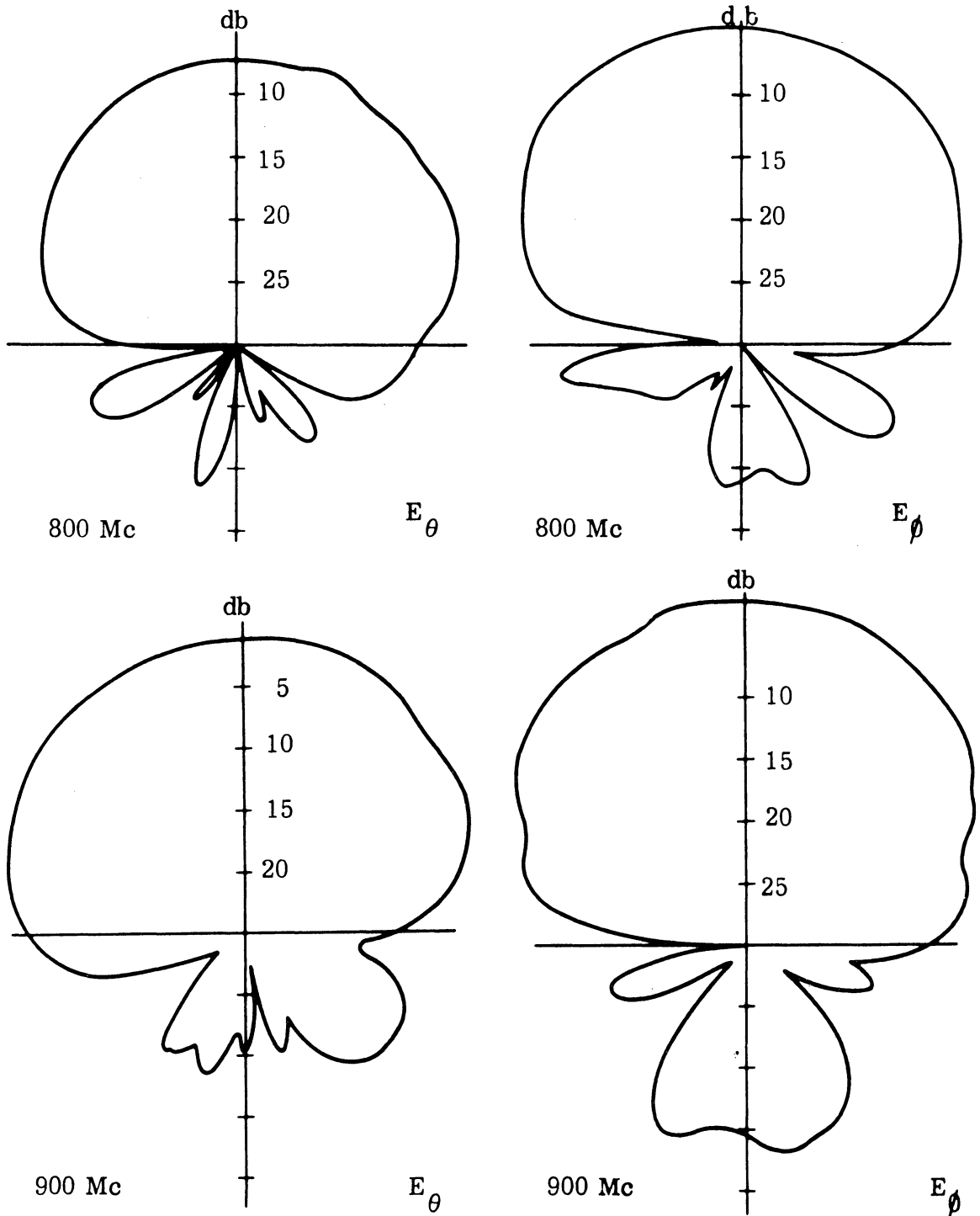
FIG. 6d: NO. 301 AIR LOADED

FIG. 6e: NO. 301 FERRITE LOADED

db

10

15

20

25

400 Mc

E_θ

db

15

20

25

400 Mc

E_ϕ

db

10

15

20

25

500 Mc

E_θ

db

10

15

20

25

500 Mc

E_ϕ

FIG. 6f: NO. 301 FERRITE LOADED

db
10
15
20
25

600 Mc

E_θ

db
10
15
20
25

600 Mc

E_ϕ

db
10
15
20
25

700 Mc

E_θ

db
10
15
20
25

700 Mc

E_ϕ
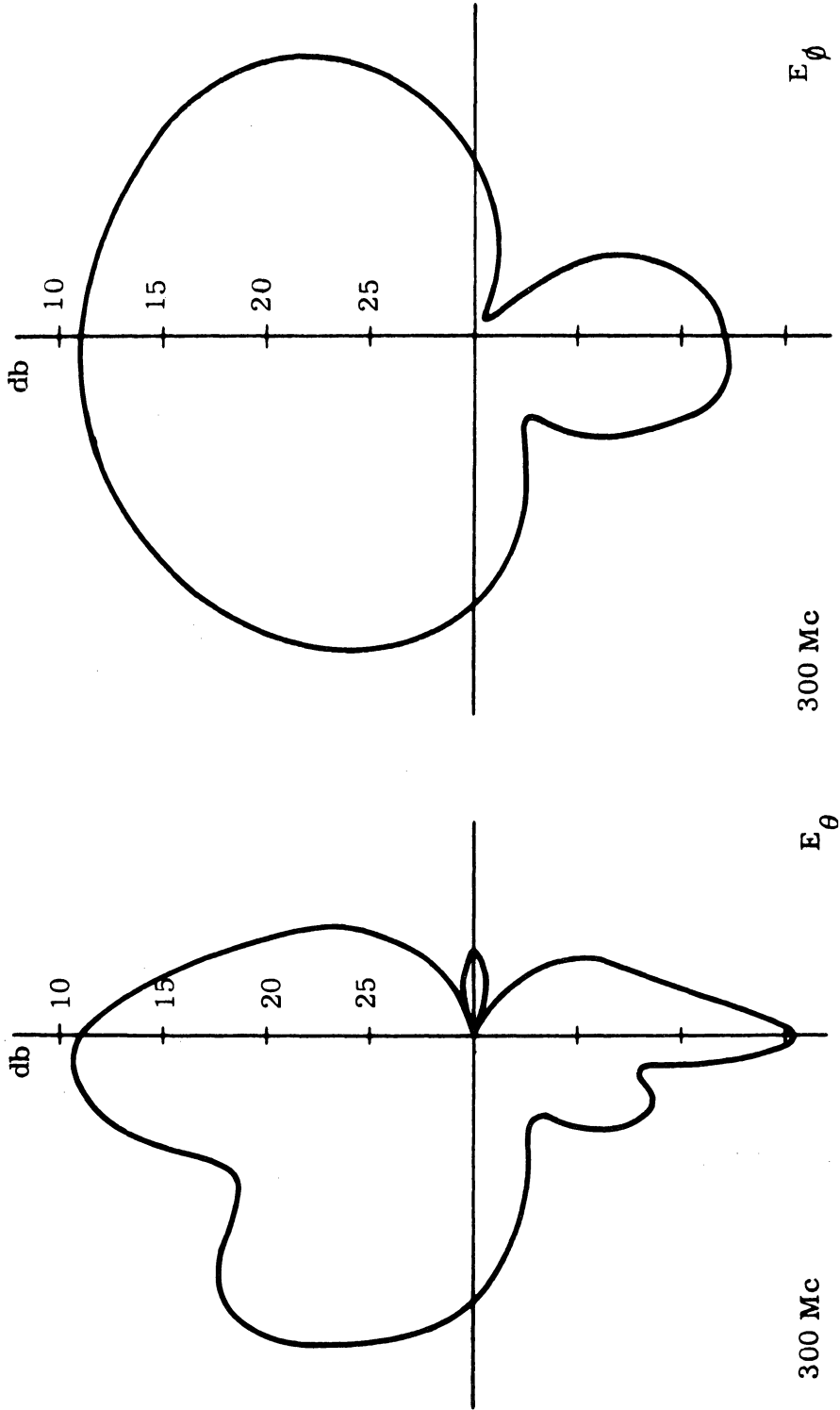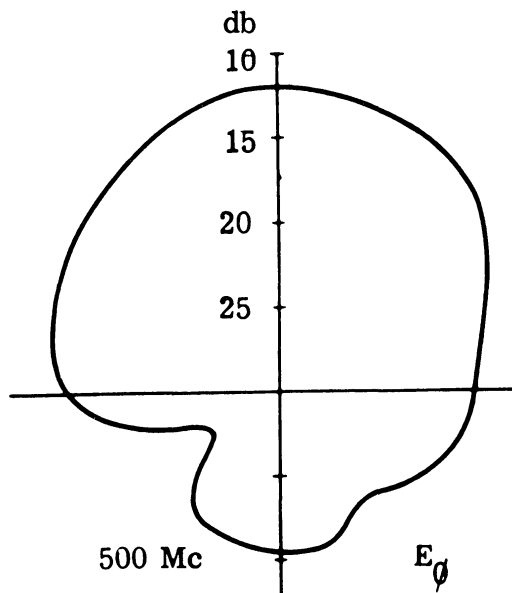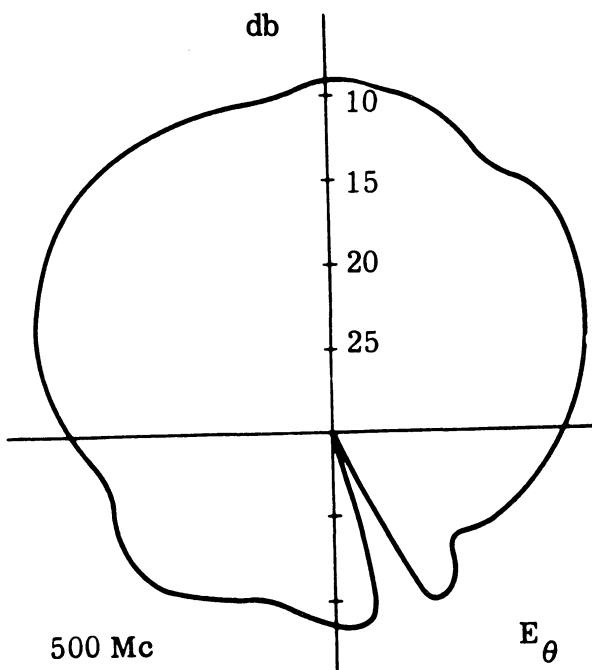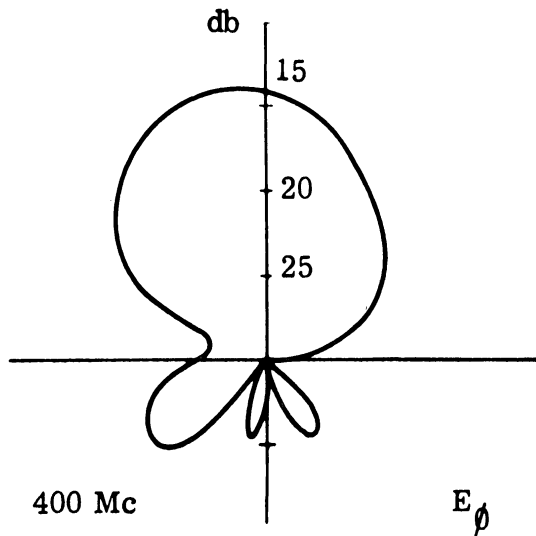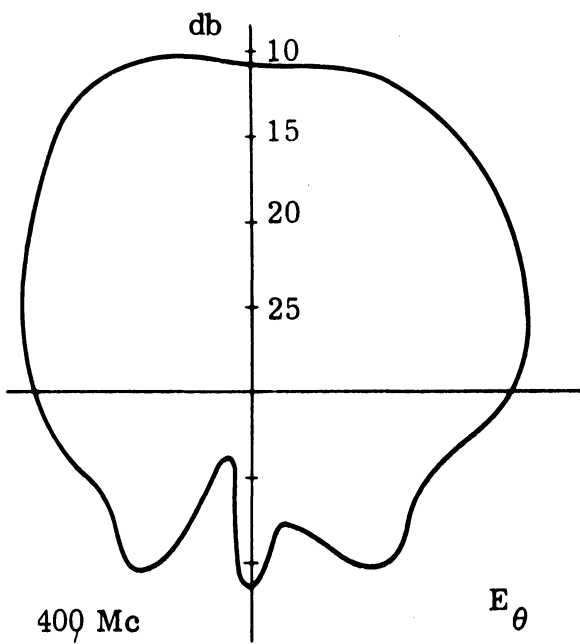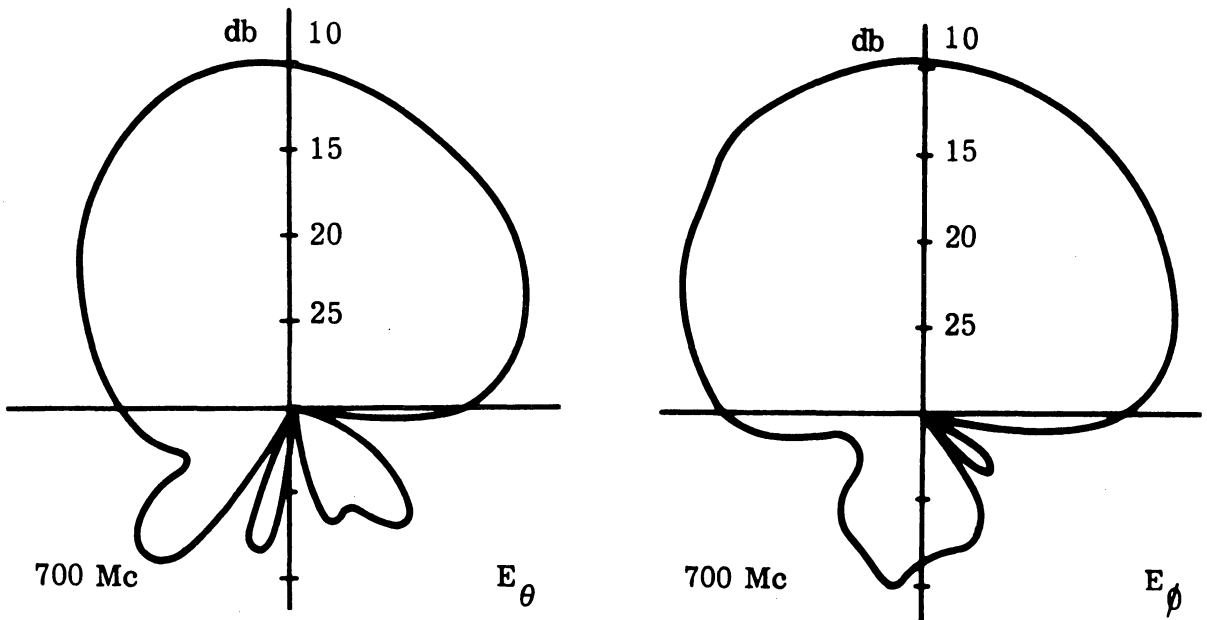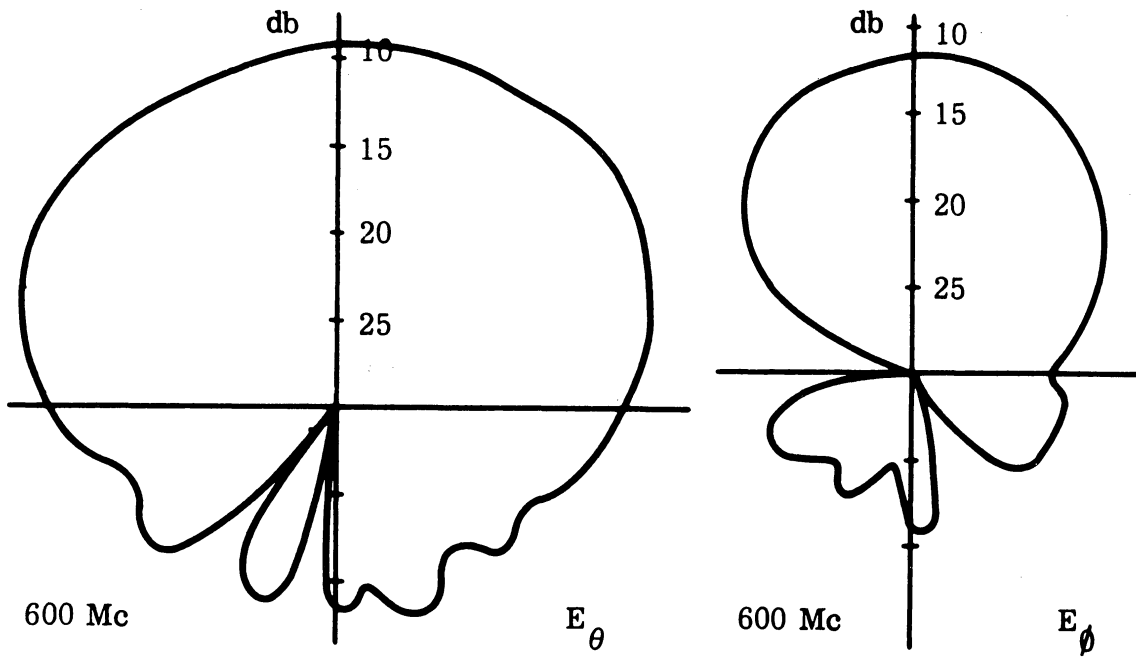
FIG. 6g: NO. 301 FERRITE LOADED
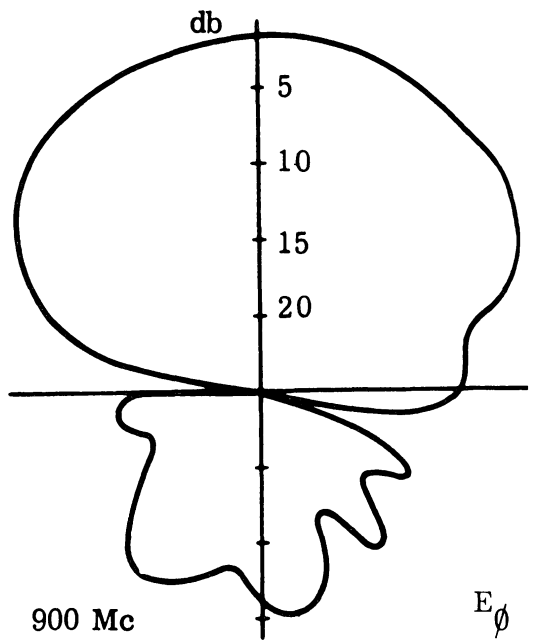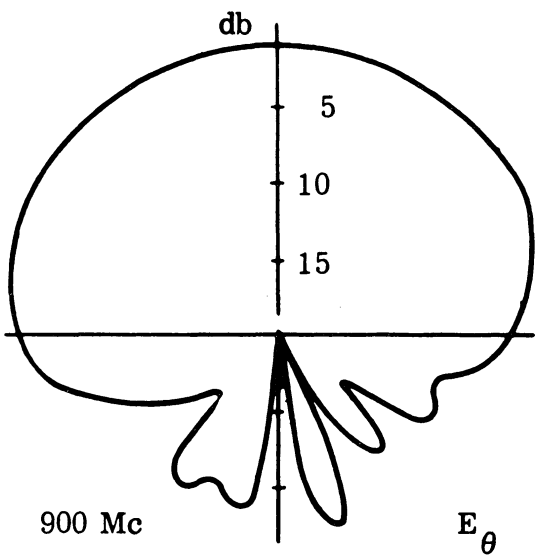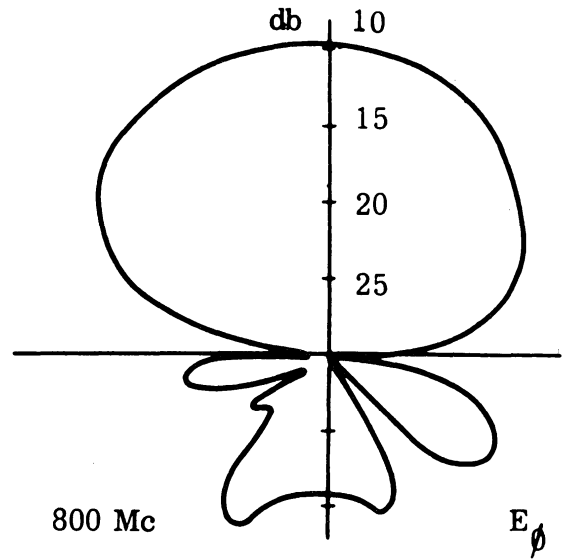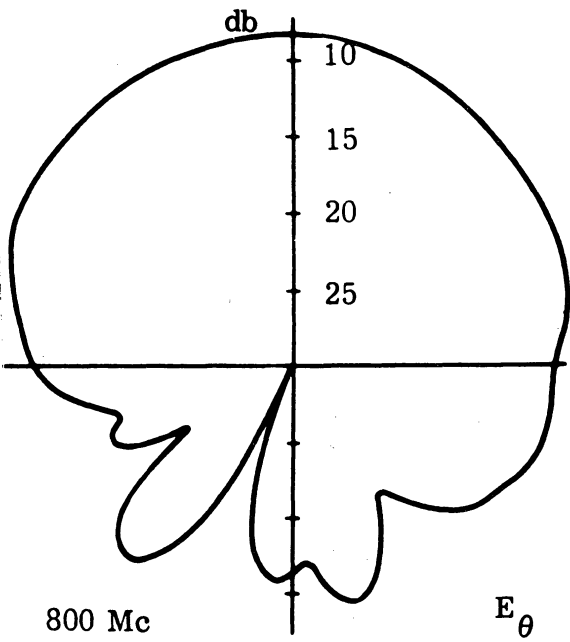
FIG. 6h: NO. 301 FERRITE LOADED

2.1.2 Theoretical Radiation Pattern of Equiangular Spiral

A mathematical expression for the radiation fields of the equiangular spiral thin-wire (or slot) antenna is now presented which is adaptable to solution using the IBM 7090 computer, if the current distribution and mode of excitation are specified.

Consider the planar monofilar spiral shown in Fig. 7, where (r', ϕ') are source coordinates, (r, θ, ϕ) are field coordinate, and $r'' = |\underline{r} - \underline{r}'|$. The magnetic vector potential for a thin current distribution in space is given by

$$\underline{A}^{(1)}(r, \theta, \phi) = \frac{\mu_o}{4\pi} \int_{spiral} \frac{\underline{I}(\ell')e^{-jkr''}}{r''} \, d\ell' \tag{1}$$

where the $e^{+j\omega t}$ time dependence is understood. In the radiation field phase variations are taken into account by

$$r'' = r - r' \sin\theta \cos(\phi - \phi') . \tag{2}$$

The equation of the equiangular spiral is

$$r' = r_o' \, e^{a\phi'} \tag{3}$$

whence

$$d\ell' = \sqrt{(dr')^2 + (r'd\phi')^2} = \sqrt{1 + a^2} \; r_o' e^{a\phi'} d\phi' \tag{4}$$

and

$$\ell' = \int_0^{\phi'} d\ell' = \sqrt{1 + \frac{1}{a^2}} \; r_o'(e^{a\phi'} - 1) . \tag{5}$$

The direction of the segment $d\ell'$ as shown in Fig. 7 is given by

$$\underline{\ell}' = \sin(\psi' - \phi')\hat{x} + \cos(\psi' - \phi')\hat{y} \tag{6}$$

where

$$\tan\psi' = \frac{dr'}{r'd\phi'} = a . \tag{7}$$
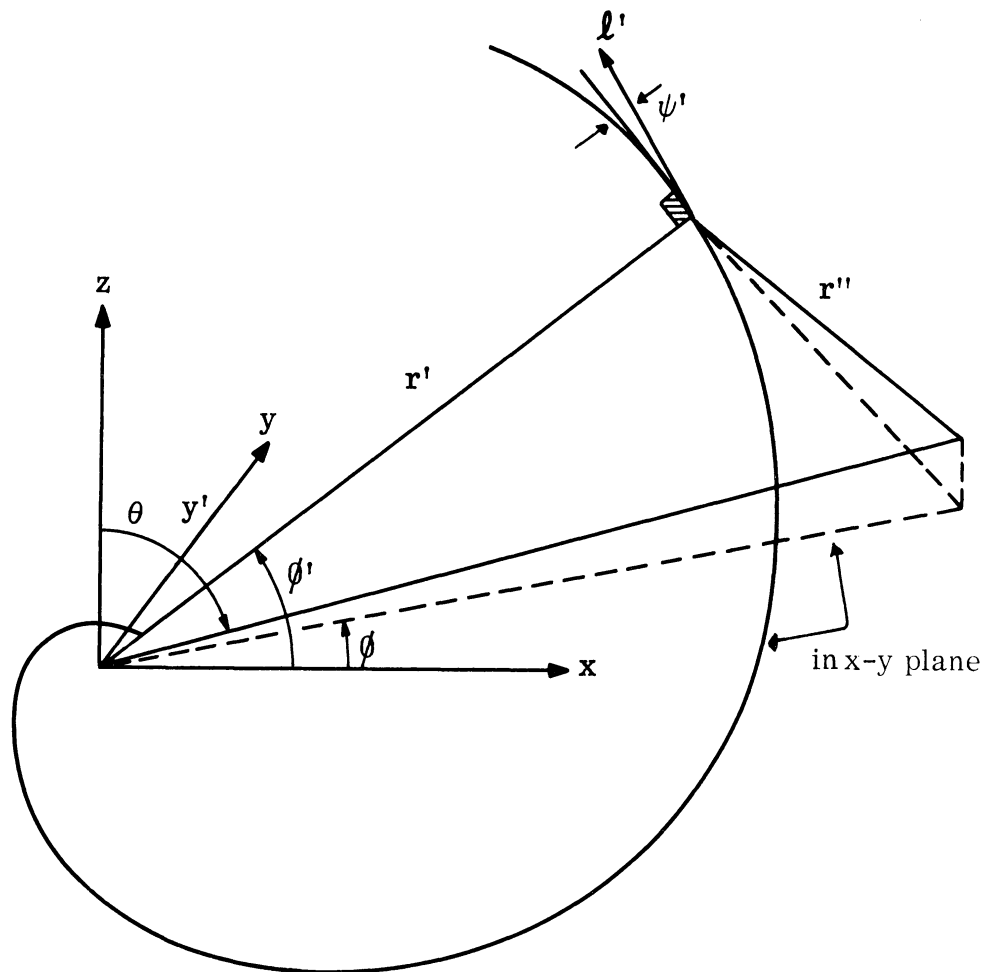
FIG. 7: SPIRAL COORDINATES

A rather crude approximation to the current is that of a curved two-wire transmission line with no coupling to surrounding elements. This gives a current depending only on the distance (ℓ') along the line from the feed point, i.e. a traveling wave,

$$\underline{I}(\ell') = I_0 \left[e^{-\gamma\ell'} + \Gamma e^{+\gamma\ell'} \right] \underline{\ell} \, ; \quad (\gamma = -\alpha + j\beta) \tag{8}$$

where $\underline{\ell}'$ is given by (5) and Γ is the reflection coefficient for current. Thus the vector potential may be written as

$$\underline{A}^{(1)}(r, \theta, \phi) = \frac{\mu_o I_o}{4\pi} \frac{e^{-jkr}}{r} \int_0^\Phi \left[e^{-\gamma\ell'} + \Gamma e^{+\gamma\ell'} \right]$$

$$\cdot \left[\exp(jkr_o' \sin\theta \cos(\phi-\phi') e^{a\phi'} \right] \left[\sin(\psi'-\phi')\hat{x} + \cos(\psi'-\phi')\hat{y} \right]$$

$$\cdot \left[\sqrt{1+a^2} \; r_o' e^{a\phi'} \right] d\phi' \, . \tag{9}$$

For total reflection at the end of the wire the reflection coefficient becomes

$$\Gamma = -e^{-2\gamma L}; \quad \left(L = \sqrt{1 + \frac{1}{a^2}} \; r_o' (e^{a\,\Phi} - 1) \right) \, , \tag{10}$$

where L and Φ correspond to the remote end of spiral. In spherical coordinates, the radiation field is related to the magnetic vector potential by

$$E_\theta = -j\omega A_\theta; \quad E_\phi = -j\omega A_\phi \tag{11}$$

where

$$A_\theta = A_x \cos\theta \cos\phi + A_y \cos\theta \sin\phi$$

$$A_\phi = -A_x \sin\phi + A_y \cos\phi \, . \tag{12}$$

Thus, if $\underline{A}$ is known the field can easily be found from (11).

Consider the bifilar spiral with the currents in the two wires out of phase by an angle Δ at the feed. Then the total magnetic vector potential will be given by

$$\underline{A}(r,\theta,\phi,t) = \underline{A}^{(1)}(r,\theta,\phi,t) + \underline{A}^{(1)}(r,\theta,\phi+\pi, t+\frac{\Delta}{\omega}) \, . \tag{13}$$

Thus for balanced excitation $(\Delta = \pi)$ the total magnetic vector potential will be

$$\underline{A}(r,\theta,\phi) = \frac{\mu_o I_o}{2\pi} \sqrt{1+a^2} \, r_o' \, \frac{e^{-jkr}}{r} \exp\left[(\alpha+j\beta)\sqrt{1+\frac{1}{a^2}} \, r_o'\right]$$

$$\cdot \int_0^{\Phi} \left\{ \left[\exp\left((-\alpha-j\beta)\sqrt{1+\frac{1}{a^2}} \, r_o' e^{a\phi'}\right) \right. \right.$$

$$-\exp\left((-\alpha-j\beta)\sqrt{1+\frac{1}{a^2}} \, r_o'(2e^{a\Phi}-e^{a\phi'})\right)$$

$$\left. \cdot \cos\left[kr_o'\sin\theta\cos(\phi-\phi')e^{a\phi'}\right] e^{a\phi'} \right\}$$

$$\cdot \left\{ \left[\sin(\psi'-\phi')\cos\phi + \cos(\psi'-\phi')\sin\phi \right] \cos\theta \, \hat{\theta} \right.$$

$$\left. + \left[\cos(\psi'-\phi')\cos\phi - \sin(\psi'-\phi')\sin\phi \right] \hat{\phi} \right\} d\phi' \, . \tag{14}$$

For convenience the following substitutions may be made:

$$z' = a\phi'; \quad Z = a\Phi; \quad \alpha' = \alpha\sqrt{1+\frac{1}{a^2}} \, r_o'; \quad \beta' = \beta\sqrt{1+\frac{1}{a^2}} \, r_o'; \quad k' = kr_o',$$

$$B = \frac{\mu_o I_o}{2\pi a} \sqrt{1+a^2} \, r_o' \, \frac{e^{-jkr}}{r} \, . \tag{15}$$

The pattern may be found for $\phi = 0$ or $\phi = \pi$ cuts. For the $\phi = 0$ cut, (14) becomes

$$\underline{A}(r,\theta,0) = B e^{\alpha'+j\beta'} \int_0^Z \left\{ \left[e^{-\alpha'+j\beta')e^{z'}} - e^{(-\alpha'-j\beta')(2e^Z-e^{z'})} \right] \right.$$

$$\left. \cdot \cos\left[k'\sin\theta\cos\frac{z'}{a}e^{z'}\right] e^{z'} \left[\sin(\psi'-\frac{z'}{a})\cos\theta \, \theta + \cos\left(\psi'-\frac{z'}{a}\right)\phi \right] \right\} dz' \tag{16}$$

Equation (16) gives a set of integrals which may easily be evaluated by numerical methods on the computer. Whence, the magnitude and phase of the field components may be tabulated for each set of parameters.

The application of this method to a ferrite loaded antenna presents a difficult boundary value problem. However, it is hoped that a thin layer loading may be simulated by merely assuming the current propagates in a 'slow-wave' mode, i. e., by assuming $\beta = \sqrt{\mu \epsilon}$ k.

A computer program was written but results did not compare well with experimental patterns, probably because the current assumed is not that observed or predicted in the 'active region' concept.

2.2 Log Zigzag Antenna

A log zigzag antenna was designed to take advantage of its reduced volume with frequency independent characteristics similar to those of the log conical spiral. The dimensions used (Tang, 1962) are shown in Fig. 8. An initial test of the VSWR for a 1/4" thick uniform layer of type "A" powder was made and compared with the air loaded case (Fig. 9).

An aluminum cavity was constructed to fit the antenna, to investigate the flush-mounted operation of the antenna. The effect of the cavity was initially tested by comparing values of VSWR for both the loaded and unloaded cavity. For ferrite loaded cavities, the powder "A" was used for a depth of approximately 5", which covered the bottom two turns only and provided a thickness of approximately 1.5". However the cavity was too small to allow adequate radiation. Further tests may be made in the future.
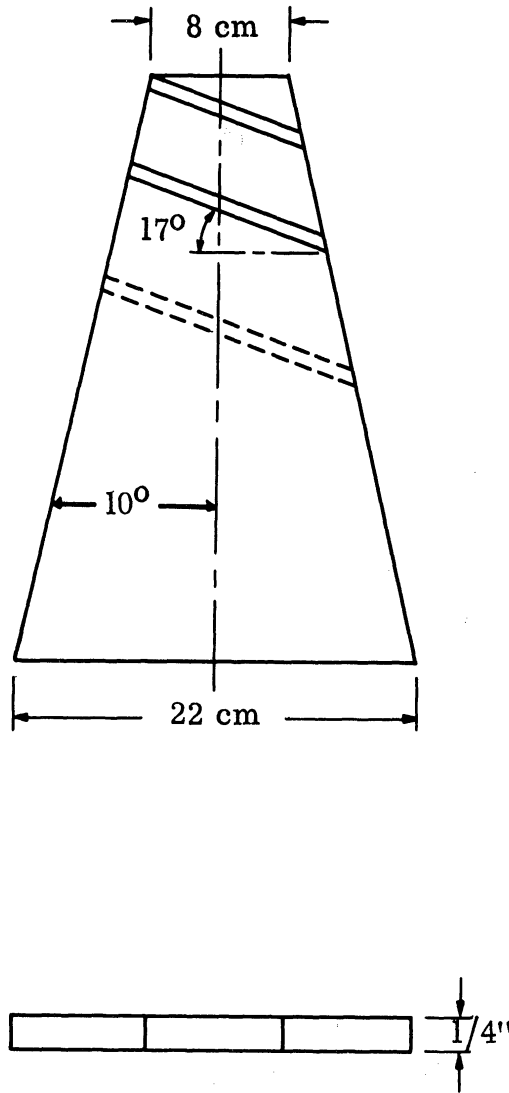
FIG. 8: LOG SPIRAL ZIGZAG ANTENNA CONSTRUCTION DETAILS.
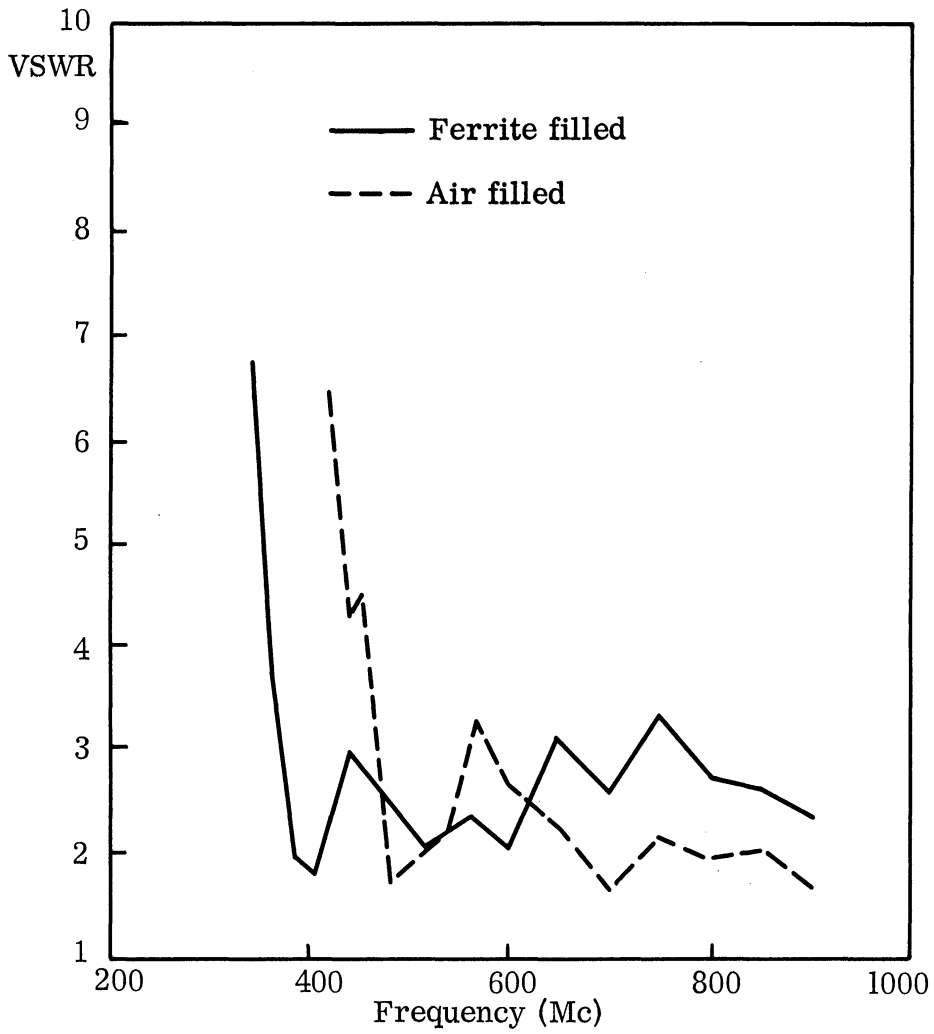
FIG. 9: FREQUENCY VS VSWR FOR LOG SPIRAL
ZIGZAG ANTENNA.

2.3 Ferrite-Loaded Helix

A ferrite-loaded helix (Fig. 10) was constructed in order to test the size reduction obtainable with such a structure. The helix was wound of No. 14 copper wire on a balsa wood cylinder of 4" diameter and 20" length. For a six-turn helix wound on this core, the pitch angle ψ, defined by

$$\tan \psi = \frac{\pi (\text{diameter})}{(\text{turn-to-turn spacing})}$$

is 14°. As shown in Fig. 10, this structure is loaded around the perimeter of the cylinder, just inside of the helical winding, with $1" \times 1/2"$ ferrite bars. The ferrite bars extend over the total length of the antenna; they are spaced 90° apart around the perimeter of the cylinder. The reason for choosing a moderate pitch angle of 14° was that most of the measurements by other workers had been concentrated in this region, and therefore data were available for comparison. The helix is fed by the center conductor of a type N connector, which is mounted on the axis of the cylinder. Figure 11 shows the measured voltage standing wave ratio for both the unloaded (balsa wood core) and the loaded (ferrite bars embedded in the surface of the basa wood core) case. The values of VSWR are quite reasonable for both cases, especially when one considers that no attempt was made to obtain a better match between the 50 ohm coaxial feeding line and the helical antenna, by any kind of an impedance transforming network. Generally, VSWR's of about 2.5 are obtained in the useful radiation regions. For the unloaded antenna, the VSWR reaches very high values at 600 Mc and below, whereas for the ferrite-loaded structure this cutoff is reduced to 450 Mc.

In Fig. 12 radiation patterns are presented for the ferrite-loaded helix from 300 - 1000 Mc. The patterns were taken with the helix being mounted on a $4' \times 4'$ aluminum ground plane. The patterns are quite unidirectional for both E_θ
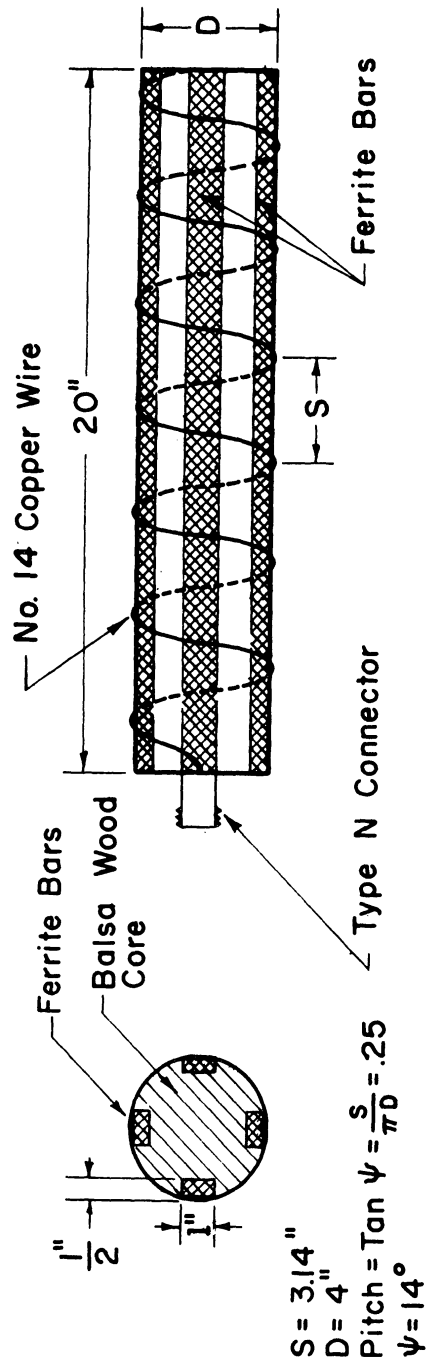
FIG. 10: HELIX ANTENNA LOADED WITH FERRITE BARS
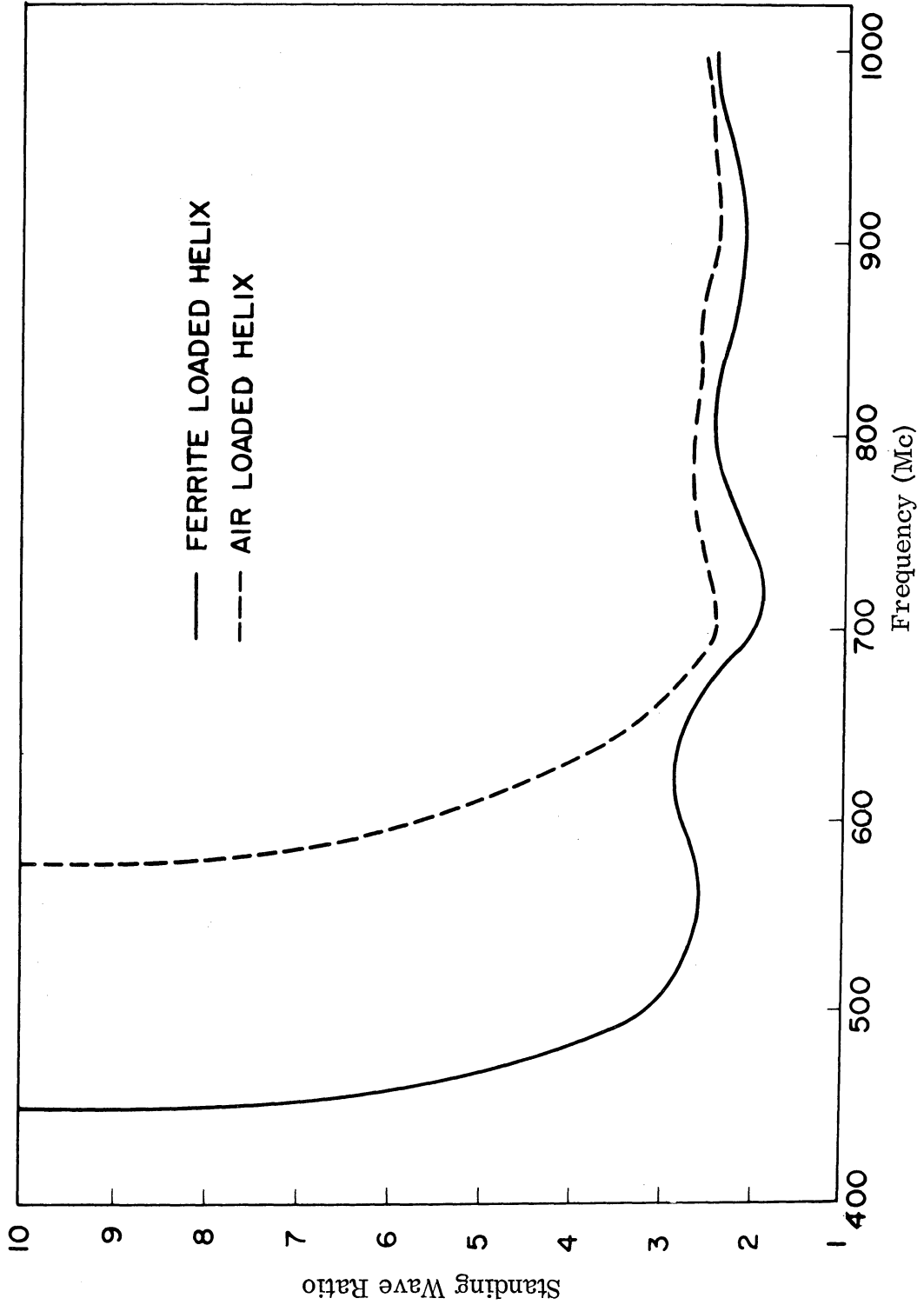
S = 3.14"
D = 4"
Pitch = Tan $\psi = \dfrac{S}{\pi D} = .25$
$\psi = 14°$

FIG. 11: VSWR FOR LOADED AND UNLOADED HELIX

300 Mc
—— E$_\phi$

400 Mc
--- E$_\theta$
—— E$_\phi$

500 Mc
--- E$_\theta$
·—— E$_\phi$

600 Mc
--- E$_\theta$
—— E$_\phi$

FIG. 12: RADIATION PATTERNS FOR FERRITE LOADED HELIX

30
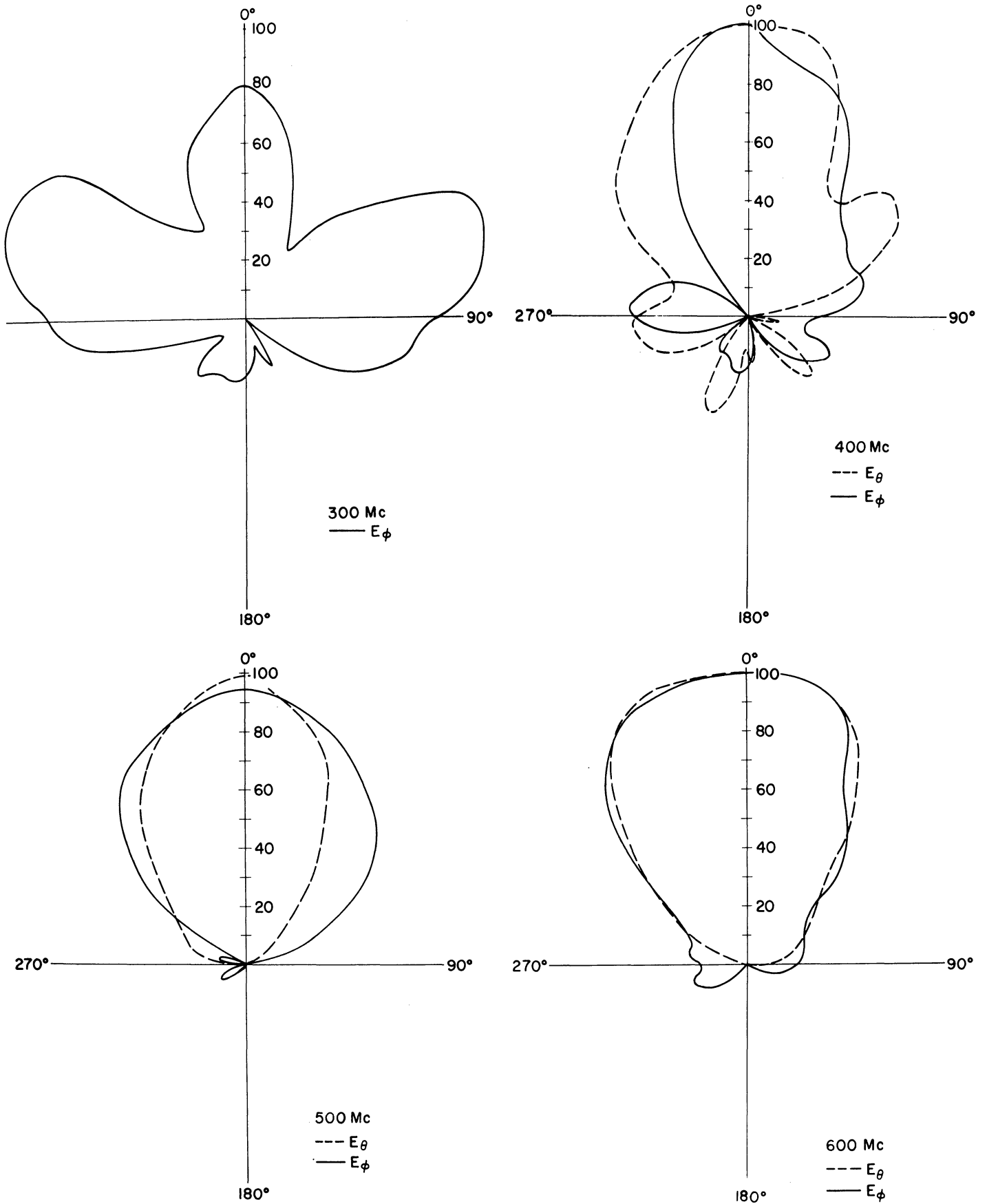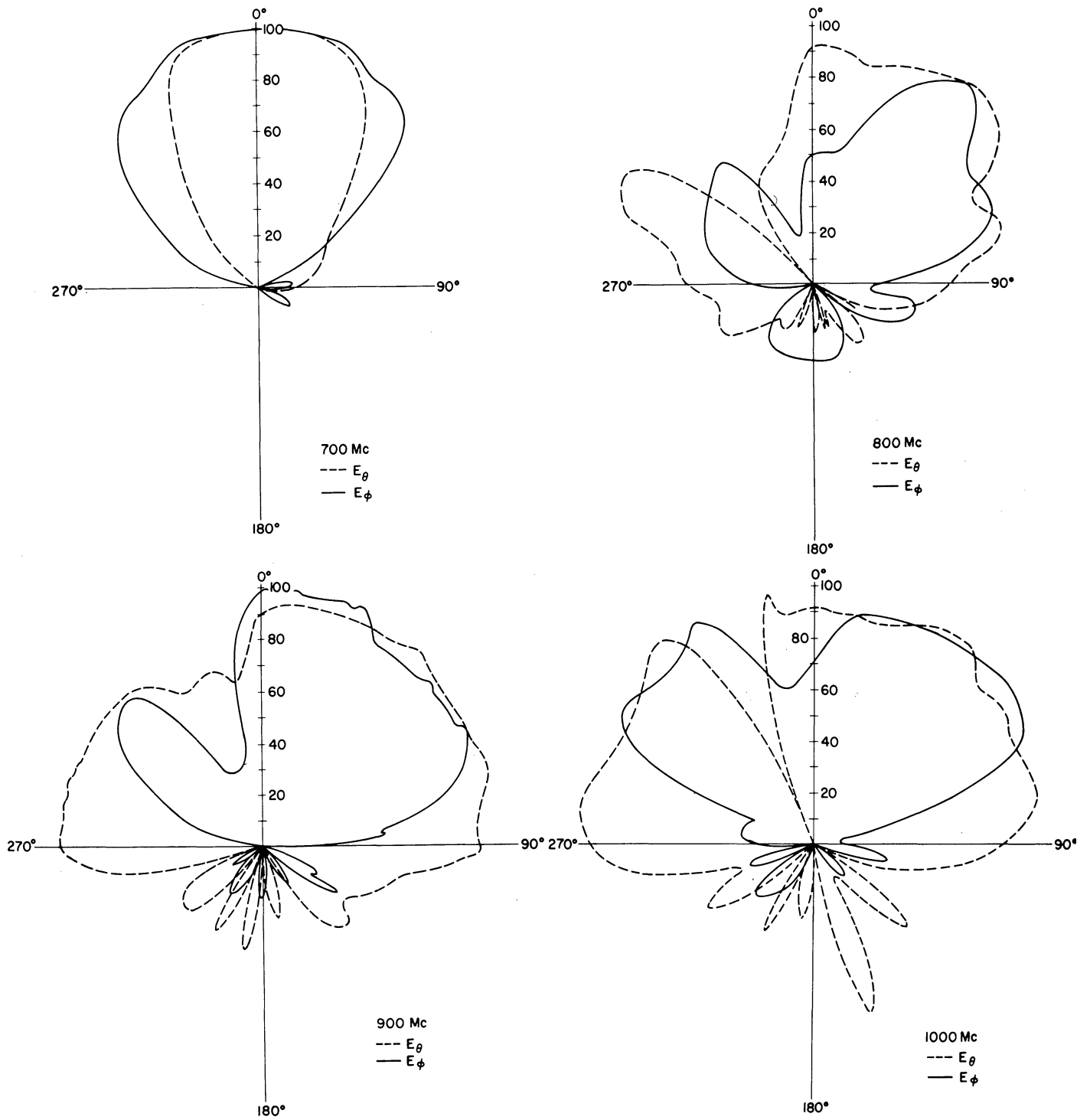
FIG. 13: RADIATION PATTERNS FOR FERRITE LOADED HELIX

and E_ϕ, with little back radiation except at the low end (300 Mc) where the wave is not properly launched yet and at the high end (800 - 1000 Mc) where the phase velocity along the helix is below that required for a single beam unidirectional pattern.

The beamwidth of the ferrite bar loaded antenna is about 80° at 400 and 500 Mc, 70° at 600 Mc, and 45° at 700 Mc; these values compare well with the electrical length versus beamwidth relationship expected. For the lengths involved ($.80\lambda$ at 500 Mc, 1.07λ at 600 Mc and 1.24λ at 700 Mc), Kraus (1950) arrives at beamwidths of approximately 70°, 60° and 50°, respectively. The unloaded antenna should operate with a well-formed beam for:

$$.77 < C_\lambda < 1.3 \, ,$$

where C_λ is the helix circumference measured in free space wavelengths. For this 10.1 cm diameter helix, the operating range should be between 727 and 1230 Mc without loading. The ratio of the upper to lower frequency is 1.69 and this is the same ratio as obtained for the ferrite-loaded helix, where $f_{min} = 400$ and $f_{max} = 700$ are the two limits. The lowest usable frequency is reduced by a factor of 1.8. This is the ratio by which the diameter of the helix has been reduced. The solid ferrite used was measured to have $\mu = 6.2$ and $\epsilon = 12.6$ at 600 Mc, where $\sqrt{\mu \epsilon} = 8.9$. In an infinite ferrite medium, the phase velocity and antenna lengths would be reduced by this factor. The actual reduction of 1.8 in helix size rather than 8.9 is mainly due to the lack of enough ferrite material: only one-third of the perimeter is loaded, and only 16 per cent of the total internal volume is loaded with ferrite bars. A size reduction of around 3.5, or 40 per cent of the theoretical limit indicated by the material parameters, seems quite feasible by using more ferrite inside the antenna.

From the $k-\beta$ diagram shown in Fig. 13, drawn for a 14° pitch unloaded helix, one can deduce the frequency band for which the helix could be an effective

$\psi = 14°$
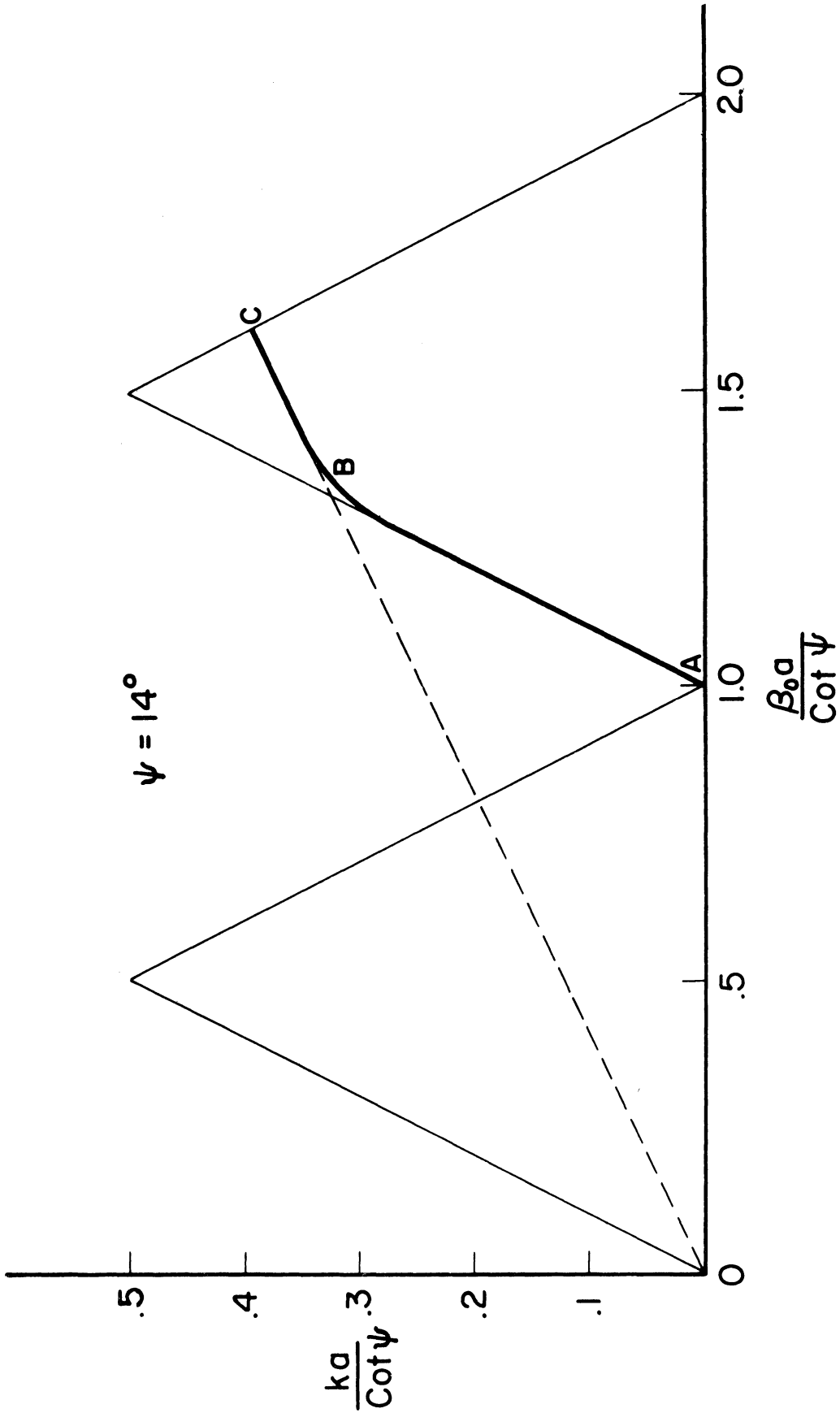
FIG. 13: k-β DIAGRAM FOR A 14° PITCH ANGLE UNLOADED HELIX

radiator. The region AB is a linear region and so is BC, however, the slope AB is suitable for realizing the Hansen-Woodyard condition whereas BC is not (Maclean, 1959). Therefore, the upper cut-off for $ka = C_\lambda$ = perimeter of helix in wavelengths, is located around B, from which point the helix wave velocity, V, is not increasing sufficiently fast with frequency to maintain a directive beam. Therefore, above this point, a breakup of the main lobe occurs.

The studies on ferrite loaded helices were very encouraging as the data which have been acquired and presented here indicate. Actually, a thorough study of the data such as presented in Fig. 11, VSWR for loaded and unloaded helices, show show that there has been considerable improvement with ferrite loading. However, the advantage of ferrite loading is even greater than shown in this figure. The ferrite material which has been used for loading deteriorates rapidly at frequencies over 600 Mc so that the full benefit of loading at frequencies over 600 Mc cannot be seen. The low frequency limit of the antenna has been reduced by approximately 100 Mc. The VSWR studies, the radiation pattern studies and efficiency studies should be made in the frequency range from 100 to 500 Mc by redesign of the helix. The trends shown for the ferrite loading of helices are encouraging.

2.4 Log Conical Spiral Antennas

Since the log conical spiral antenna has a very large inherent bandwidth, it was decided to load this antenna with ferrite in hopes that a large bandwidth would be maintained, in contrast to the very narrow bandwidth of the ferrite loaded rectangular slot antenna. The free standing log conical antenna was loaded with layers of ferrite; in addition, attempts at placing the log conical antenna in a cavity were made in order to allow flush mounted operation. Table I gives the specifications of the antennas and their identification numbers. Figures 14 and 15 are photographs of these antennas.
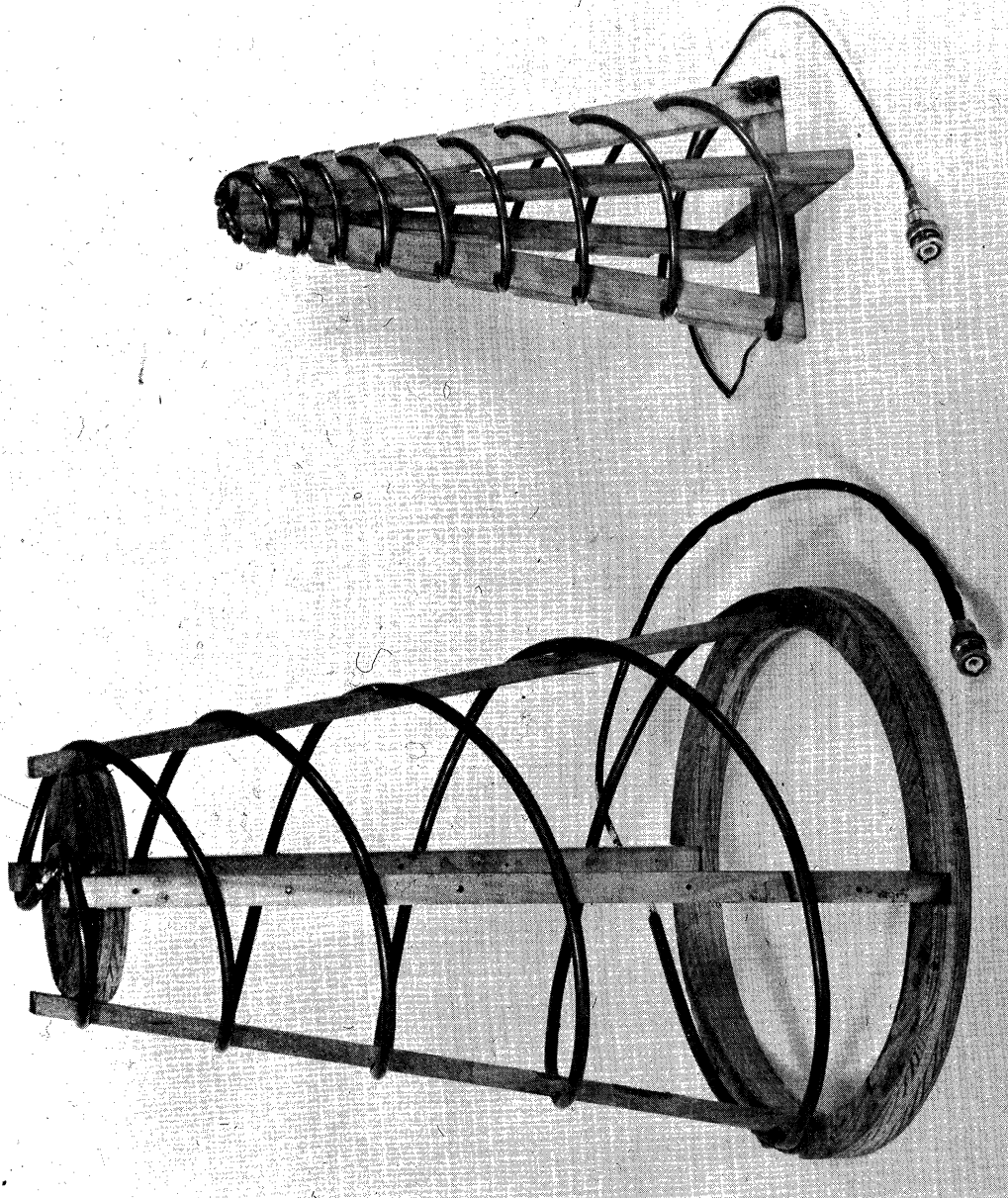
FIG. 14: LARGE AND SMALL LOG CONICAL SPIRAL ANTENNAS
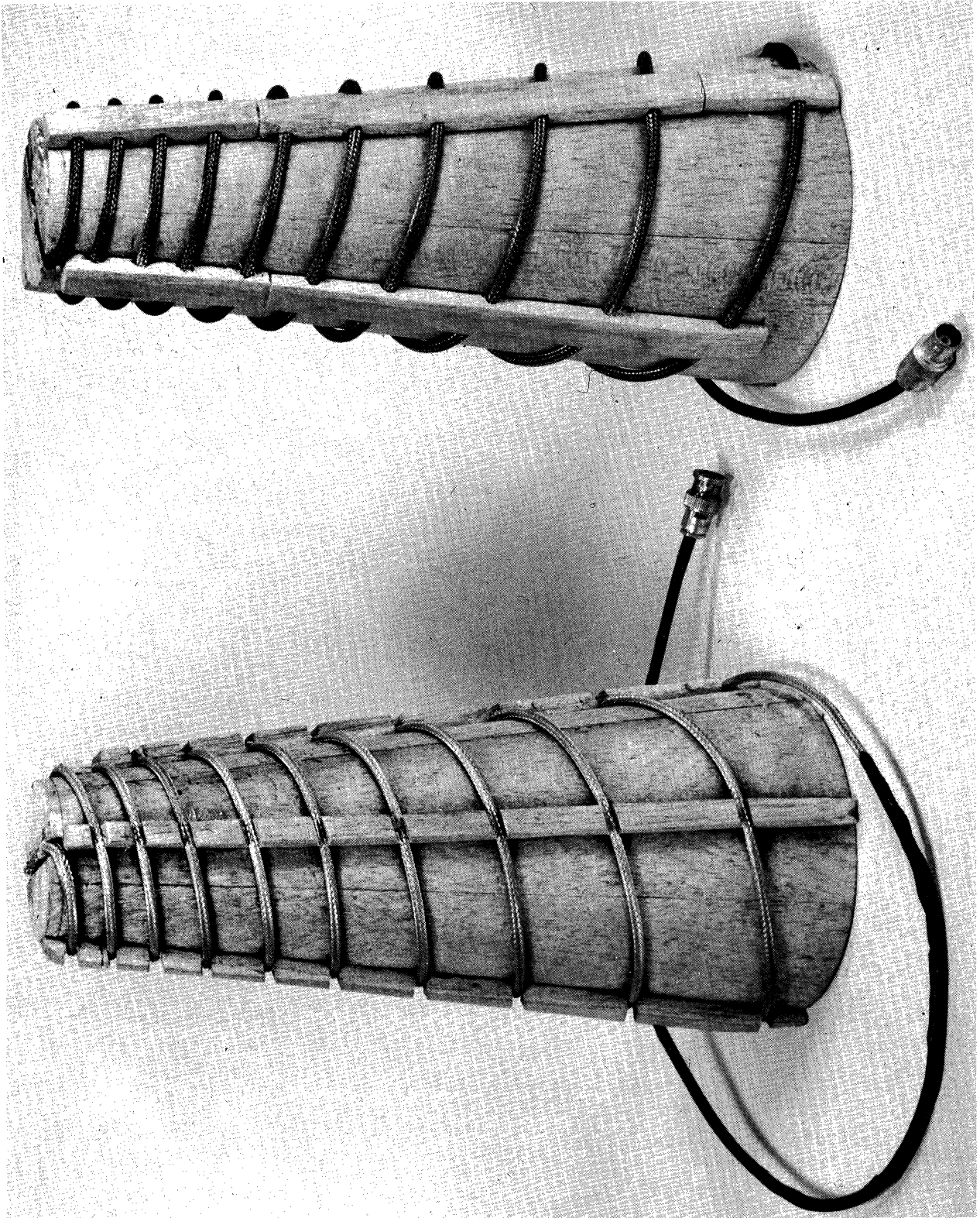
FIG. 15: MODELS OF LOG CONICAL ANTENNAS

TABLE I: LOG CONICAL SPIRAL ANTENNA SPECIFICATIONS

Identification Number	200	201	202-202a	204	208, 209
Base Diameter	26.5cm	17.5cm	12.5cm	11cm	13 cm
Apex Diameter	10.5	5.5	6	5	3
Height	39	47	30	27.5	27.5
Apex Angle	10°	10°	7°	6°	10°
Pitch Angle	73°	73°	80°	73°	73°
Outer Conductor	1/4" copper tube	1/4" copper tube	50Ω bare cable RG141U	50Ω bare cable RG141U	3/16" copper tube
Inside of Cone	hollow	hollow	balsawood	hollow	hollow

2.4.1 Log Conical Antenna Without Cavity

Two log conical antennas, with loading (No. 208) and without loading (No. 200) are depicted in Fig. 16, along with the VSWR characteristics. The unloaded antenna was actually larger than the loaded one, rather than being the same size as shown. It is seen that the lower bound of operating frequency has been reduced from above 300 Mc to below 200 Mc, as judged by the VSWR characteristics even though size reduction was also achieved. Figure 17 shows radiation patterns of the log conical antenna without cavity and shows that the lowered operating frequency range is maintained in radiation characteristics as well as VSWR curves. The loading of the smaller log conical antenna (No. 208) was by a ferrite powder everywhere inside the log conical antenna and 1/8" beyond the conductors, retained by a thin polyethylene sheet. The efficiency of this free standing loaded log conical antenna (No. 208) was approximately 23 per cent.

Loadings other than the solid core loading above are possible. Initial attempts at loading were with layers. Figure 18a shows Antenna 201 loaded with a layer of ferrite, and Antenna 202 unloaded. Figure 18b shows various partial loadings that were attempted with the large log conical spiral antenna (No. 201). The type "A" ferrite material of Fig. 18b(a) is the least lossy available ($Q_{mag} \cong 30$) and could be used in a thin layer loading only, since there was not a sufficient amount of this material available for loading with thick layers. As a result a more lossy type "B" material was used for the thicker loadings. With the more lossy material, VSWR curves would mean little; however, it was determined from numerous radiation patterns (see Bimonthly 5549-6-P on this contract) that at the higher frequencies, the thickness of loading did not effect the radiation pattern shapes significantly. At low frequencies, the thicker layers significantly improved the radiation patterns, whereas much less improvement was obtained when using the thin layers of material. Use of a thick layer resulted in a lower minimum possible operating frequency by a factor of .08 based upon constant VSWR level, or by a factor of 0.7 based upon maintaining the radiation pattern. No efficiency measurements were
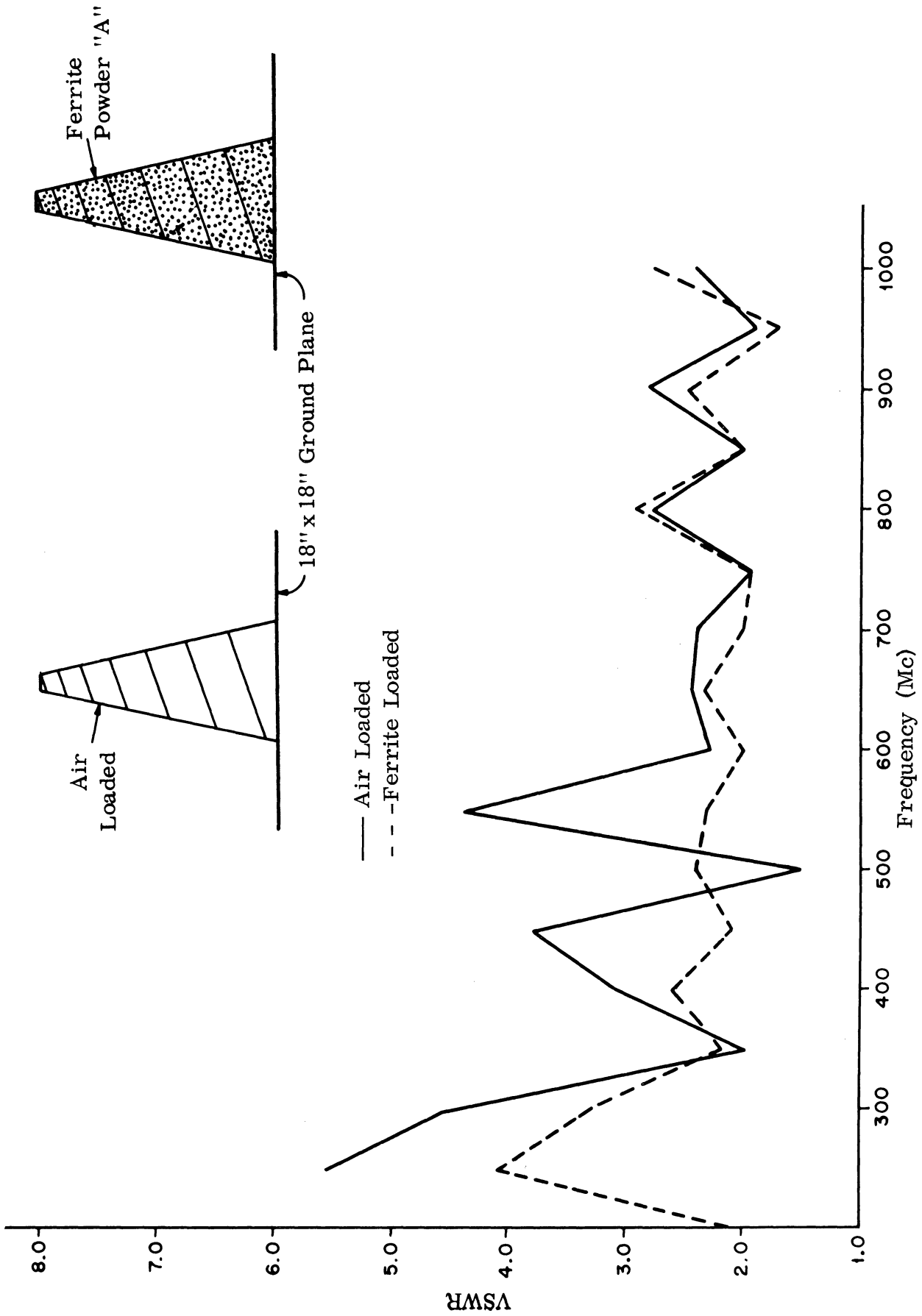
FIG. 16: VSWR VS FREQUENCY. ANTENNA NO. 208.

E_ϕ

400 Mc

500 Mc

--- FERRITE

— AIR
--- FERRITE

600 Mc

700 Mc

— AIR
--- FERRITE

— AIR
--- FERRITE

800 Mc

900 Mc

— AIR
--- FERRITE

— AIR
--- FERRITE

FIG. 17a: RADIATION PATTERNS WITHOUT CAVITY

5549-1-F

E_θ

400 Mc

—— AIR
--- FERRITE

500 Mc

—— AIR
--- FERRITE

600 Mc

—— AIR
--- FERRITE

700 Mc

—— AIR
--- FERRITE

800 Mc

—— AIR
--- FERRITE

900 Mc

—— AIR
--- FERRITE
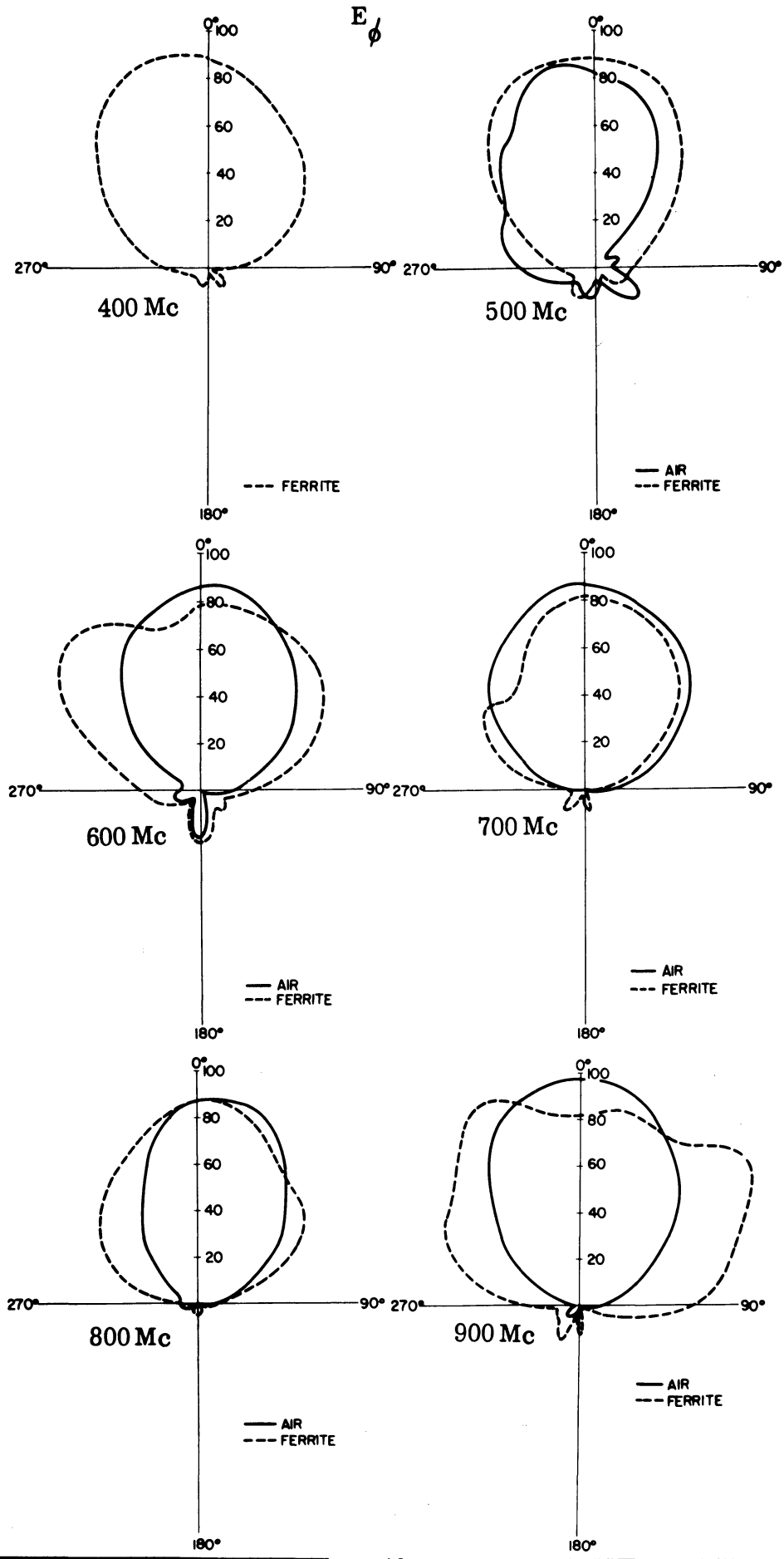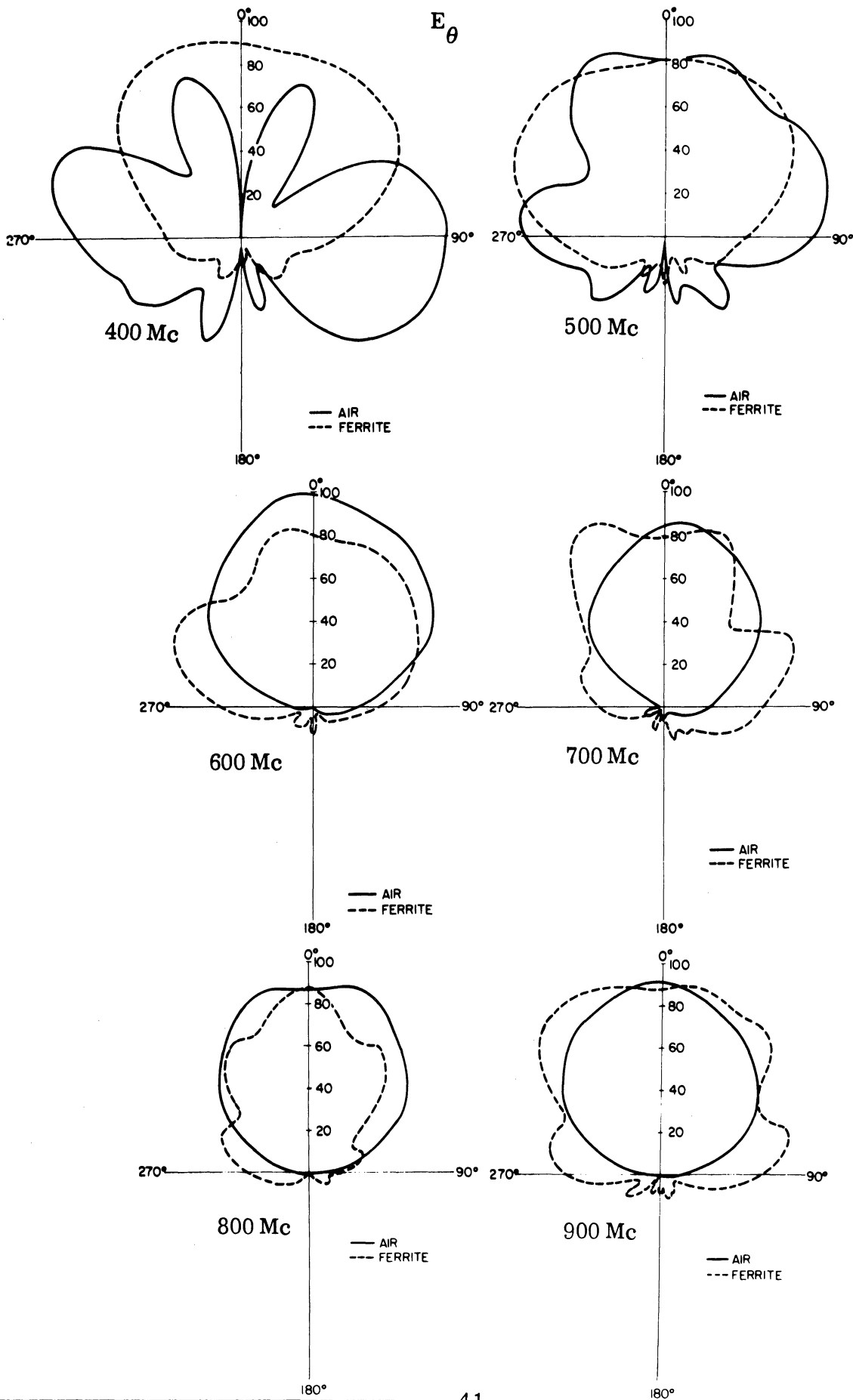
FIG. 17b: RADIATION PATTERNS WITHOUT CAVITY

41
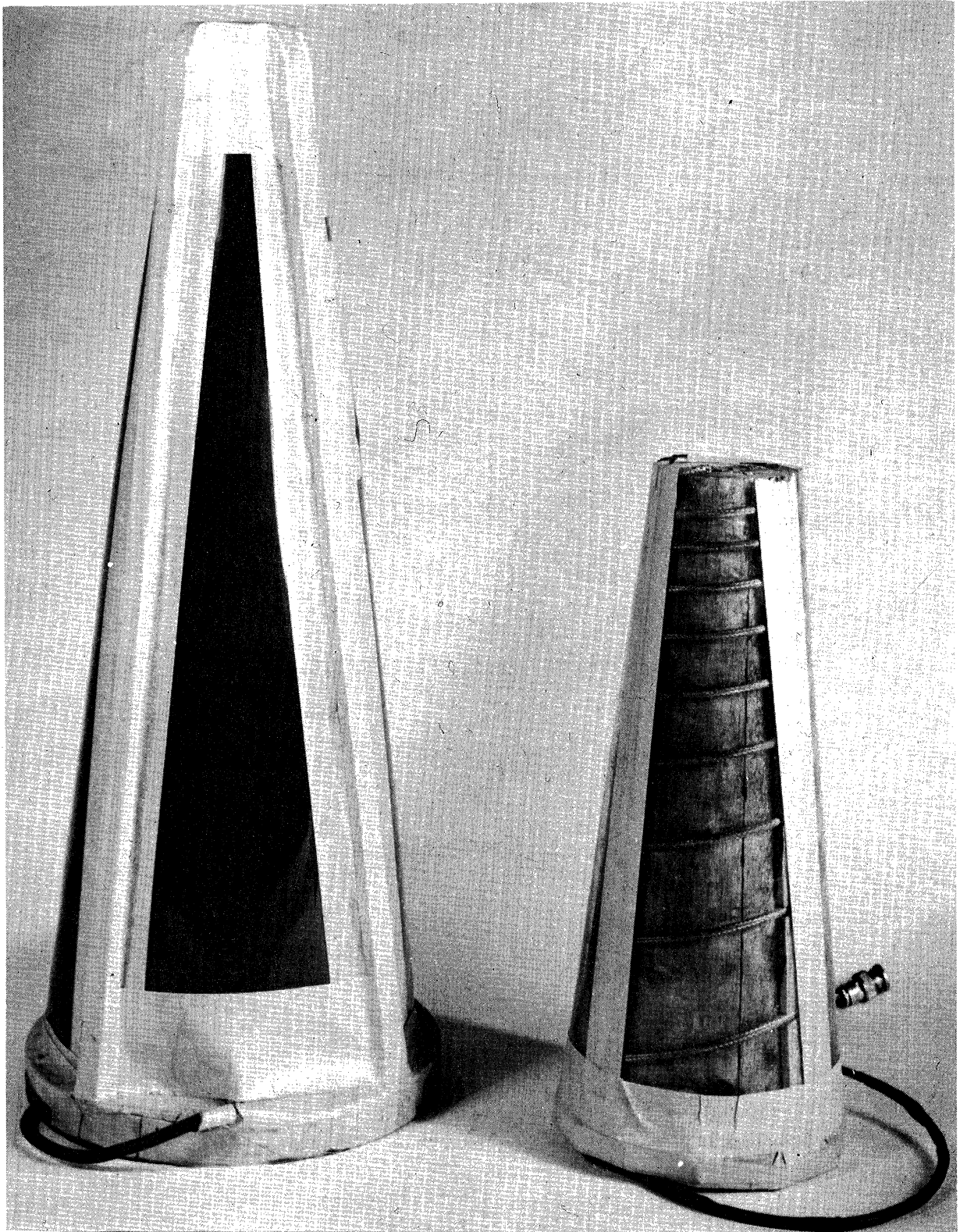
No. 201   No. 202

FIG. 18a: MODELS OF LOADED AND UNLOADED LOG CONICAL SPIRALS
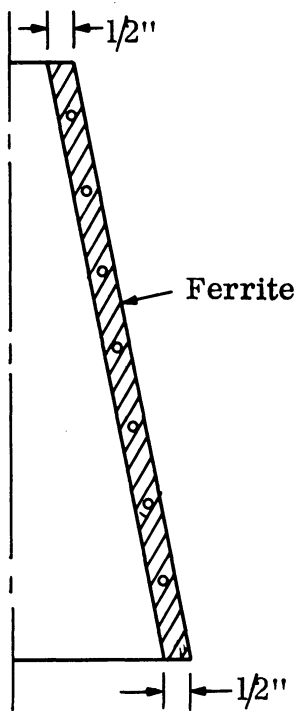
Ferrite

Thin uniform layer, type A material.
(a)
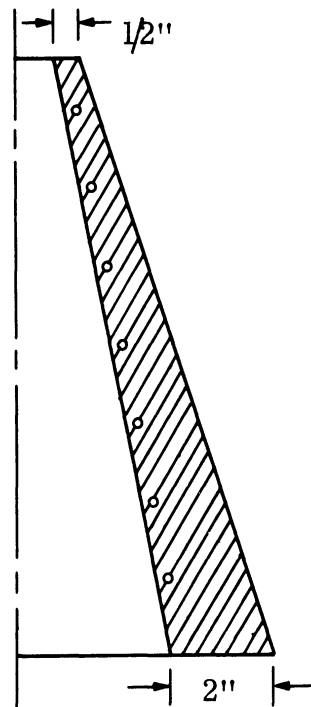
Tapered thick layer, type B material.
(b)

8 1/2"
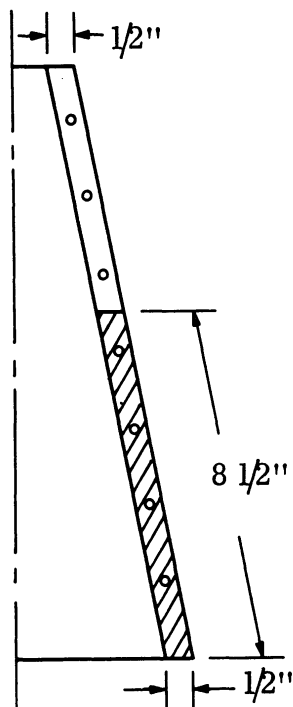
Uniform thin layer, bottom half.
(c)

8 1/2"
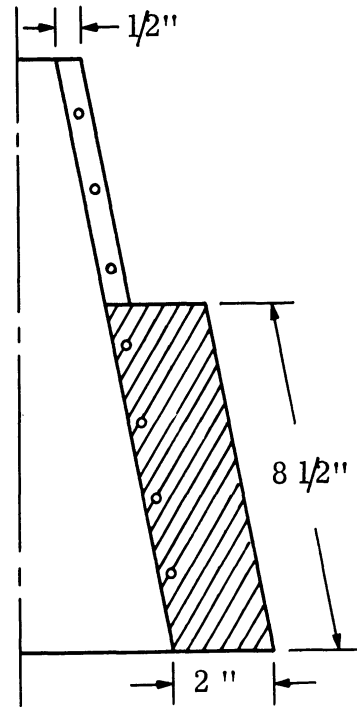
Uniform thick layer, bottom half.
(d)

FIG. 18b: FERRITE LOADING FOR LARGE LOG CONICAL SPIRAL ANTENNA.

made on these early models.

2.4.2 Log Conical Antenna Inside a Cavity

In order to achieve flush mounted operation, the free standing log conical antenna as discussed in the last paragraph, could be mounted on a missile nose cone, or other conical aerodynamic shape. Another way of flush mounting is to place the antenna (No. 209) mounted in a cavity (5.5" dia., 15" deep). The figure also displays VSWR characteristics vs frequency. The ferrite loading is seen to improve these VSWR characteristics considerably, although much of the improvement may be due to ferrite losses. However, as seen in Fig. 20, the radiation patterns of the ferrite loaded antenna with cavity are vastly superior to those without cavity, probably due to the fact that the ferrite loading allows the lowest dominant mode in the cavity whereas cutoff characteristics of the air loaded cavity appear to dominate below 900 Mc. It would seem that the ferrite loading allowed operation down to 300 Mc. rather than 900 Mc, which is a tremendous improvement.

The cavity and antenna No. 209 are shown in Fig. 21. For loading, the entire cavity was filled with ferrite powder. A considerable decrease in efficiency was noted over the free standing air loaded conical antenna in a cavity with loading.

The loading of the log conical antennas with a completely filled cavity was the final of a long series of experiments attempted at loading these antennas. Other kinds of loading are possible. The log conical antenna originally used is No. 202 (Fig. 15).

The results of early tests using a cast cavity are shown in Fig. 22, as a plot of VSWR vs frequency for the ferrite-filled and air-filled cavity with log conical spiral antenna (No. 202). A reduction in more than 2 : 1 is seen in the lower operating frequency due to the ferrite loading. Figure 23 shows several types of loading used with this original log conical antenna wound on a balsa wood core. The results shown in Fig. 22 were from loading as in Fig. 23b. In addition, partial loadings (Figs. 23c and 23d) were tried, with the results as shown in Fig. 24. It is
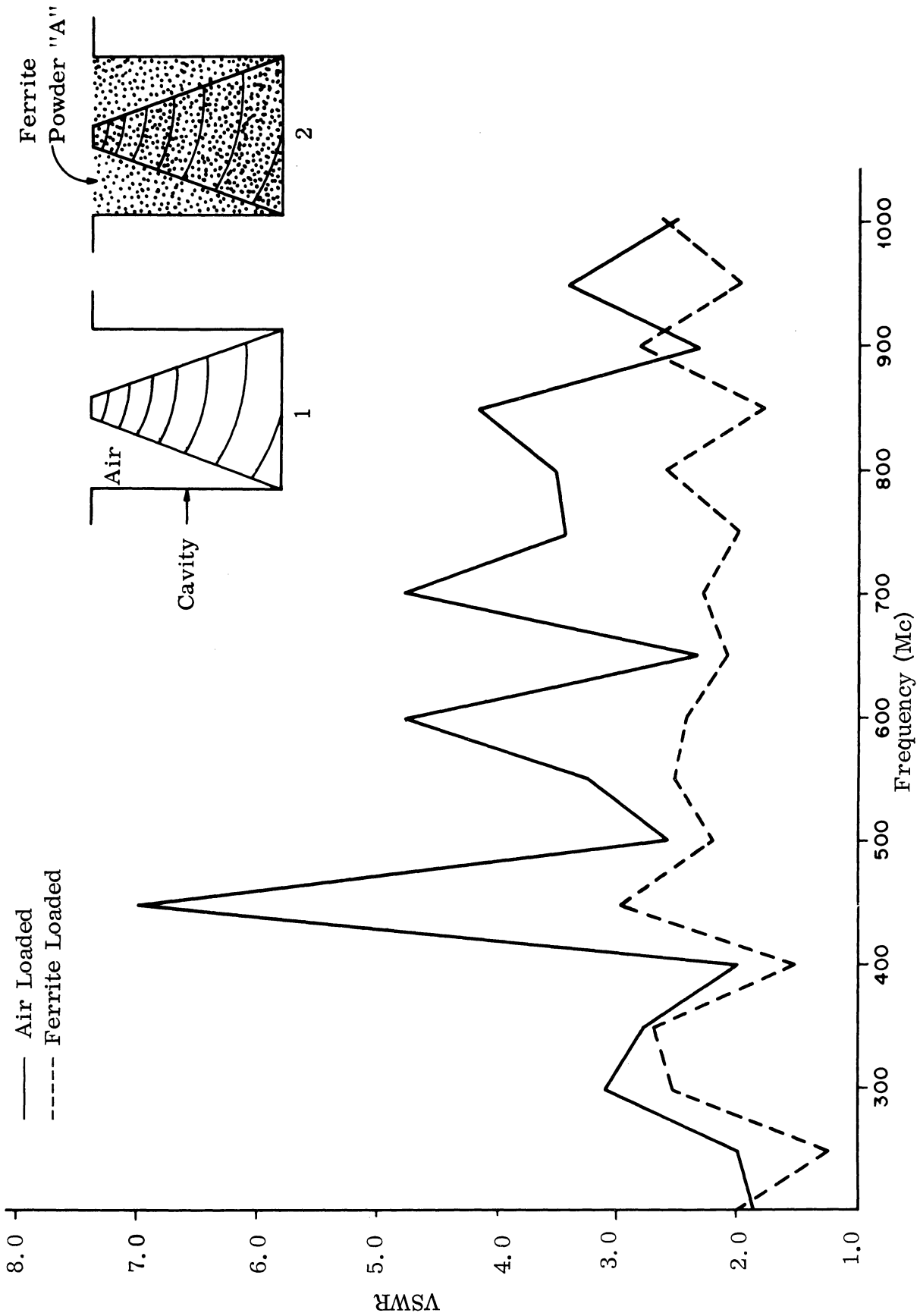
FIG. 19: VSWR VS FREQUENCY. ANTENNA NO 208 WITH CAVITY

FIG. 20a: RADIATION PATTERNS OF LOG CONE WITH CAVITY

E_ϕ

300 Mc
—— AIR
--- FERRITE

400 Mc
—— AIR
--- FERRITE

500 Mc
—— AIR
--- FERRITE

600 Mc
—— AIR
-- FERRITE

700 Mc
—— AIR
--- FERRITE

800 Mc
—— AIR
-- FERRITE

900 Mc
—— AIR
--- FERRITE

1000 Mc
—— AIR
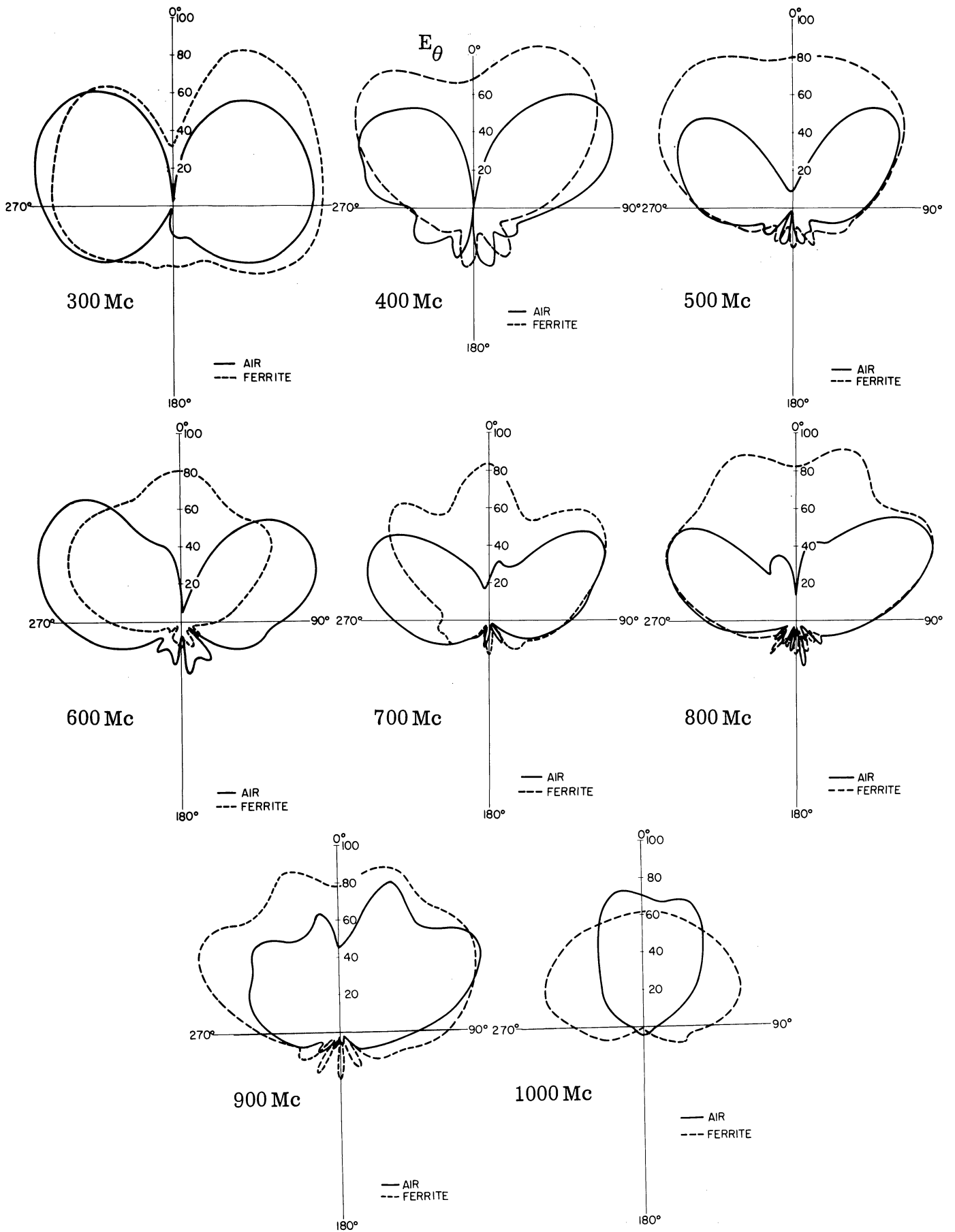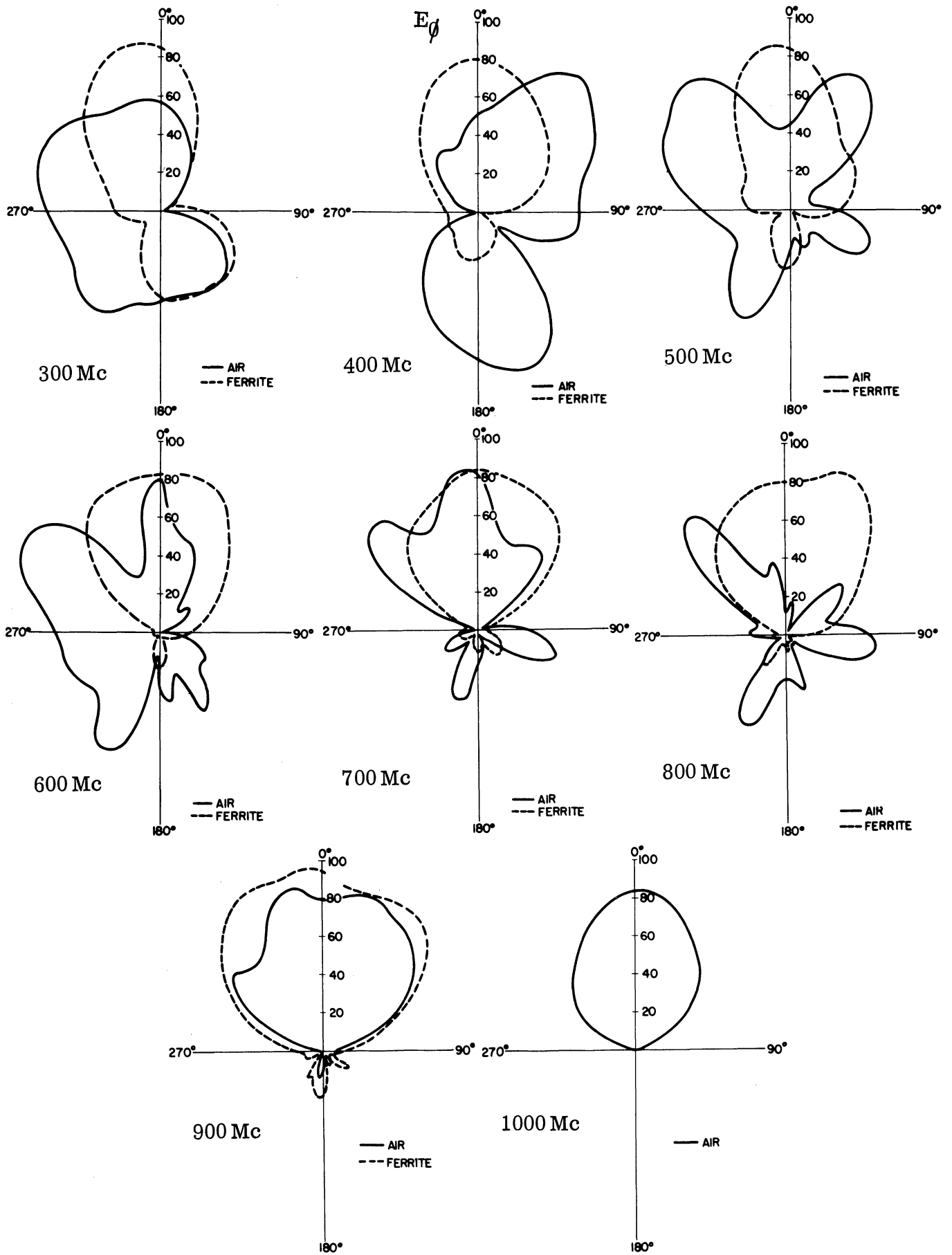
FIG. 20b: RADIATION PATTERNS OF LOG CONE WITH CAVITY

47
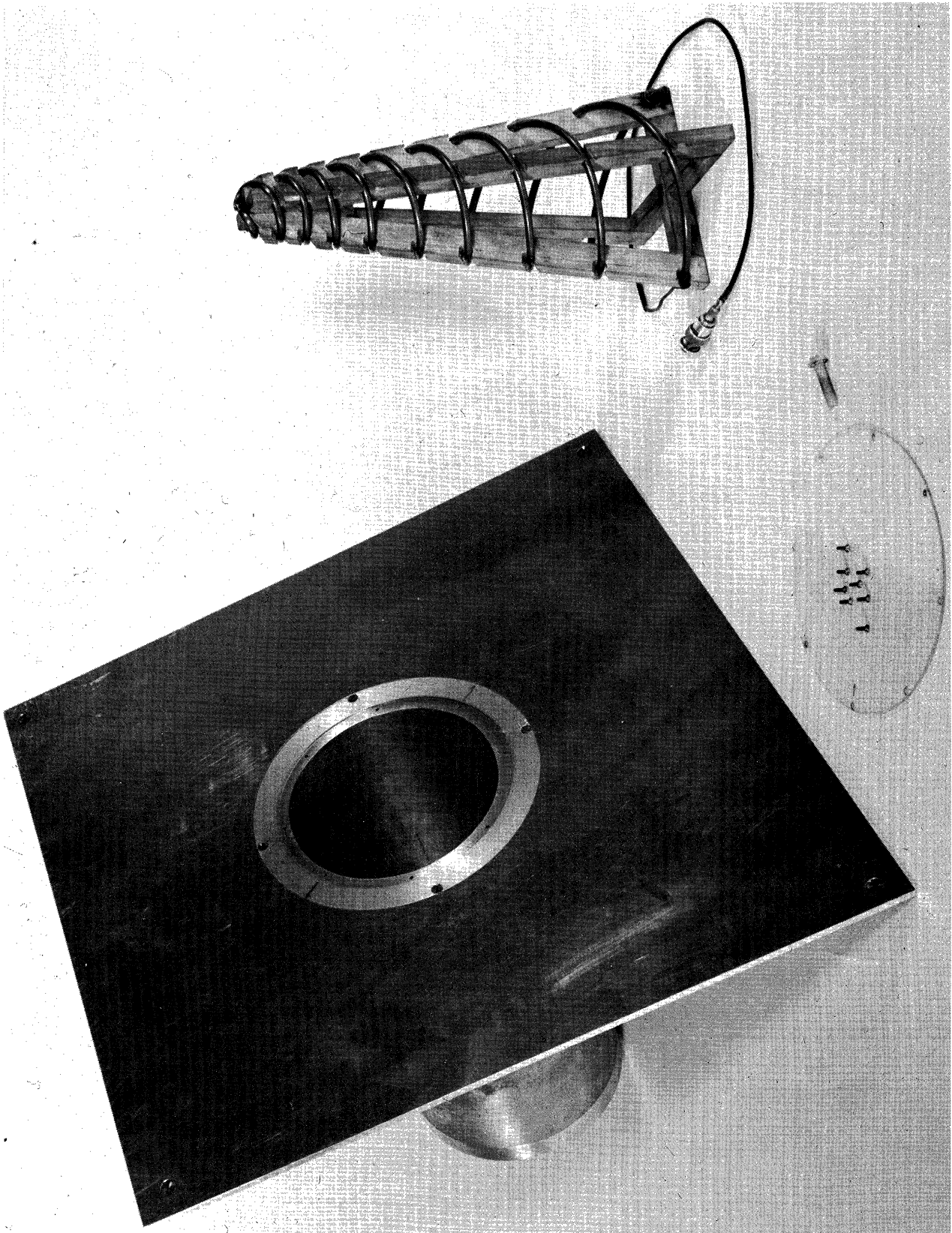
FIG. 21: CAVITY-BACK LOG CONICAL ANTENNA
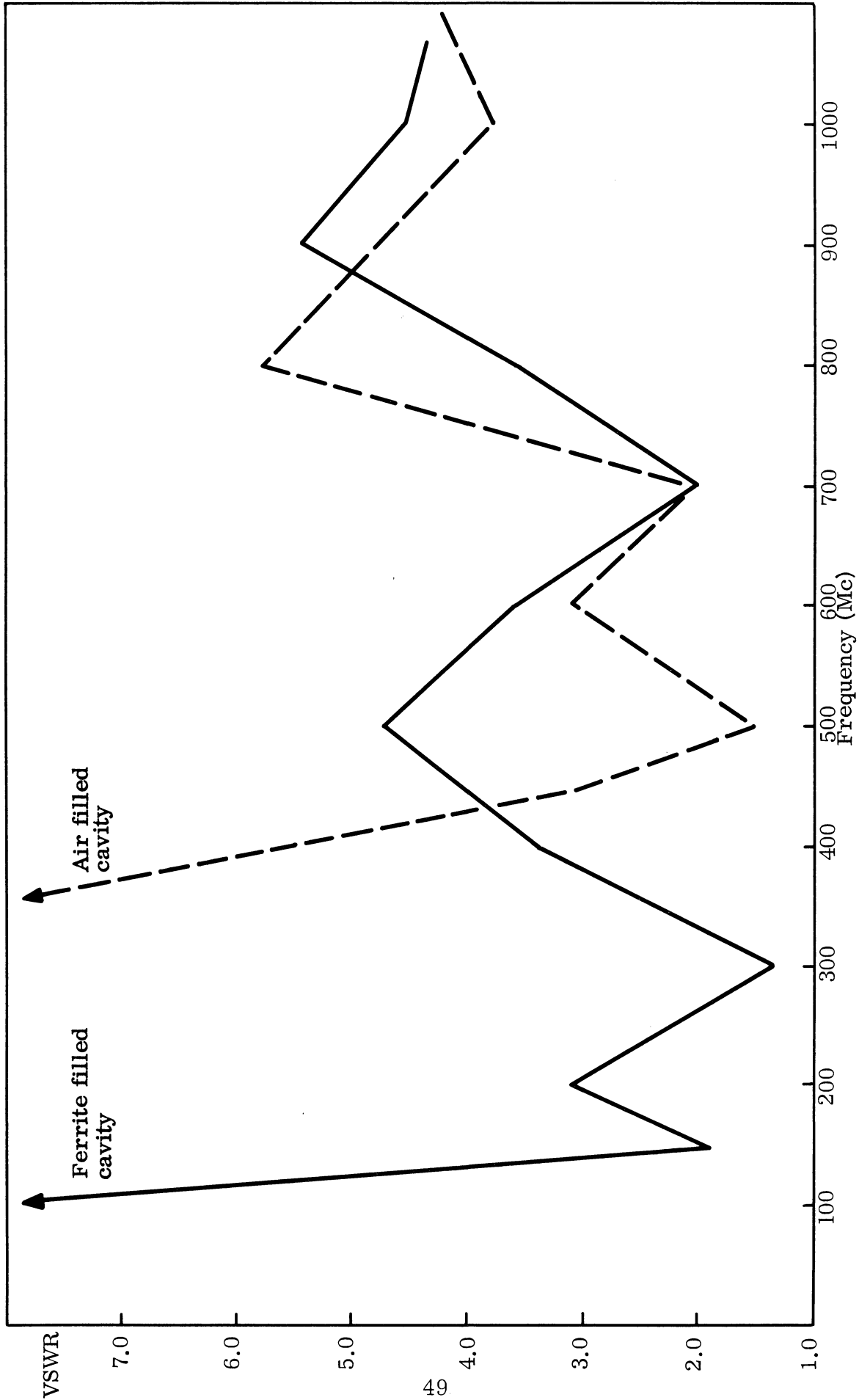
FIG. 22: VSWR FOR LOG CONICAL SPIRAL ANTENNA.
$\theta = 10^{\circ}$, $\alpha = 73^{\circ}$, $b = 0.053$.

(a)

(b)

(c)

(d)
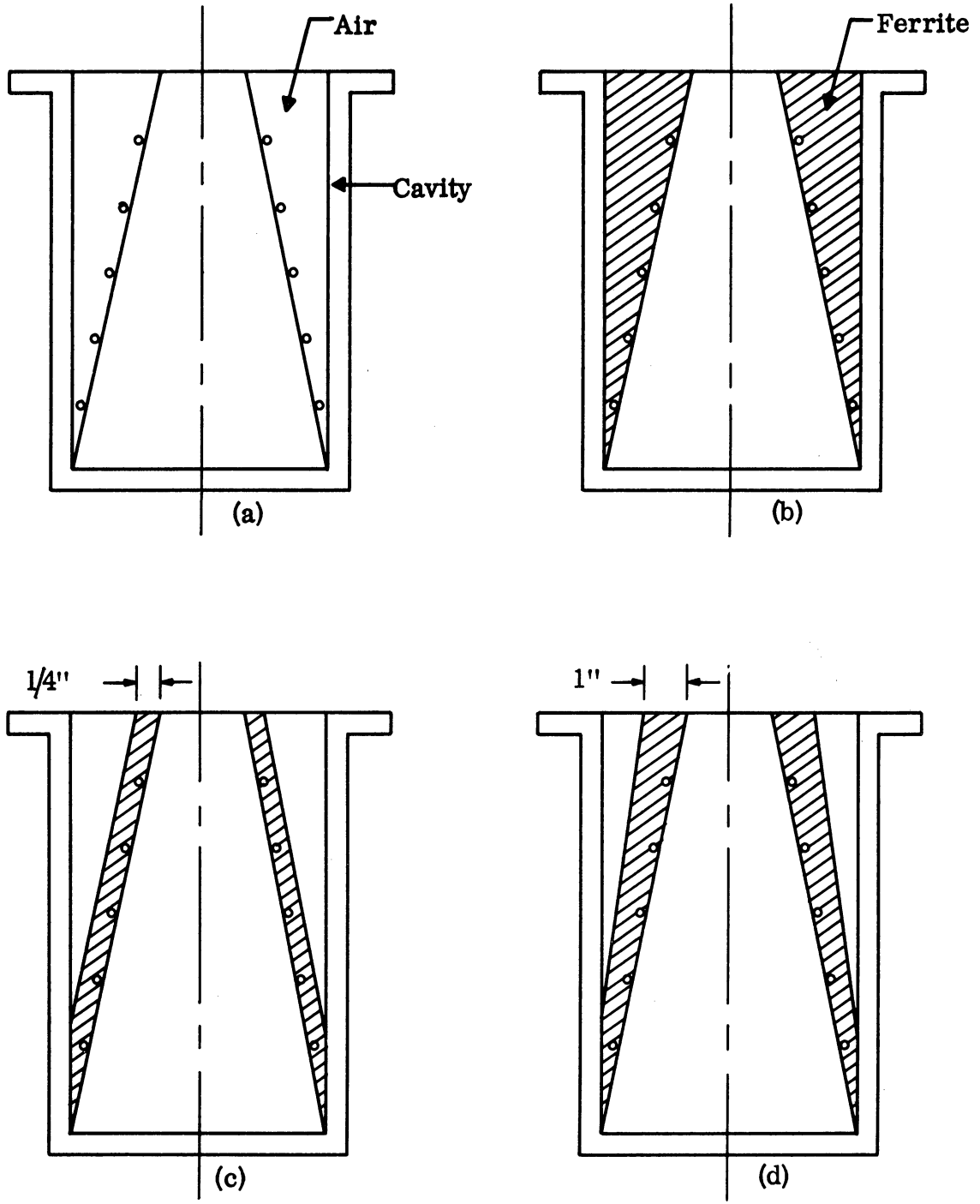
FIG. 23: FERRITE LOADING FOR SMALL LOG CONICAL SPIRAL
ANTENNA IN A CAVITY.

Cavity filled with ferrite

Uniform thin layer ferrite (cavity backed)

Cavity with air

Tapered layer (thick on top part)

Voltage Standing Wave Ratio
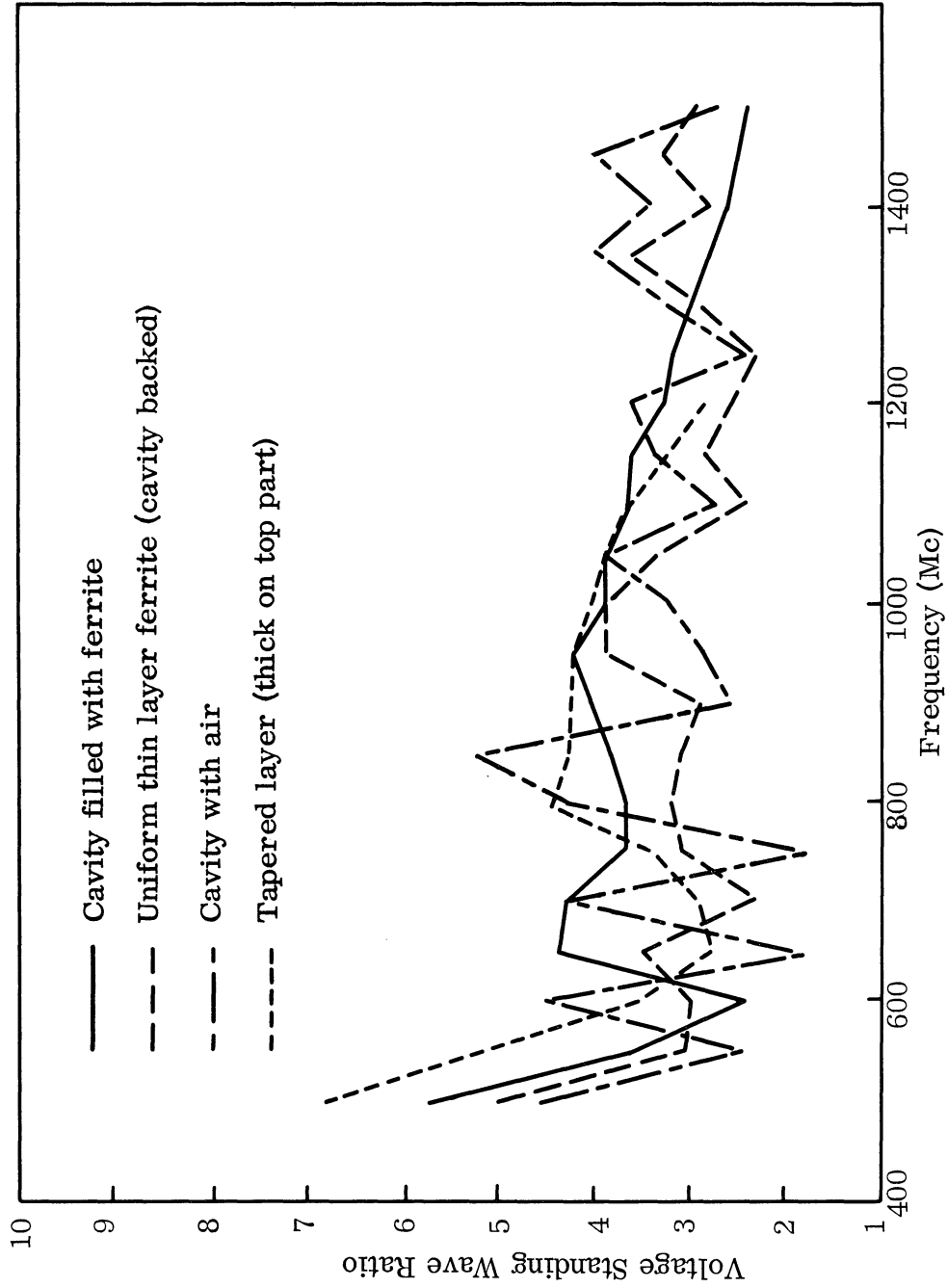
Frequency (Mc)

FIG. 24. FREQUENCY VS VSWR FOR SMALL LOG CONICAL SPIRAL WITH CAVITY.

interesting to note that the various ferrite loadings appeared to make little difference in VSWR. The original cavity with an aluminum cast cavity was finally replaced with a superior, machined cavity (Figs. 19 - 21 apply to the machined cavity).

2.4.3 Evaluation and Future Work on Log Conical Spiral Antennas

Numerous experiments were designed and tests were made involving this type of antenna. The experiments so far performed do not completely cover the whole range necessary. However, results have been sufficiently encouraging so that more critical experiments are being designed.

Unfortunately the range of experiments with and without a metal cavity are not sufficiently complete. It was found that there was considerable deterioration of efficiency when the log conical spiral was mounted in the cavity. Different arrangements of the ferrite material should be tried in order to more fully determine what is the most appropriate arrangement of material. Also, there appears as a result of the experiments performed so far, the need for possibly using more than one type of absorbing material just inside the curved cavity wall. It would be informative to use the log conical spiral inside a metal cavity with the ferrite material concentrated entirely inside of the cone formed by the active antenna conductors.

In view of the experimental results found so far, certain types of partial loading of the log conical spiral should be attempted. In the early experiments some partial loading was attempted. It is now believed that the more methodical program with two or more layers of ferrite inside the conical structure may yield results far better than any shown in this final report. There is the distinct possibliity that such an arrangement will increase efficiency through two possibly changes; a) the smaller amount of core material and thereby a smaller amount of magnetic loss associated with the volume of material, and b) a smaller amount of loss due to additional reflection present at an air-ferrite interface. Appropriate design of this last interface may result in improved radiation.

III
SLOT ANTENNA

The ferrite-filled rectangular slot antenna was the major subject of the report by Adams (1964). Since then, additional studies have been made of variations in the slot antenna, particularly those due to magnetic tuning, slot geometry (changes by the addition on metal or air in place of some of the ferrite), and changes due to temperature of the ferrite.

3.1 Magnetic Tuning

Since the ferrite-filled slot antenna has a rather narrow bandwidth (16 - 20 Mc) it has been expected that some tuning of this slot antenna would be achieved by the application of a d - c magnetic field. Originally, experiments were carried out with a permanent magnet as the source of a unidirectional magnetic field. More recently, an electromagnet was fashioned so that continuous changes in magnetic field can be achieved. Since the three characteristics of the antenna, VSWR, antenna patterns and efficiency, were studied as the unidirectional magnetic bias field was varied, these three characteristics will be discussed separately.

3.1.1 VSWR Curves

The first attempt at shifting the resonant frequency of the ferrite-filled slot antenna was with permanent magnets as shown in Fig. 25. Figure 26 shows the effect of applying a permanent magnet to the back of the slot antenna. In order to get a variation in the intensity of the applied magnetic field, the magnet was applied both with and without an aluminum plate as shown in Fig. 26. A shift in the resonant frequency of 70 Mc was achieved with the strongest magnetic dield. In addition, no marked change in the bandwidth occurred. Figure 27 shows a more extensive set of measurements made with two magnets placed in various combinations on the side of the slot antenna. Most of the configurations are seen to produce only a small change in the resonant frequency of the antenna. However, in using Configuration No. 7, where the applied magnetic field is along the wide dimension of the aperture, the

53
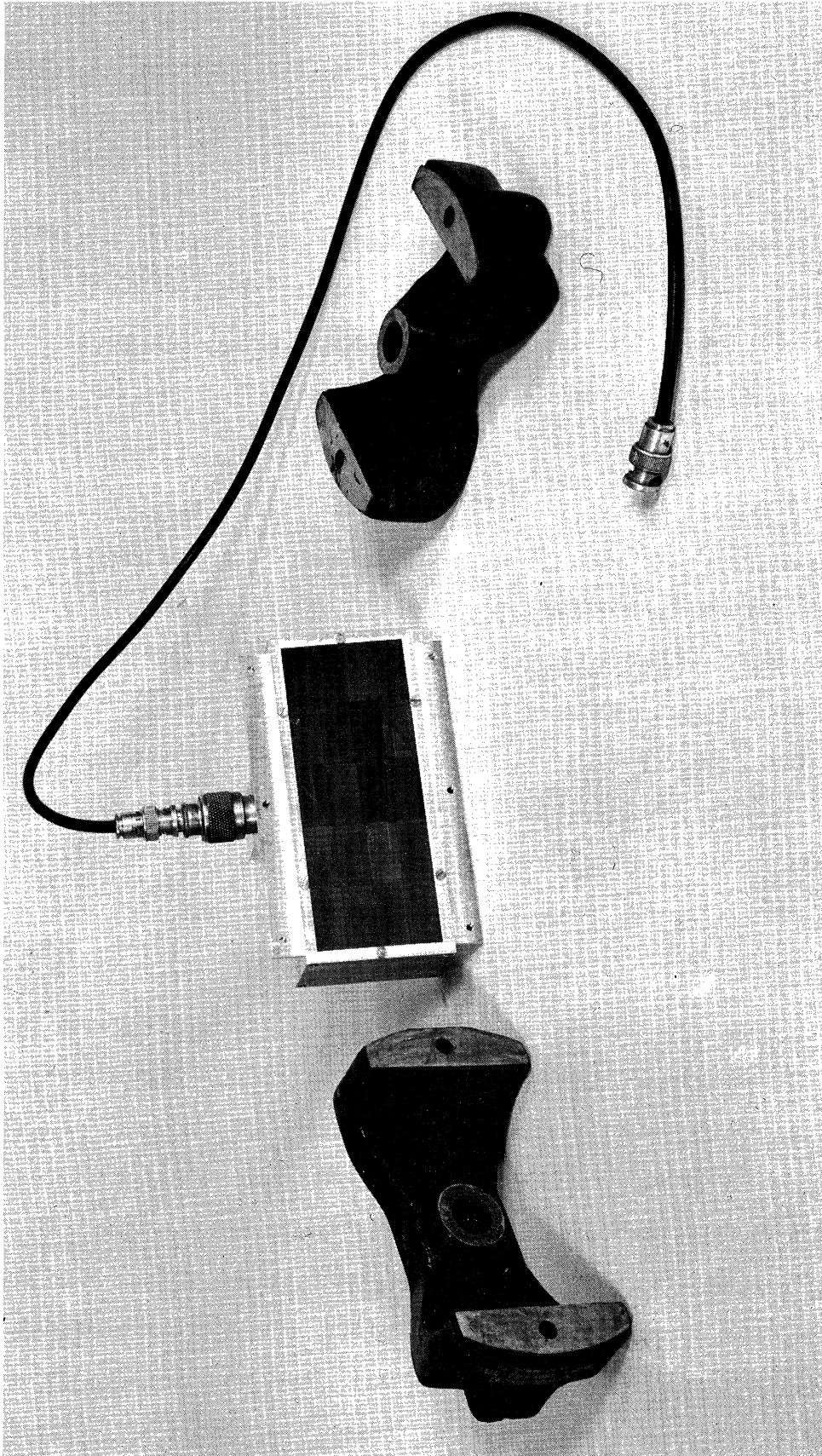
FIG. 25: FERRITE LOADED SLOT ANTENNA WITH PERMANENT MAGNETS.
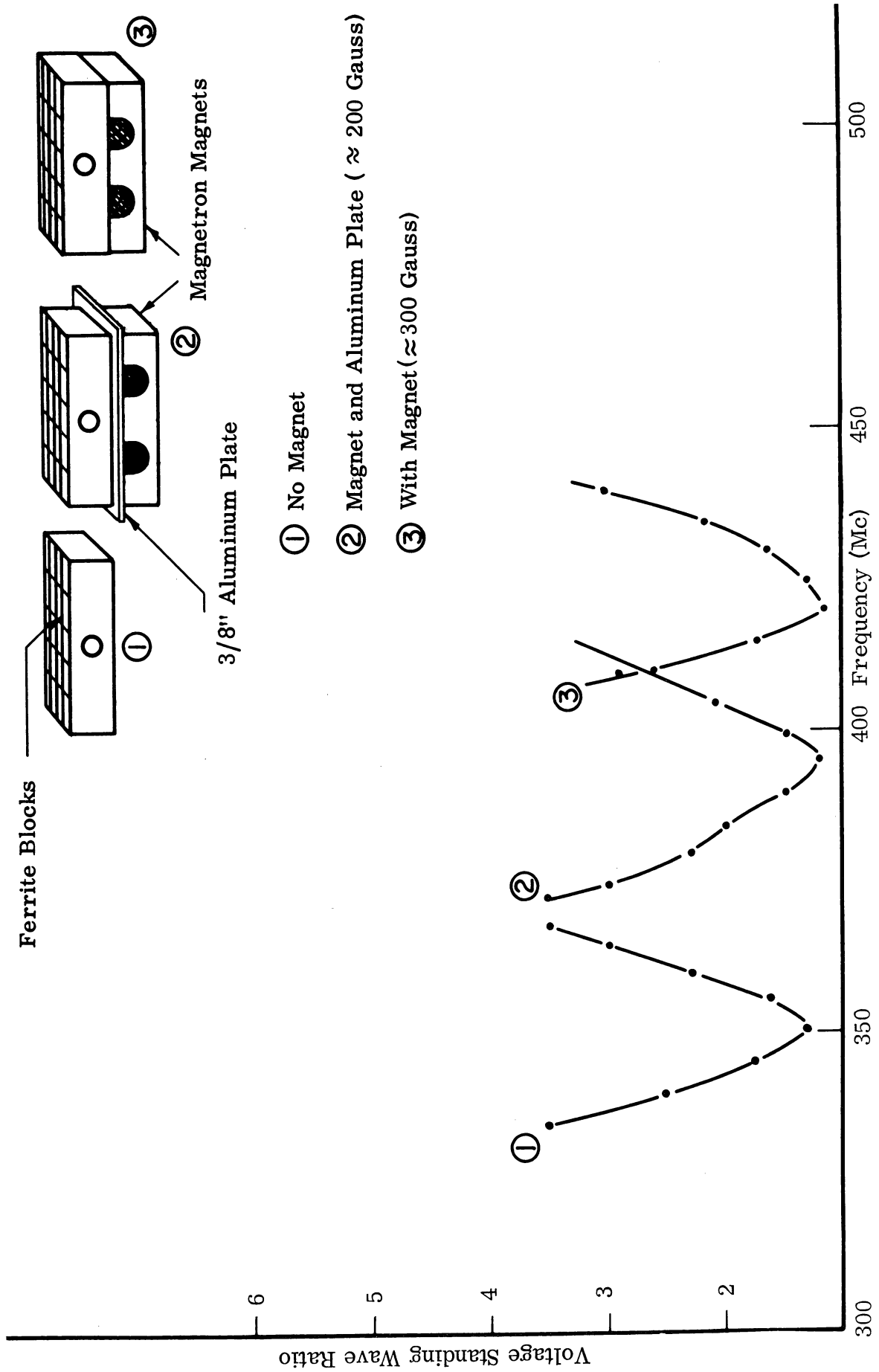
FIG. 26: VSWR VS FREQUENCY FOR RECTANGULAR FERRITE SLOT ANTENNA NO. 101
WITH PERMANENT MAGNETS
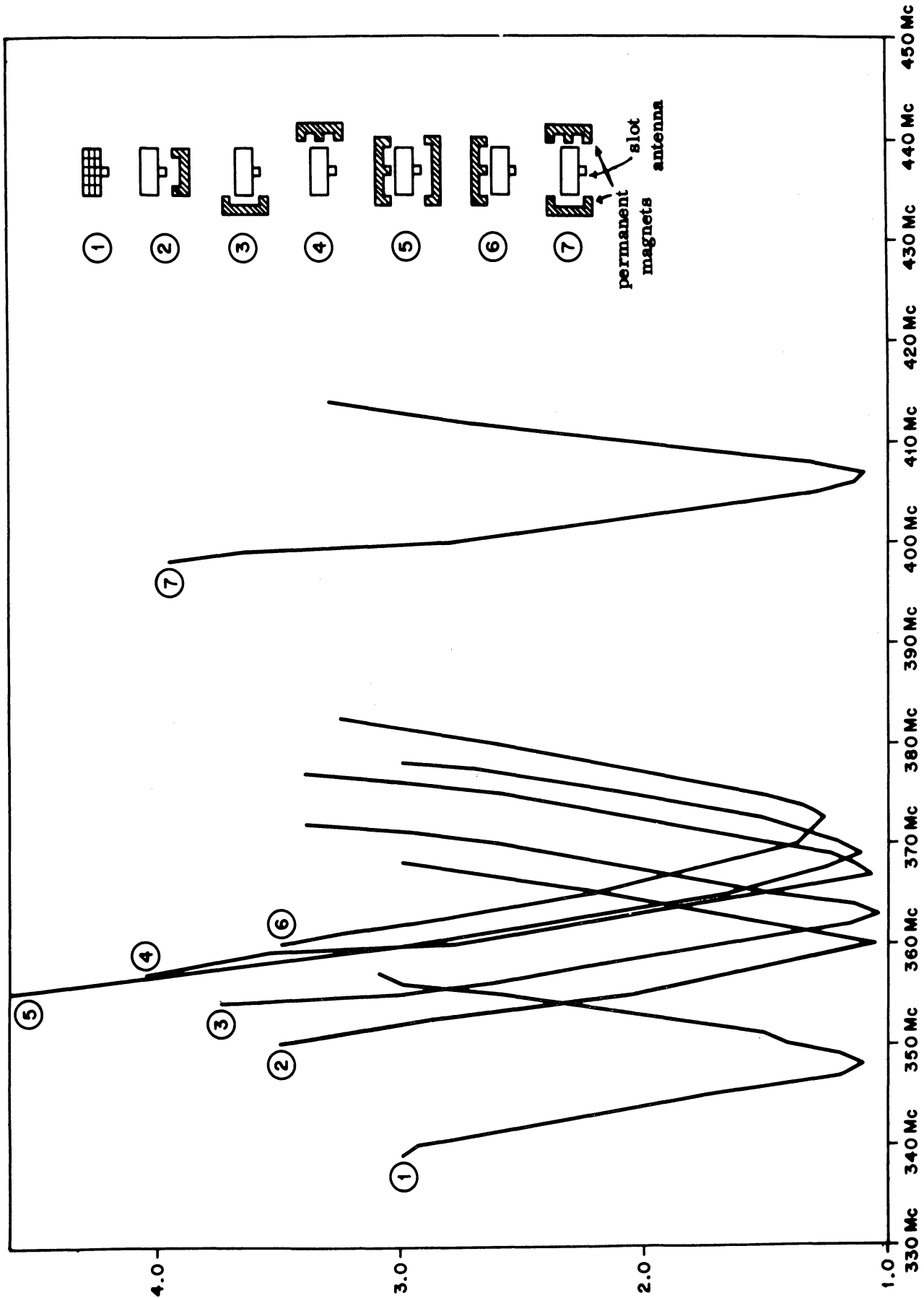
FIG. 27: FREQUENCY-VSWR BEHAVIOR OF FERRITE FILLED SLOT ANTENNA FOR VARIOUS ARRANGEMENTS OF MAGNET OR MAGNETS

shift is again quite large (about 60 Mc). Again, there were no major changes in the bandwidth about the resonant point of the slot antenna. Figure 28 shows the effect upon VSWR of using an electromagnet to provide a unidirectional bias field along the wide dimension of the aperture. In this case, a shift of 120 Mc in the resonant frequency of the antenna was achieved with the largest bias field of 1100 gausses. The bandwidth of the antenna was again substantially unchanged. Figure 29 shows the tuning curve of magnetic bias vs shift in the resonant frequency for the same magnet configuration as in Fig. 28. In order to achieve greater magnetic bias, it appeared necessary to fabricate wot electromagnets, because severe heating effects were encountered with one magnet at field strengths greater than 1000 gausses. Figure 30 shows the VSWR curve with two magnets along the wide face of the antenna aperture. Little additional tuning shift over that for the single magnet was observed because the ferrite was saturating; thus, a higher magnetic flux in the ferrite was not achievable. Figure 31 shows a different electromagnet configuration with the resulting VSWR curves vs frequency. It was noted in the permanent magnet configurations that magnetic fields across the short face of the aperture did not cause large shifts in resonant frequency. The experimental results shown in Fig. 31 confirm these results for the electromagnet case. However, it is noticed that a second minimum occurred with this configuration that did not occur in the unbiased slot antenna (Fig. 31) for B = 0. Figures 32 and 33 show configurations with the electromagnet biasing fields on opposite sides of the aperture opposing each other. Note that the biasing in Fig. 33 differs from that in Fig. 30 because of the top bias field in Fig. 33 opposing that bias on the bottom. In Fi.g 30, the two bias fields are both in the same direction. Again significant shifts in the resonant frequency did not occur. A second minimum VSWR occurs as in Fig. 31, but only for a very large magnetic bias. An attempt was made to wind the electromagnet directly around the cavity part of the slot antenna so that the plane of the coils was parallel to the aperture face and directly behind it, causing the magnetic field to be normal to the aperture. This attempt failed to affect the resonant frequency, possibly due to a weak magnetic field. Heating was also a severe problem.
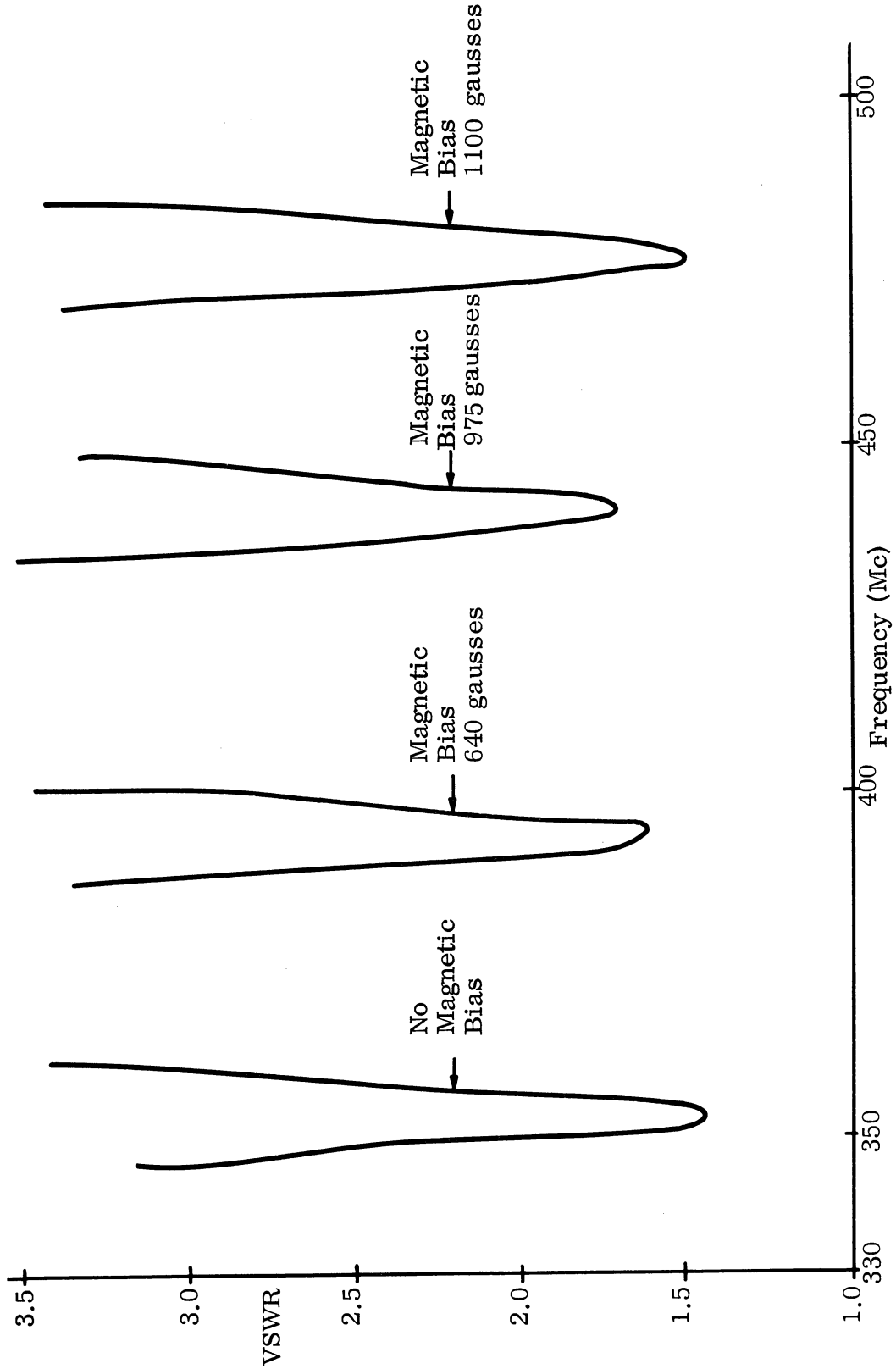
FIG. 28: VSWR VS FREQUENCY FOR MAGNETIC TUNING
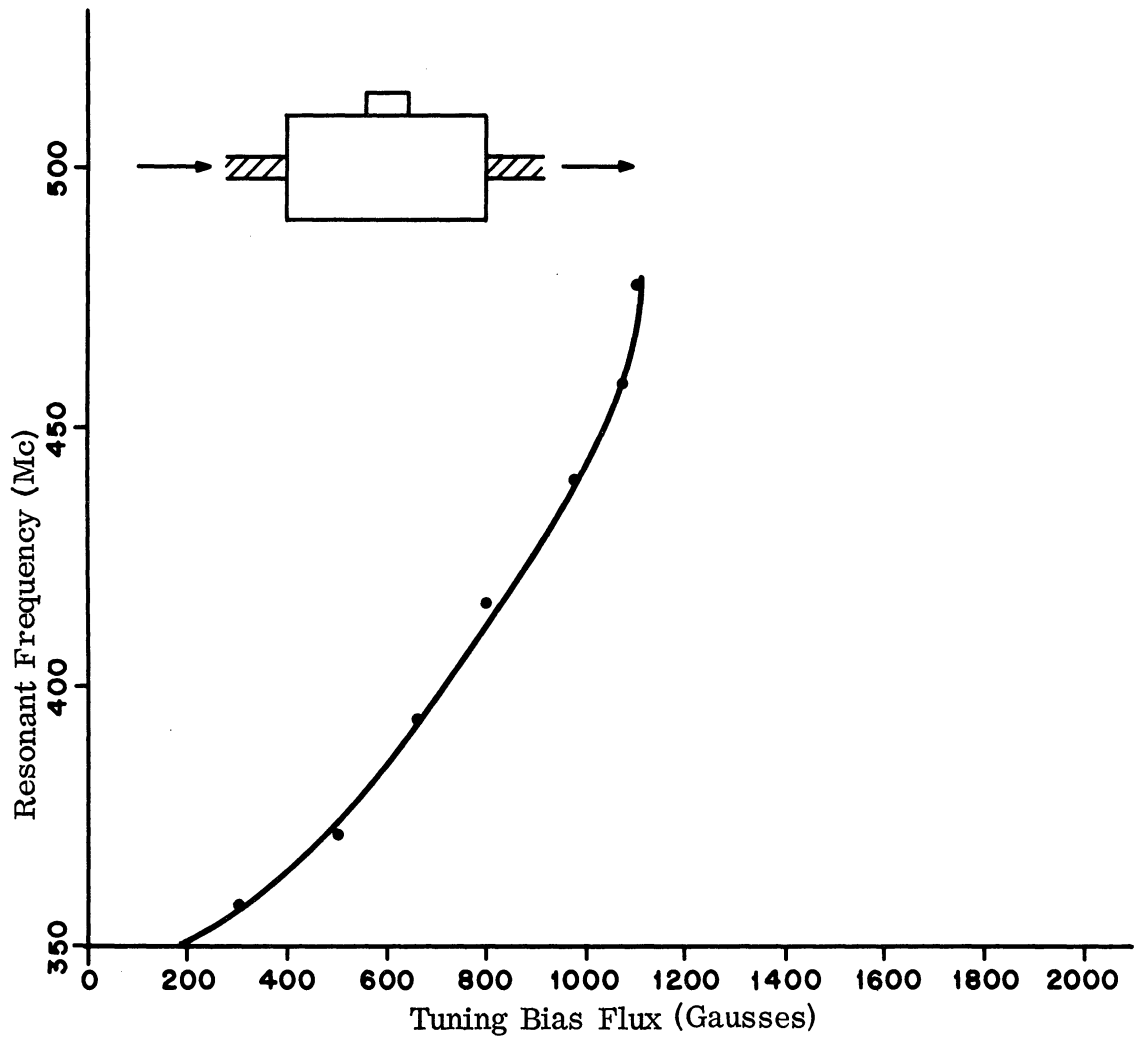
FIG. 29: TUNING BIAS VS RESONANT FREQUENCY
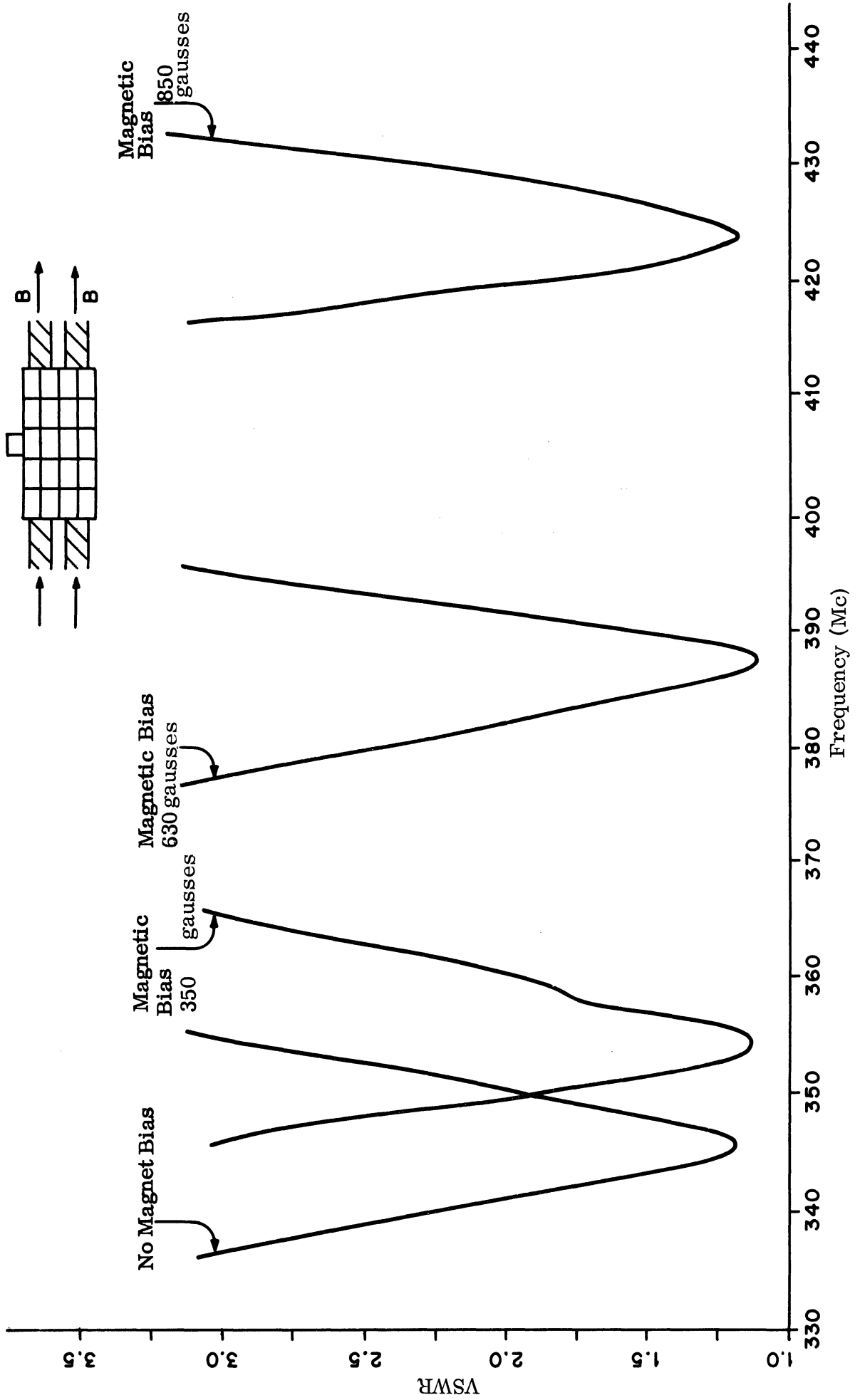
FIG. 30: VSWR VS FREQUENCY – ELECTROMAGNET TUNING
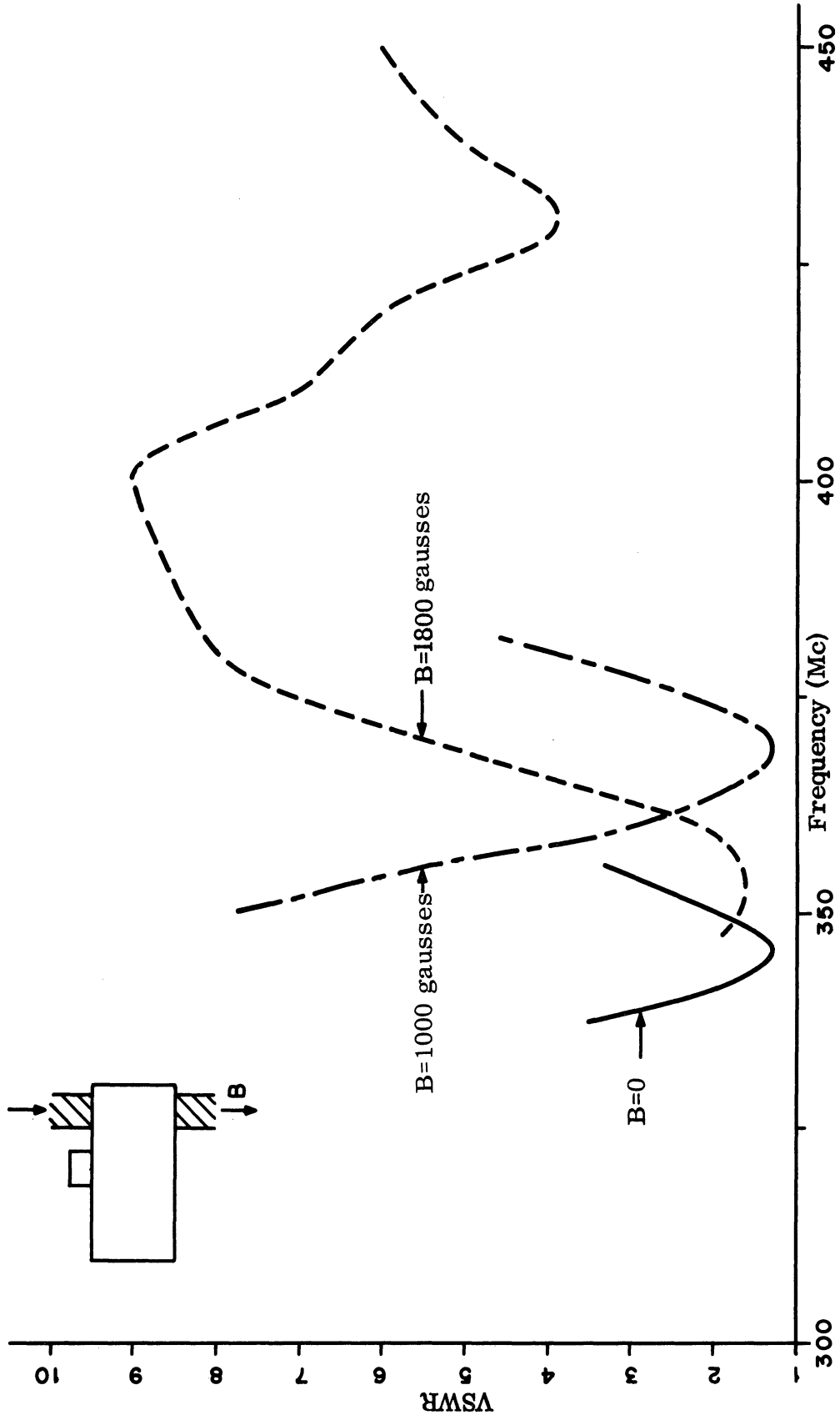
FIG. 31: VSWR VS FREQUENCY - ELECTROMAGNET TUNING
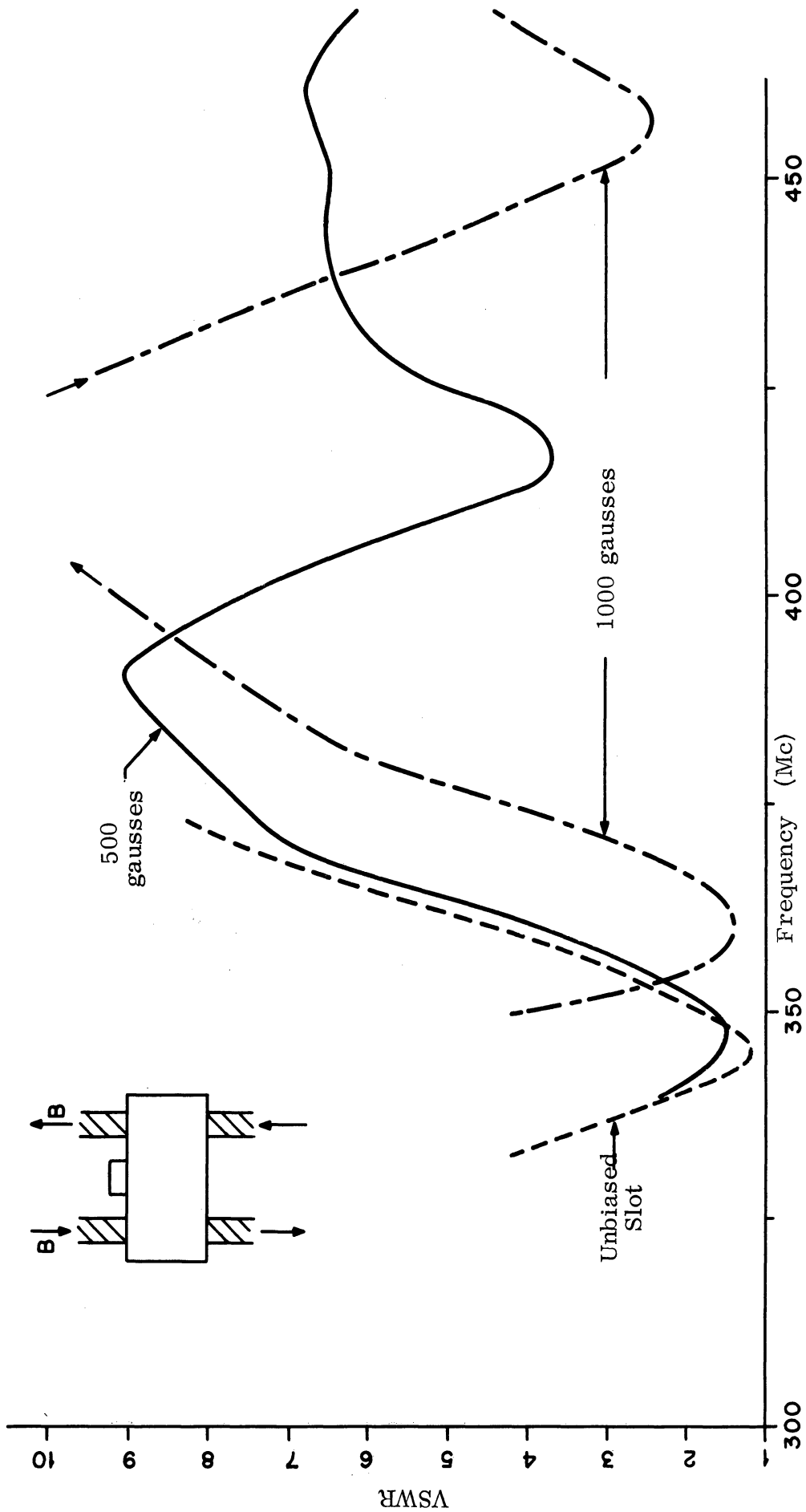
FIG. 32: VSWR VS FREQUENCY – ELECTROMAGNET TUNING
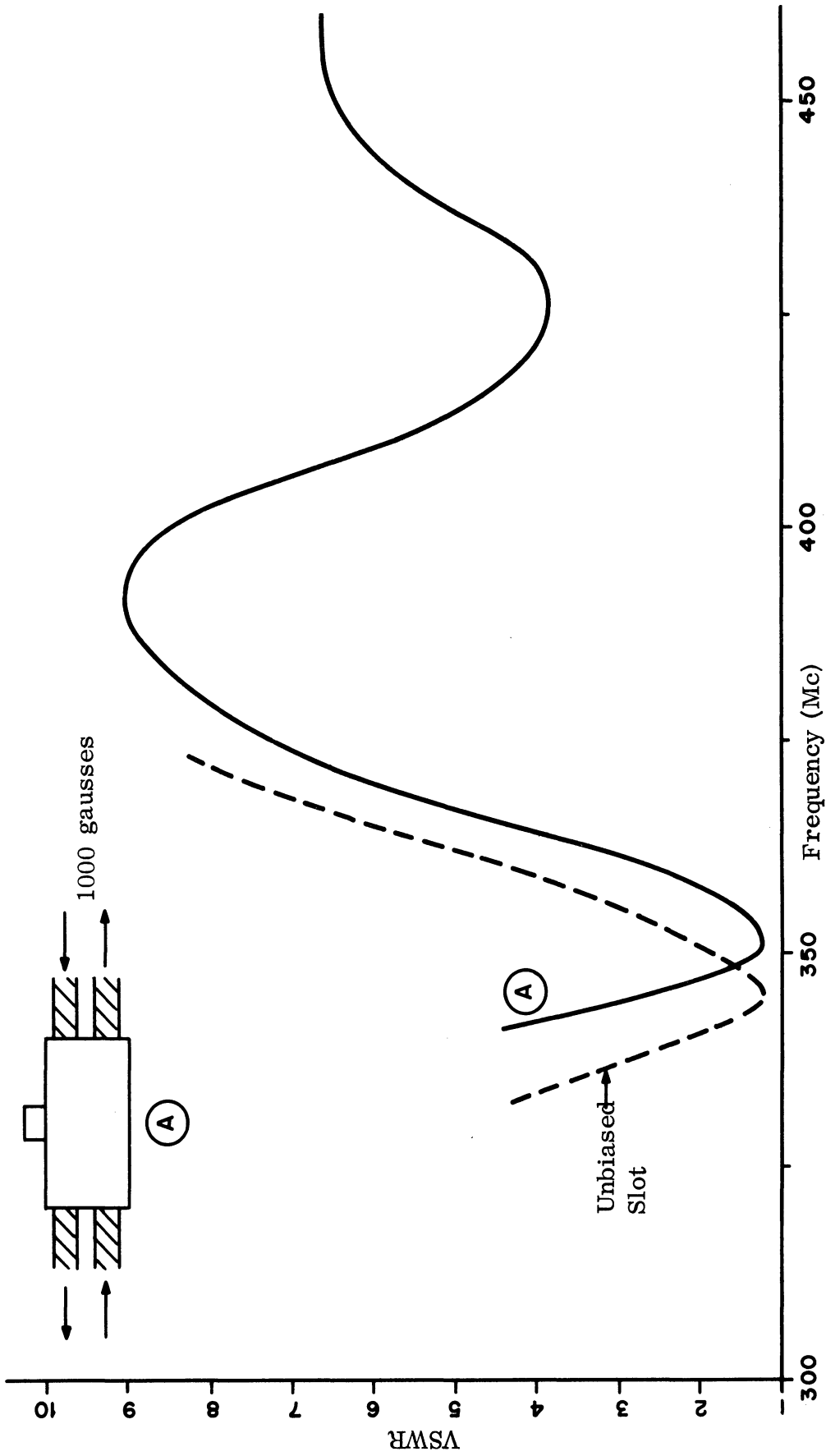
FIG. 33: VSWR VS FREQUENCY - ELECTROMAGNET TUNING

3.1.2 Antenna Patterns

It is important that the magnetic tuning should not impair the ferrite slot antenna patterns. Figure 34 shows a series of antenna patterns taken for the original permanent magnet tuning experiments shown in Fig. 26. It is seen that the backlobes are somewhat affected by magnetic tuning and that the essential dipole pattern of the ferrite slot is preserved. No pattern deterioration occurred for bias in any other direction, since only the TE_{10} mode can exist in the slot cavity. Changes in the lobe direction have been reported in the literature for situations where higher modes existed.

3.1.3 Efficiency

It is essential that the magnetic tuning of the ferrite slot antenna not reduce the efficiency of the slot antenna. Efficiency measurements have been made for both permanent and electromagnet biasing. The efficiency changed from the original unbiased 30 percent efficiency to a biased efficiency of 25 per cent for the permanent magnet on back and 22 per cent for the electromagnet aligned as in Fig. 29. Thus, it appears that the effect of magnetic tuning on the efficiency of the ferrite-filled slot antenna is not intolerable.

3.1.4 Theory

More extensive derivations of the effect of unidirectional magnetic bias on a ferrite rectangular slot antenna are planned in the future. However, it is felt that the results just presented may be explained. The ferrite is a highly anisotropic media, which means that if a unidirectional magnetic bias is in the direction of the short dimension of the aperture, the μ in the long direction of the antenna aperture will not be effected. Since the dominant mode in the cavity is with the H vector along the wide dimension of the aperture, it is to be expected that the only significant effect in μ in this wide direction will be when the magnetic bias is in the wide direction. In addition, the wide dimension of the aperture determines cut-off frequency and resonant cavity size. Therefore, when the bias is in this wide direction, the effective size of the cavity is altered; when it is not in this direction, the effective size of the cavity is essentially unaltered.
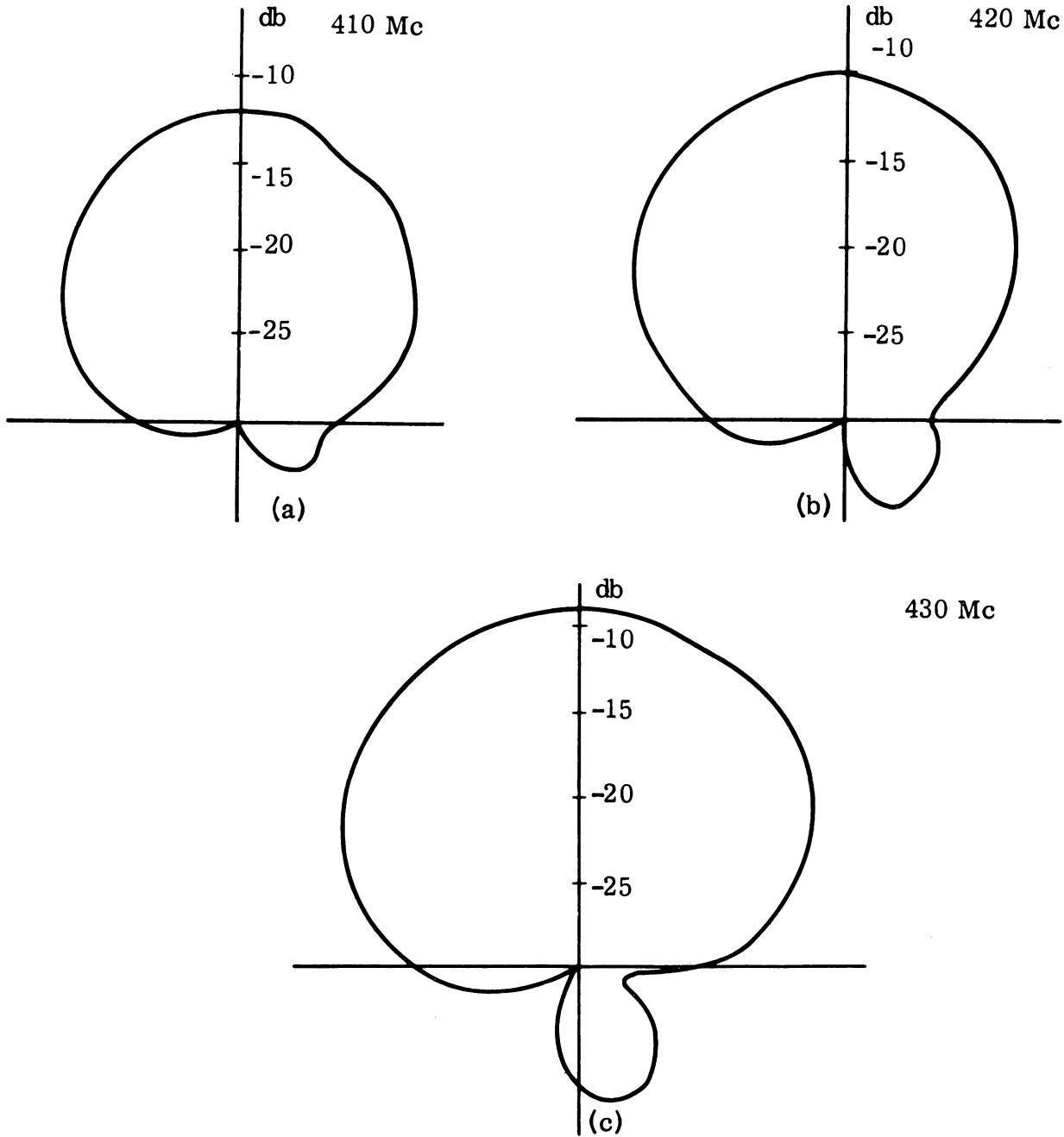
FIG. 34a-c: RADIATION PATTERNS (E_ϕ) FOR ANTENNA NO. 101 WITH MAGNET. RESONANT FREQUENCY = 420 MC
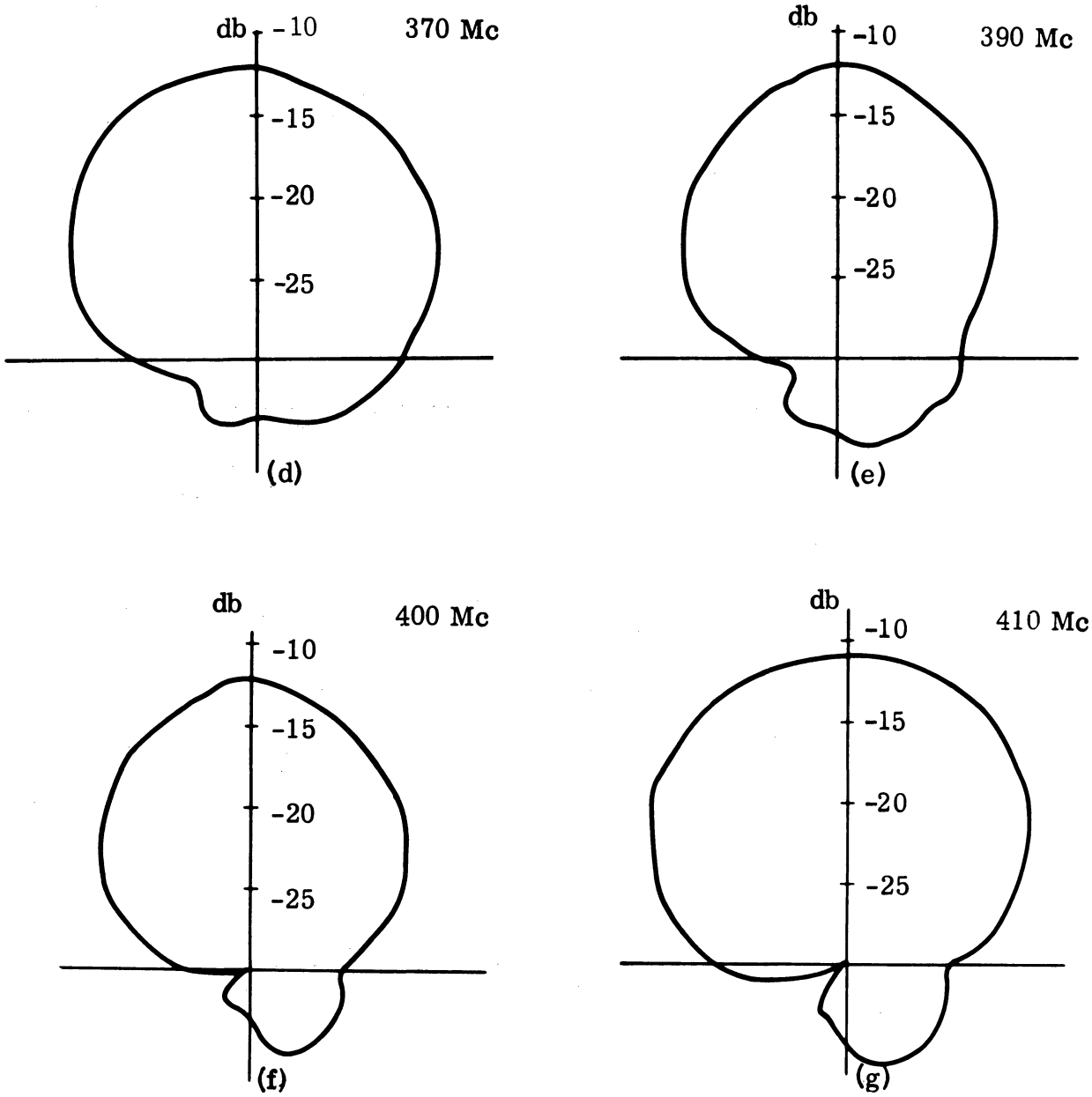
FIG. 34d-g: RADIATION PATTERNS (E_ϕ) FOR ANTENNA NO. 101 WITH MAGNET AND ALUMINUM PLATE. RESONANT FREQUENCY = 395 MC

db 340 Mc

- -10
- -15
- -20
- -25

(h)

db 350 Mc

- -10
- -15
- -20
- -25

(i)

db 360 Mc

- -10
- -15
- -20
- -25

(j)
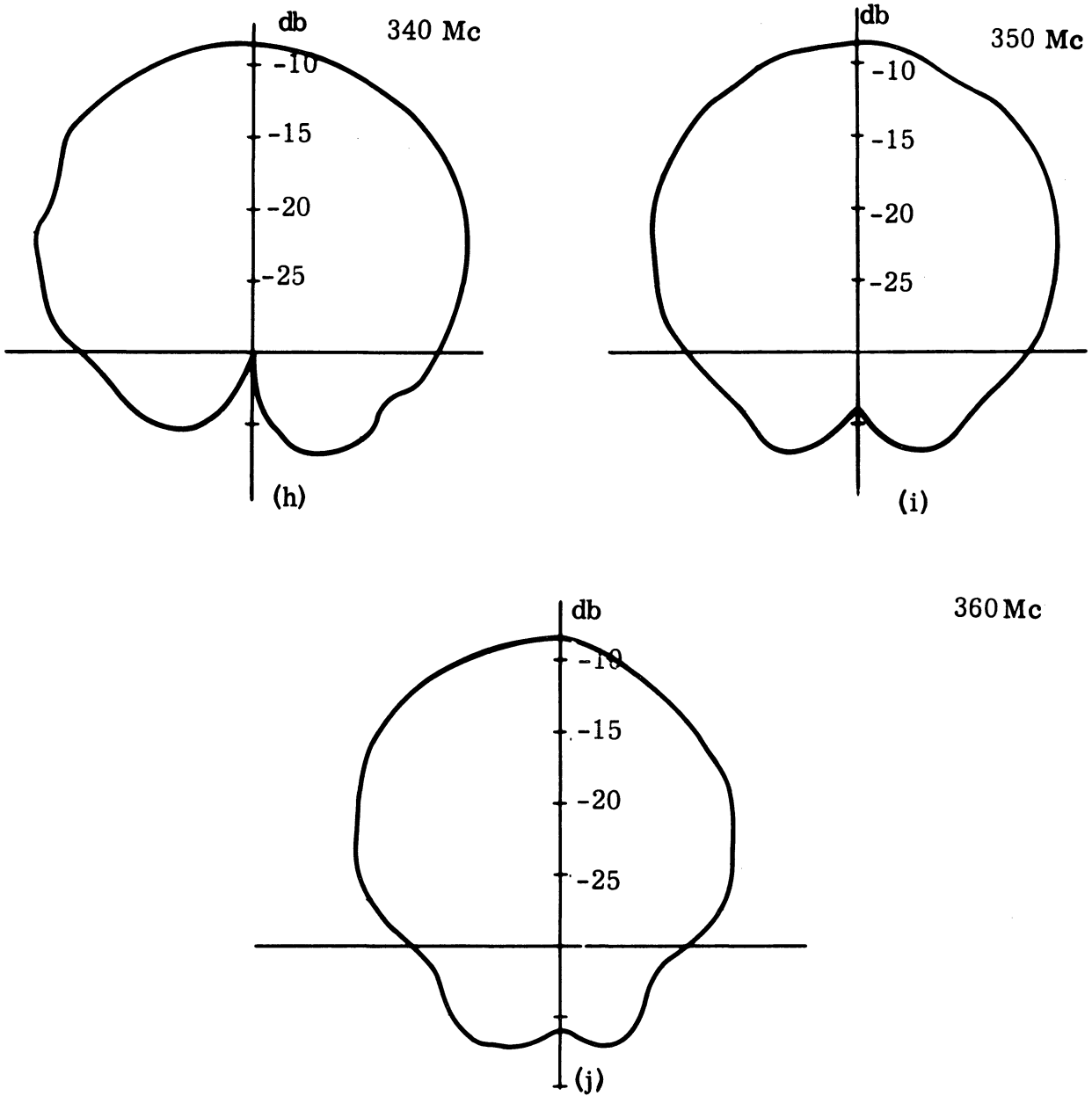
FIG. 34h-j: RADIATION PATTERNS (E_ϕ) FOR ANTENNA NO. 101 WITHOUT MAGNET. RESONANT FREQUENCY = 350 MC.

3.2 Changes in Slot Geometry

From observations on the ridged waveguide it may be anticipated that configurations other than the rectangular slot will give far greater bandwidth of operation. Some measurements of the ridged waveguide, ferrite-powder-filled slot antenna were taken two years ago on this project. Initial experiments were recently performed on the solid-ferrite-filled slot antenna with various segments of the ferrite replaced with low dielectric material (balsa wood) or with metal segments replacing the ferrite.

3.2.1 VSWR

Figure 35 shows the effect of replacing single cells of ferrite with balsa wood (essentially air). Curve A shows the original VSWR curve for a completely filled ferrite slot antenna. Curve B represents the effect of replacing a single outer cell with balsa wood. Curve C depicts the effect of replacing an interior cell with balsa wood. It is evident that an interior cell is more important than an exterior cell in shifting the resonant frequency. However, no significant change in bandwidth occurs. Figure 36 shows the effect of replacing horizontal rows of cells with combinations of solid metal and air. Unfortunately, this curve was not extended down to 300 Mc for comparison with the original resonant frequency minimum on the VSWR curve. In the frequency range 500 to 800 Mc the ferrite in the slot becomes quite lossy and low VSWR curves are probably caused by this loss rather than a well matched radiating antenna. The VSWR of the completely ferrite-filled slot antenna is shown for comparison and the low VSWR effect above 500 Mc is observed. Figure 37 shows the effect of replacing vertical columns of ferrite cells with balsa wood. In this curve, the crucial 300 to 500 Mc frequency range is covered. The most significant effect is seen in Curve B of Fig. 37, which shows a very large increase in bandwidth occurring when the outer vertical columns of cells are replaced with balsa wood and then blocked off at the aperture with a metal iris. Effects such as shown in Curve B will be much more thoroughly explored in future work.

A - All blocks ferrite.

B – Block 1, 6, 11, 16, 5, 10, 15 or 20
replaced with balsa, one at a time
replaced with balsa.

C – Block 7 or 9 replaced with balsa.
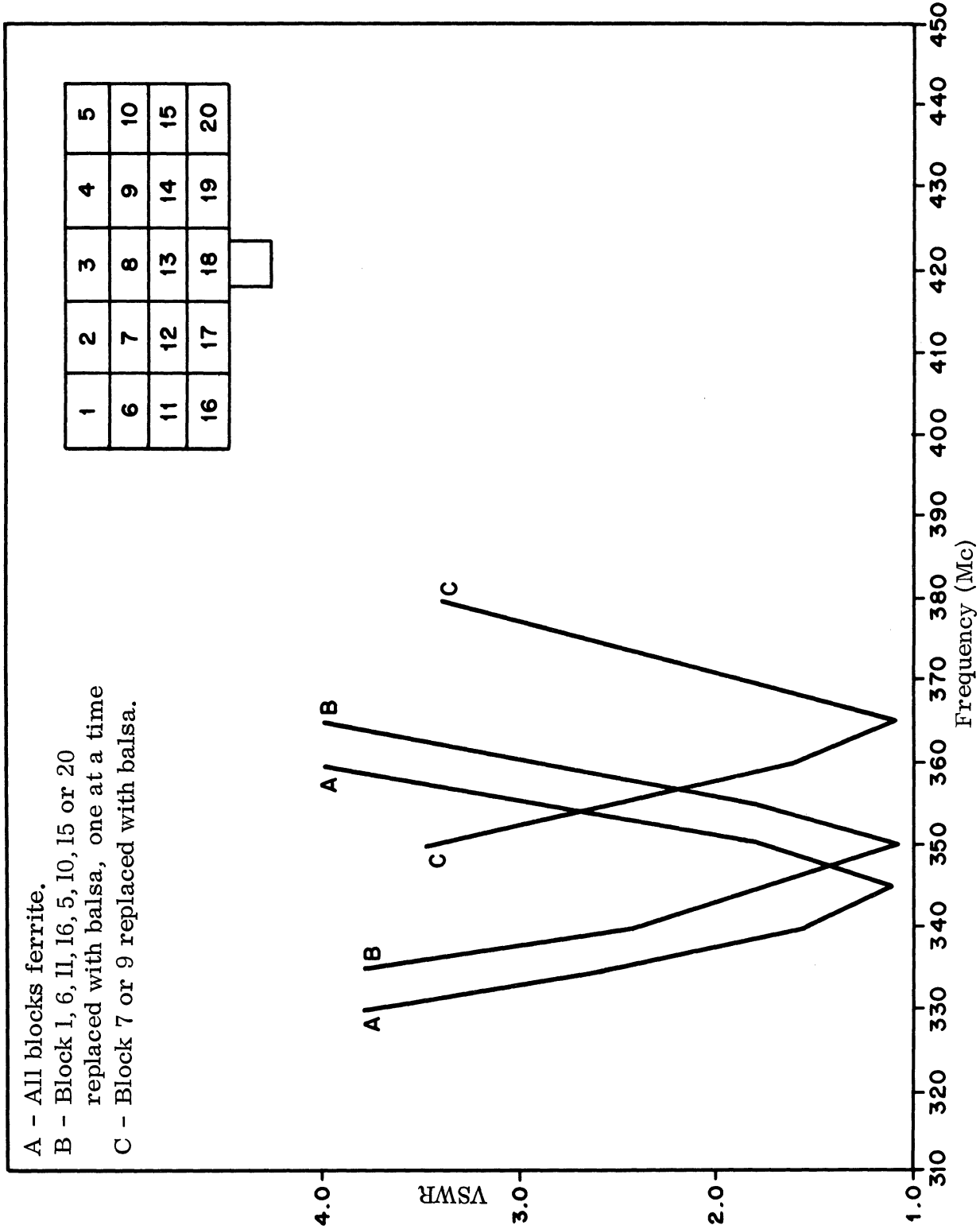
FIG. 35: EFFECT ON VSWR OF REPLACEMENT OF SINGLE CELLS OF FERRITE
IN A RECTANGULAR APERTURE.

Original all-ferrite slot antenna, for comparison

Blocks 1 - 5 replaced with solid metal and 6 - 10 replaced with balsa.

Blocks 6 - 10 replaced with balsa.

Blocks 1 - 10 replaced with balsa.
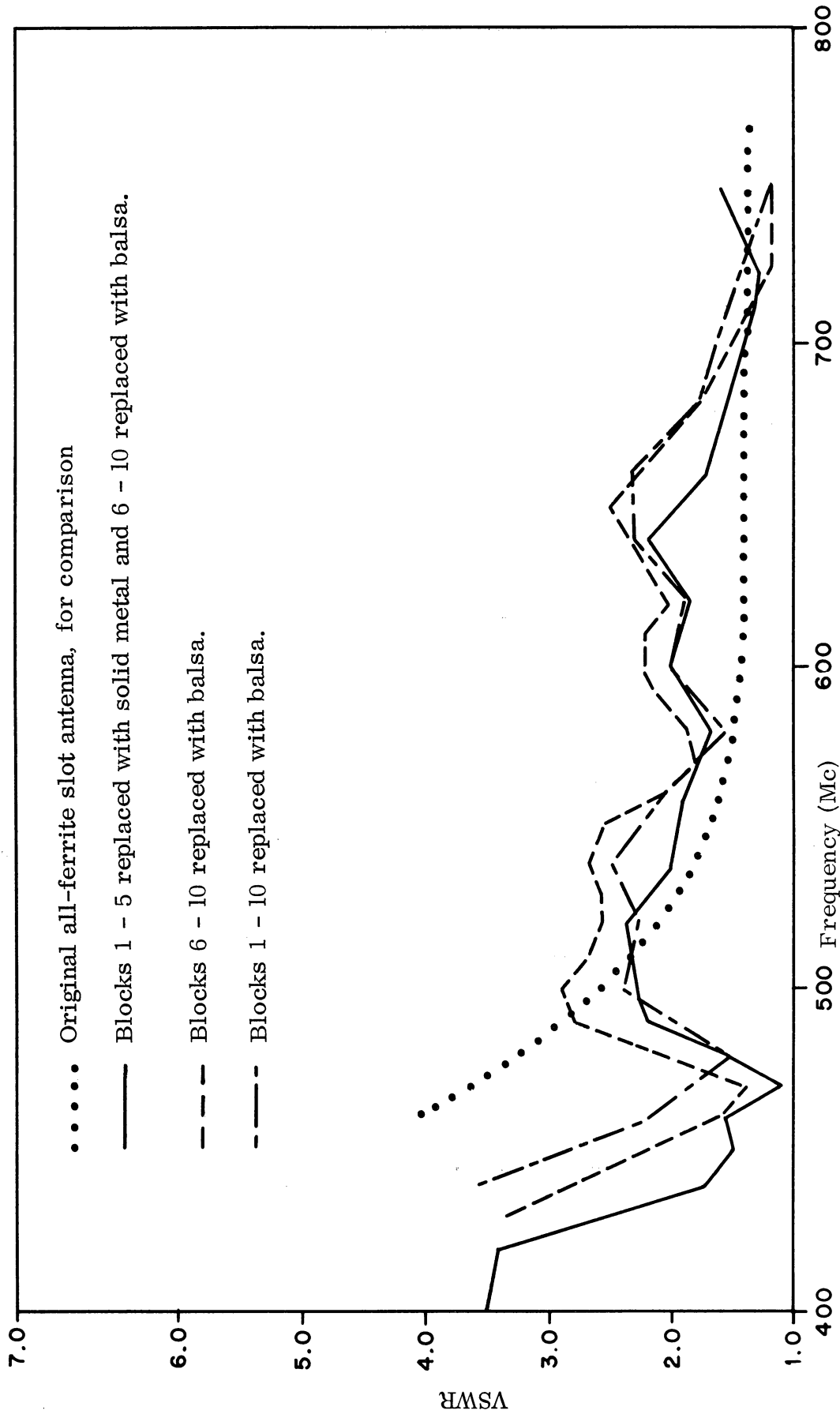
FIG. 36: EFFECT ON VSWR OF REPLACEMENT OF HORIZONTAL ROWS OF CELLS OF FERRITE IN A RECTANGULAR APERTURE.

A = Blocks 1, 6, 11, 16, 5, 10, 15 and 20 replaced with balsa.

B = Blocks 1, 6, 11, 16, 5, 10, 15 and 20 replaced with balsa – balsa section
of slot blocked off with metallic iris.

C = Blocks 16 and 20 replaced with balsa.

D = Original all-ferrite slot antenna.
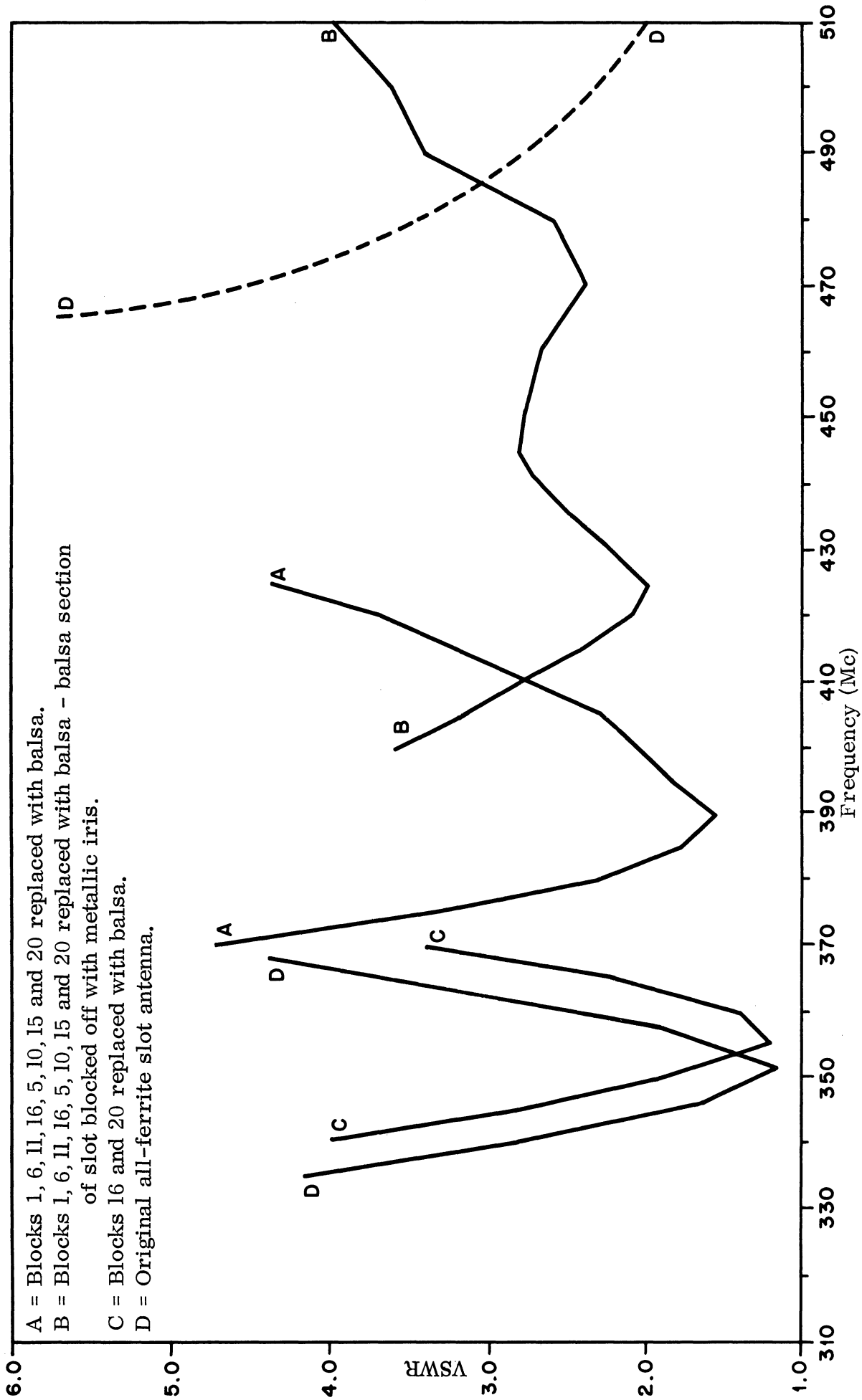
FIG. 37: EFFECT ON VSWR OF REPLACEMENT OF VERTICAL COLUMNS OF CELLS OF FERRITE
IN A RECTANGULAR APERTURE

71

3.2.2 Other Characteristics

The other antenna characteristics have not been well investigated as yet. Several antenna patterns taken for the case of balsa wood replacement of ferrite showed that no large change in the dipole-like pattern of the antenna occurred. No measurements on efficiency were taken.

3.3 Temperature Effects on Efficiency

In Section IV the effect of temperature on ferrite characteristics will be discussed, and it is apparent that high temperatures lead to greatly increased losses in ferrite materials. In this section, a theoretical study of the effect of a change in material Q on the efficiency of the slot antenna is reported. Figure 38 shows a plot of the magnetic Q of the material vs temperature for the ferrite presently being used to load antennas. These curves come from dividing the experimentally determined loss permeability μ'' into the permeability μ'. It will be shown that the parameter magnetic Q is the most important parameter in determining slot antenna efficiency. It can be seen from Fig. 38 that magnetic Q deteriorates very rapidly above $100^\circ C$. The effect on efficiency of the slot antenna is shown in Fig. 39 for a ferrite powder filled cavity. It is seen that for temperatures above $100^\circ C$, the efficiency deteriorates quite rapidly at most frequencies, although for 300 Mc, good efficiency is maintained up to $150^\circ C$. These curves are theoretically calculated values and were obtained as follows.

The loaded ferrite cavity antenna has been fully investigated theoretically (Adams, 1964). Formulas from this reference give efficiency as

$$\eta = \frac{1}{1 + P_L/P_r} \tag{17}$$

where

$$\frac{\bar{P}_L}{\bar{P}_r} = \frac{\mu''}{\mu'} \frac{\left[k^2 a^2 (\frac{2d}{a}) + \frac{\sin 2\beta_{10} d}{\sqrt{k^2 a^2 - \pi^2}} (k^2 a^2 - 2\pi^2) \right]}{(1 - R^2) \sqrt{k^2 a^2 - \pi^2}} \tag{18}$$
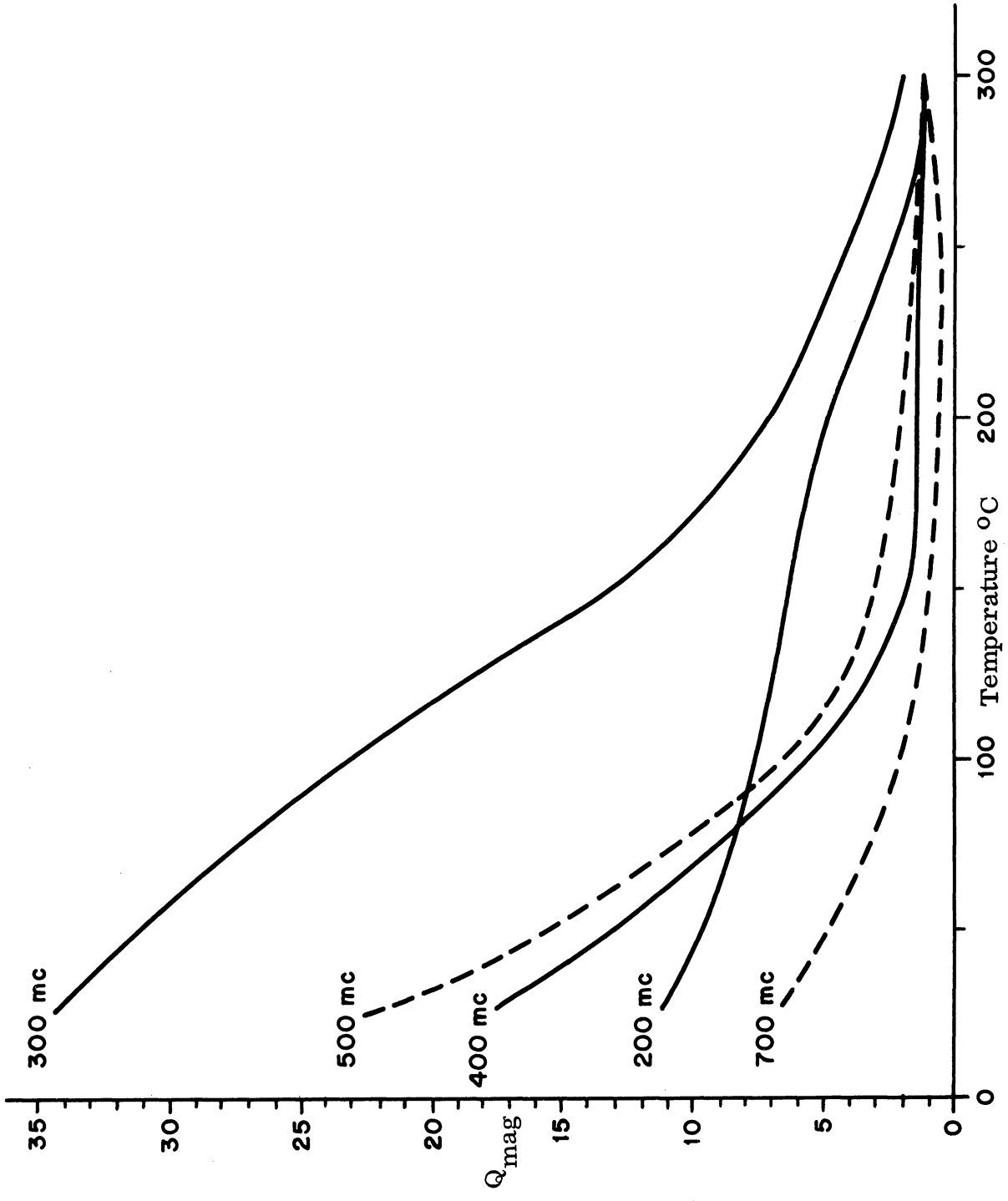
FIG. 38: Q_{mag} VS TEMPERATURE FOR CO_2Z
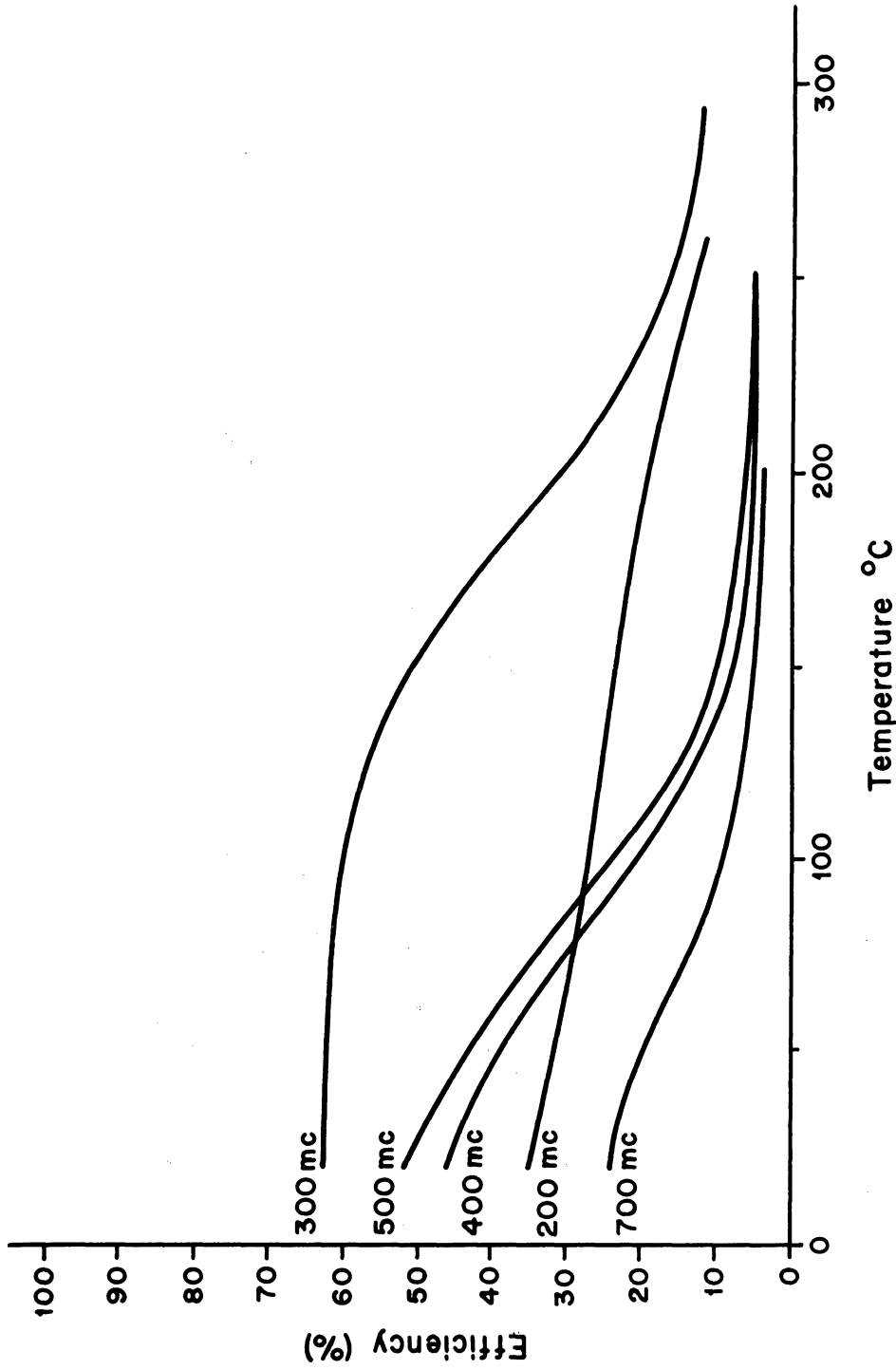
FIG. 39: EFFICIENCY VS TEMPERATURE FERRITE-POWDER-FILLED CAVITY ANTENNAS. $ka/\pi = 1.8$.

and

P_L, P_r are power lost and radiated, respectively

μ', μ'' are components of permeability

$k = \omega\sqrt{\mu\epsilon}$ in the cavity

d, a   are the depth and long aperture dimension of the cavity, respectively

β_{10} is the phase propagation constant in the cavity

R   is the absolute value of the voltage reflection coefficient of the aperature for the incident dominant waveguide mode.

The following assumptions were made in this formula:

a) The perturbation approach was used in calculating losses, thus limiting accuracy at low efficiencies.

b) The cavity was assumed resonant.

c) Wall losses and dielectric losses were assumed negligible.

d) The entire cavity was considered as one region for the boundary value problem.

e) The ferrite was homogeneous and isotropic.

More complex formulas without these assumptions were also derived in Adams (1964).

Equation (18) may be simplified to

$$\frac{P_L}{P_r} \approx \frac{2kd}{Q(1-R^2)\sqrt{1 - \dfrac{\pi^2}{k^2 a^2}}}, \qquad (19)$$

where $Q = \mu'/\mu''$.

The second numerator term of (18) is small except very near cutoff, and has been neglected. Since in the region far from cutoff, R and k are not too

$$\eta \cong \frac{1}{1+K/Q} \, , \text{ where } K = \frac{2kd}{(1-R^2)\sqrt{1- \dfrac{\pi^2}{k^2 a^2}}} \tag{20}$$

K is almost constant and room temperature values are used in the computations.

Equation (20) is useful to obtain first-order loss effects on a slot antenna. Nevertheless, since μ' changes considerably with temperature (19) should be used in any exact computations. Note that while (19) appears simple, the variable R is available only be extrapolating graphs in Adams (1964) and the numerator, kd, must be computed from R in order to give caivty resonance. This calculation is tedious. Note also that for a given cavity antenna in resonance at room temperature, a rise in temperature detunes the cavity, thus violating assumption (b). In the computations, a termperature compensating tuner was assumed. Figure 38 shows the plots of Q for various solid ferrites vs temperature. Figure 39 indicates the effect of this Q on powdered ferrite slot antennas using the crude approximation (20). Note that, in the case of the powdered ferrites, it has to be assumed that Q was the same as for solid ferrites at a given temperature. This was found approximately true at room temperature. In addition, if equation (19) were used, scaling of μ' and μ'' would have to be assumed. Figure 40 shows a comparison between calculations using (19)[+] and its approximation (20).

The efficiencies of the example slot antennas are very low for $T > 200^\circ$ C. Actually, to find the optimum size and balance between ϵ', ϵ'', μ' and μ'' a computer study should be made; this is tentatively planned. A new method of calculating the reflection coefficient R other than the numerical integration given by Adams (1964) appears to make such an optimization feasible.

The μ' and μ'' measurements appear to be consistent and correct. The same instrumentation was used for 200, 300 and 400 Mc; however, no explanation is yet offered as to why the efficiency drops at 200 Mc.

[+] The result of (18) is then substituted in (17), of course.
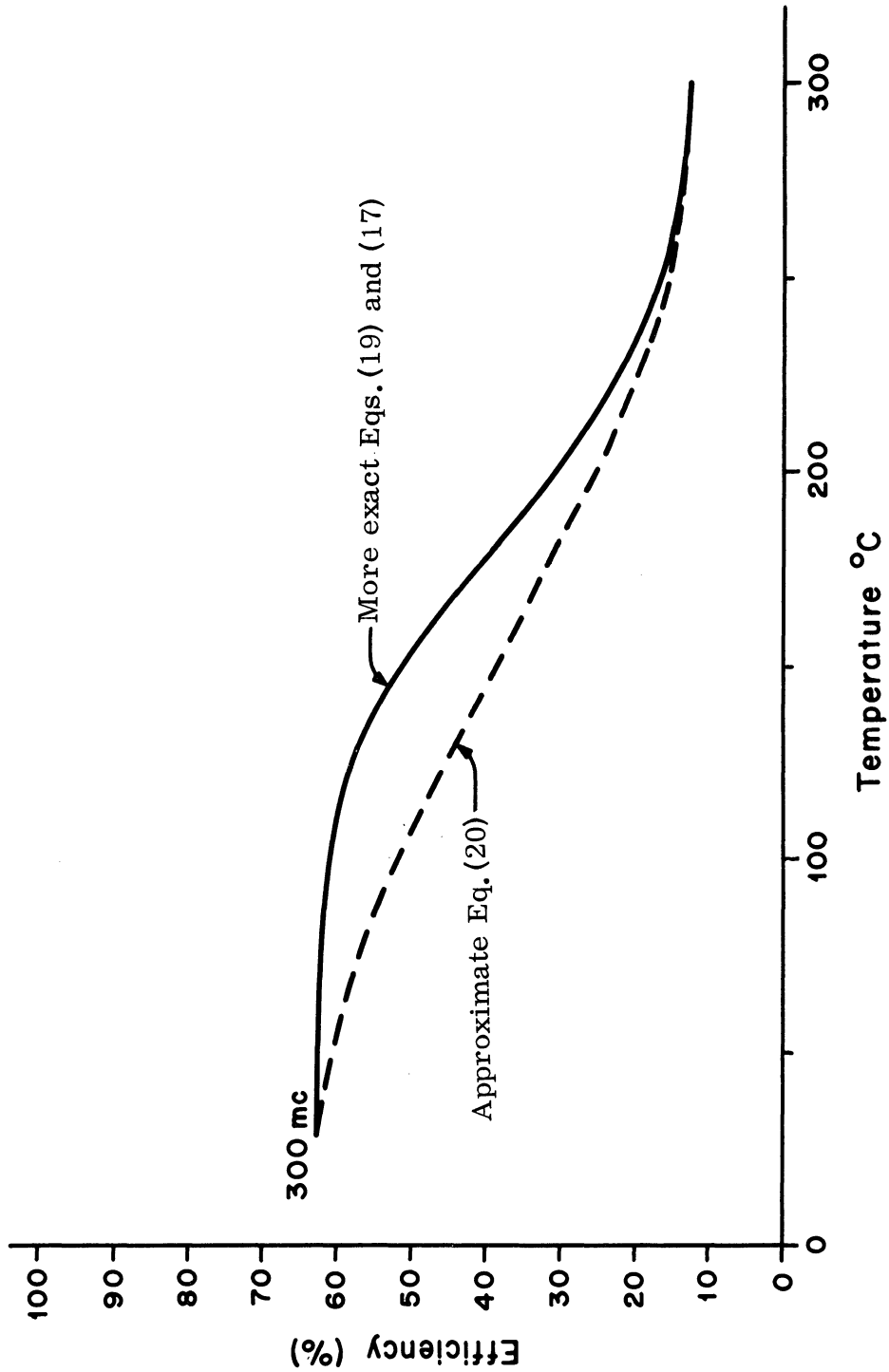
FIG. 40: EFFICIENCY VS TEMPERATURE. RESONANT SLOT FERRITE POWDER FILLED ANTENNA. $b/a = .255$. $ka/\pi = 1.805$ at $27^\circ C$.

IV
FERRITE MATERIALS

4.1 Temperature Dependence of Magnetic Properties of Ferrite

The ferrite antenna characteristics described throughout the report have been obtained at very low power levels and at room temperature. In anticipation of the use of ferrite antennas at high power levels and possibly high ambient temperatures, studies have been made on the magnetic properties of the ferrite at various temperatures and frequencies. The type "A" ferrite used is that previously described in other reports by the following formula:

$$Ni_{.9696}Zn_{.0404}Co_{.03}Fe_{1.84}Al_{.04}O_4.$$
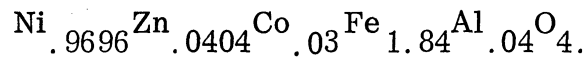
Figure 41 shows the apparatus used for permeability measurements at elevated temperatures. This equipment provides the means of heating a sample to a specified temperature. The sample is in the form of a toroid which fills a small coaxial cavity. Measurements are taken on the two components of permeability μ', the real component of relative permeability, and μ'' the loss component of relative permeability, using the techniques of Rado (1953) and Lax (1962).

Figure 42 shows a plot of μ' and μ'' vs temperature. From these measurements of characteristics it is apparent that the temperature may impose a severe restriction on the use of ferrite antennas. The heating of aerospace vehicles upon re-entry is an example where a severe temperature may limit the use of a ferrite antenna unless special provisions are made to shield the ferrite material. However, in initial tests with moderate (10 watts) transmission power th the antenna , no significant change in slot temperature was noted; thus, internal heating may not be a problem.
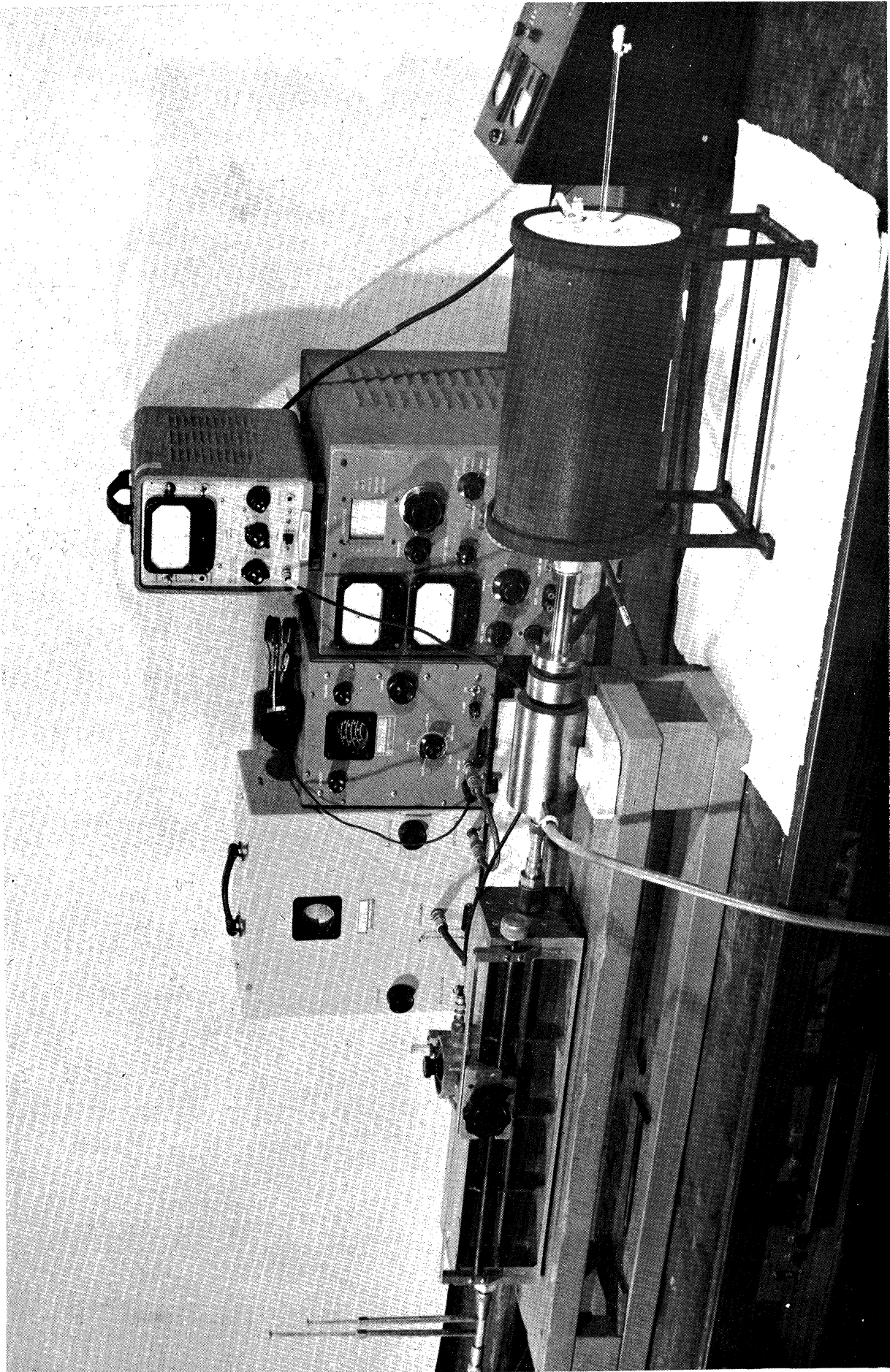
FIG. 41: PERMEABILITY VS TEMPERATURE MEASURING EQUIPMENT
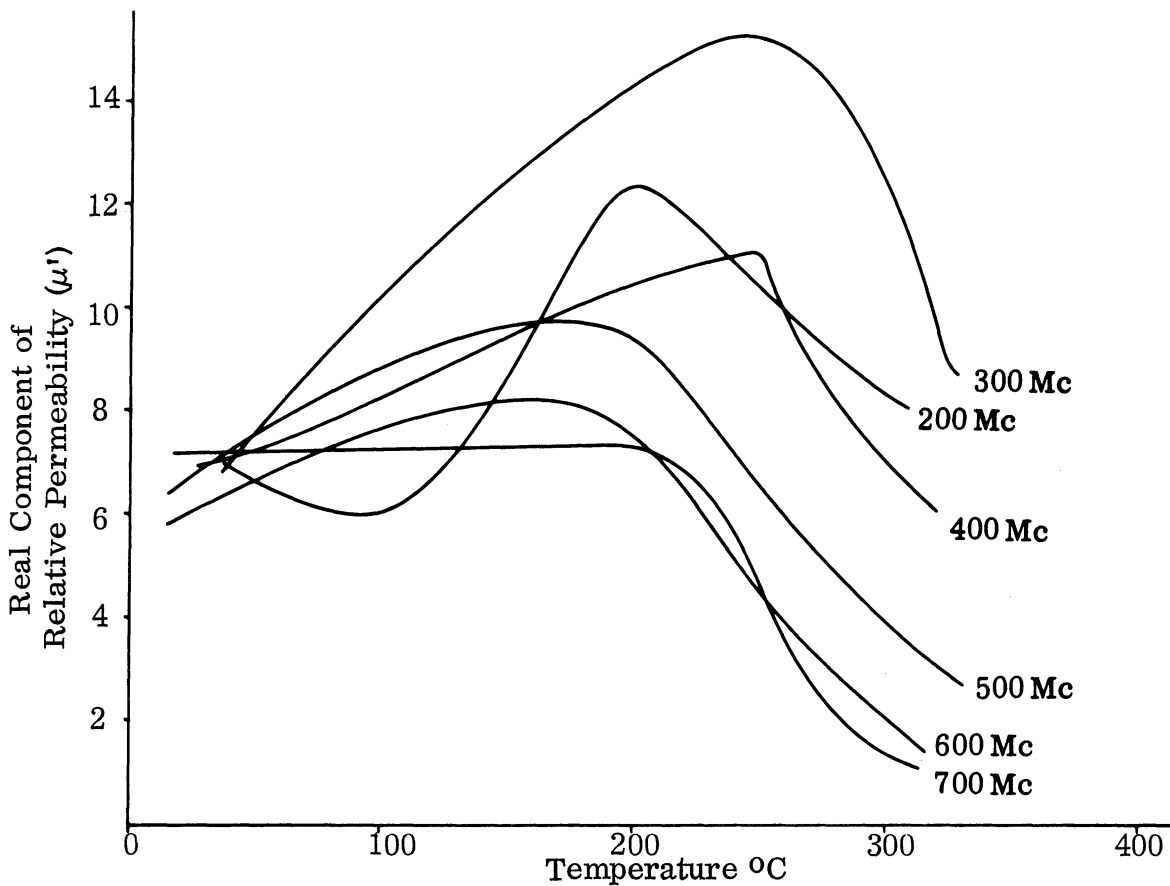
FIG. 42a: RELATIVE PERMEABILITY (μ') VS TEMPERATURE FOR $CO_2 Z$.
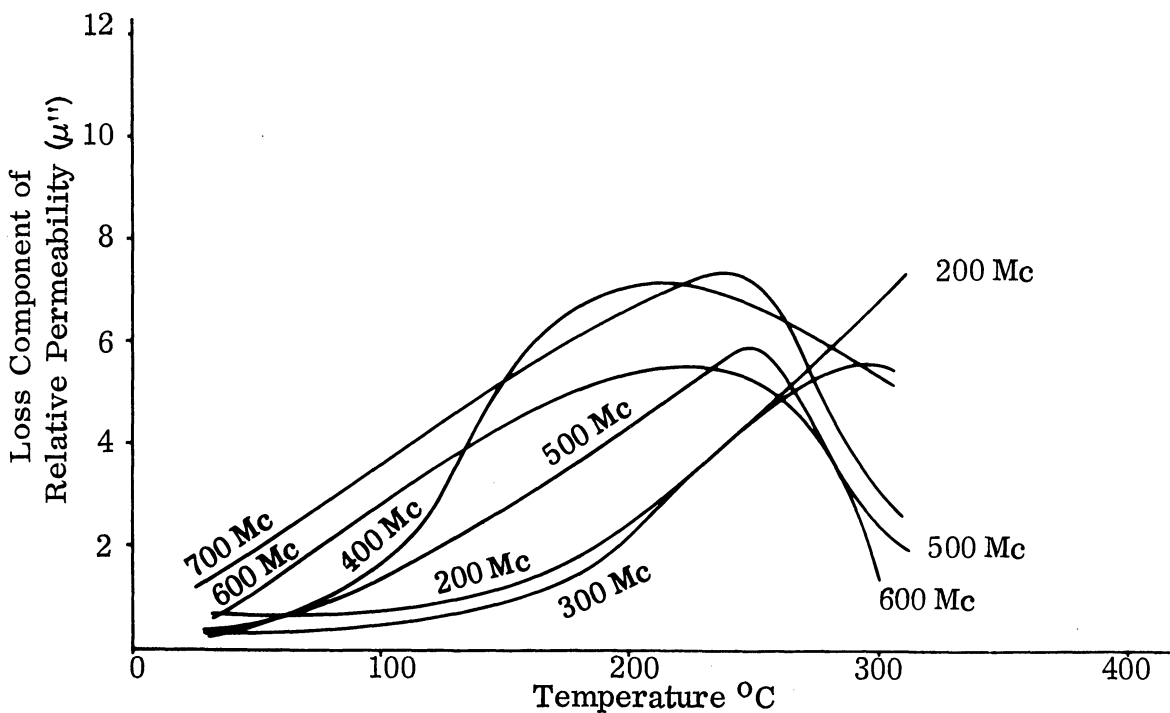
FIG. 42b: RELATIVE PERMEABILITY (μ'') VS TEMPERATURE FOR $CO_2 Z$.

4.2. Basic Limitations and Future Potential of Ferrites

4.2.1 Introductory Comments

A magnetic dipole of moment $\underline{m}$, in the presence of an external magnetic field, $\underline{H}$, is subject to a torque $\underline{T}$:

$$\underline{T} = \mu_o \underline{m} \times \underline{H} \ . \tag{21}$$

The torque equals the time rate of change of angular momentum L, or:

$$\underline{T} = \frac{d\underline{L}}{dt} \ ,$$

(true either for a whole or unit volume) and

$$\frac{M}{L} = \frac{ge}{2m} \ , \tag{22}$$

where $\underline{M}$ is the magnetic moment per unit volume,

   g is the spectroscopic splitting factor

   m is the mass of an electron (scalar)

   e is the change on an electron.

Putting these three equations together and using $\gamma = \mu_o ge/2m$, the gyromagnetic ratio, the result is

$$\frac{dm}{dt} = \gamma \underline{m} \times \underline{H} \ . \tag{23}$$

In a magnetic material with magnetization $\underline{M}$, not only the effective value of $\underline{H}$ inside the material must be considered but also the torques produced through interactions between the separate dipoles. The interaction can be phenomenologically substantiated through the expedient of a power series expansion for the magnetization in terms of the applied field, i.e.

$$\frac{\partial \underline{M}}{\partial t} = \gamma \underline{M} \times \underline{H}_t - \frac{\lambda}{M} \underline{M} \times (\underline{M} \times \underline{H}_t) \tag{24}$$

where H_t is the sum of applied $\underline{H}_o$ and internal fields, $\underline{H}_i$ and λ is the loss constant. The magnetic energy in the absence of an external field, must be produced by and have the symmetry of the magnetic material. This can be introduced by expanding the magnetic energy density for a single crystal in a power series expansion as:

$$U_i = U_0 + (K_b^1 \alpha_1^2 + K_b^2 \alpha_2^2 + K_b^3 \alpha_3^2) + (K_e^1 \alpha_1^4 + K_c^2 \alpha_2^4 + K_c^3 \alpha_3^4) + 0(\alpha^6) \tag{25}$$

where the K's are constants of the material at a given temperature and the α's are direction cosines. Those materials with a large value of U_o, the exchange energy density, are ferrimagnetic. Of interest are hexagonal and cubic structures, and only the lowest trivial value of K will be considered. For hexagonal material it follows that $K_b^2 = K_b^3$ and

$$U_i = U_o^1 + K_1 \sin^2 \theta \tag{26}$$

while for cubic material,

$$U_i = U_o^1 + K_1 (\alpha_1^4 + \alpha_2^4 + \alpha_3^4), \tag{27}$$

remembering that $\alpha_1^2 + \alpha_2^2 + \alpha_3^2 = 1$. The four cases of interest are: cubic and hexagonal each with $K_1 < 0$ or $K_1 > 0$. Table II lists the anisotropy category of many room temperature ferromagnets.

Referring back to Eq. (25), the exchange energy density U_o produces an effective torque which aligns the magnetic moments of each atom to be nearly parallel. The subsequent terms produce torques which are dependent upon crystalographic direction. These torques are describable as effective magnetic fields H_{an}, and result in the magnetization being oriented along certain preferred or "easy" directions in the crystal. The effective magnetic fields produced are given in Table III. Turning to a nonoriented polycrystalline sample, the maximum value of magnetization possible for the different symmetries is also listed.

TABLE II: CONPOSITIONS BY ROOM TEMPERATURE ANISOTROPY

Cubic, $K_1 < 0$	Cubic, $K_1 > 0$
$NiFe_2O_4$	$CoFe_2O_4$
$MnFe_2O_4$	Fe (metallic)
Fe_3O_4	
Ni (metallic)	
$MgFe_2O_4$	Very small anisotropy $\rightarrow Y_3Fe_5O_{12}$
$Li_{1/2}Fe_{2\ 1/2}O_4$	

Hexagonal, $K_1 < 0$	Hexagonal, $K_1 > 0$
$Ba_2Mg_2Fe_{12}O_{22}$ (Mg_2Y)	$BaFe_{12}O_{19}$
$Ba_2Ni_2Fe_{12}O_{22}$	Co (metallic)
$Ba_2Zn_2Fe_{12}O22$	$BaFe_{18}O_{27}$
$Ba_2Co_2Fe_{12}O_{22}$ (Co_2Y)	$BaNi_2Fe_{16}O_{27}$
$Ba_3Co_2Fe_{24}O_{41}$ (Co_2Z)	

TABLE III:

Mg is the spontaneous magnetization in each single crystal. M max is the maximum magnetization for a non-oriented polycrystalline material.

	Cubic		Hexagonal	
	$K_1 > 0$	$K_1 < 0$	$K_1 > 0$	$K_1 < 0$
H_{an}	$2K_1/\mu_o M_s$	$-4K_1/3\mu_o M_s$	$2K_1/\mu_o M_s$	$2K_2/\mu_o M_s$
$\dfrac{M_{max}}{M_s}$	0.831	0.866	0.500	0.785

The Curie temperature is that temperature at which the thermal energy density is essentially equal to U_o. Above that temperature thermal disorder predominates and there is only a magnetic moment in the presence of an applied field. Magnetic material is useless, as such, more than a few degrees above that temperature. The Curie temperature of many substances is listed in Table IV.

4.2.2 Permeability Spectrum

The frequency dependence of the permeability is determined from equation (24). It is necessary in all cases to account not only for the fields listed in Section I, but also fields due to discontinuities in magnetizations both at the surface of the magnet and internally to it. These discontinuties produce fields which at times completely cancel the driving field and at other times become essentially infinite. These effects produce a shift in the effective resonant frequency of the sample. To avoid such complexities the discussion here will apply to an infinite sheet of material magnetized perpendicular to the plane. Under these circumstances the field is

$$\underline{H} = \underline{H}_o e^{j\omega t} + \underline{H}_{an} \tag{28}$$

which must be substituted into (24). It is assumed that

$$\left| H_{an} \right| \gg \left| H_o \right| \quad \text{and} \quad \left| M_s \right| \gg \left| H_o \right| .$$

The results, for cubic symmetry, or for hexagonal symmetry with $K_2 > 0$, are;

$$\chi = \chi' - j\chi'' = \frac{dM}{dH} = \frac{\omega_M}{D} \left\{ \omega_o(\omega_o^2 - \omega^2) + \omega^2 \omega_o \lambda^2 - j\lambda\omega \left[\omega_o^2 + \omega^2(1+\lambda^2) \right] \right\} .$$

$$D = \left[\omega_o^2 - \omega^2(1+\lambda) \right]^2 + 4\omega^2 \omega_o^2 \lambda^2 , \tag{29}$$

where $\omega_M = \gamma M_s$ and $\omega_o = \gamma H_{an}$. Equation (29) for low loss material (i.e., $\lambda \ll 1$) becomes:

TABLE IV: CURIE TEMPERATURES $^\circ C$

Material	T_c
Fe	770
Co	1131
Ni	358
+$NiFe_2O_4$	585
+$MnFe_2O_4$	300
+Fe_3O_4	585
+$MgFe_2O_4$	440
+$Li_{.5}Fe_{2.5}O_4$	670
+$CoFe_2O_4$	520
$BaFe_{12}O_{19}$	450
$BaFe_{18}O_{27}$	455
$BaNi_2Fe_{16}O_{27}$	>520
++$Ba_2Mg_2Fe_{12}O_{22}$	280
$Ba_2Ni_2Fe_{12}O_{22}$	390
$Ba_2Zn_2Fe_{12}O_{22}$	130
$Ba_2Co_2Fe_{12}O_{22}$	340
+++$Ba_3Co_2Fe_{24}O_{41}$	410*
$Y_3Fe_5O_{12}$	287

+The Curie temperature can be decreased from this value towards absolute zero by partially replacing the divalent cation with Zn or Cd.

*Undergoes an anisotropy change at about $280^\circ C$.

++A sample of composition Me_2Y where Me = Mg.

+++A sample of composition Me_2Z where Me = Co.

$$\chi' \approx \frac{\omega_M \omega_0 (\omega_0^2 - \omega^2)}{(\omega_0^2 - \omega^2)^2 + 2\lambda\omega^2(\omega_0^2 + \omega^2)}$$

$$\chi' \approx \frac{\lambda\omega_M \omega_0 (\omega_0^2 + \omega^2)}{(\omega_0^2 - \omega^2)^2 + 2\lambda\omega^2(\omega_0^2 + \omega^2)} \ . \tag{30}$$

The real part of the susceptibility resonates at $\omega = \omega$, i.e. the frequency corresponding to the anisotropic field. In the limit of low frequency, the susceptibility is:

$$\chi_0 \approx \frac{\omega_M}{\omega_0} = \frac{M_s}{H_{an}} \ , \tag{31}$$

or

$$\chi_0 \omega_r = \omega_M \tag{32}$$

where ω_r is the resonance frequency. Equation (32) contains a basic limitation upon the use of nonsaturated ferrites. The product of the magnitude of the low frequency susceptibility and the resonant frequency is parabolic. The factor ω_M varies only slightly from material to material while ω_0 varies widely from about 0.1 to 20,000 Mc. From (30) it is evident that χ'' will be substantially small only if $\omega < \omega_0$, so if the usable frequency range is to be increased ω_0 must be increased but this can only be done by decreasing χ' !

A very large value of ω_M is $2\pi \times 8400$ Mc, so an initial susceptibility of 10 can, at best, have a resonant frequency of 840 Mc, and a usable frequency range to about 300 Mc.

The situation is altered for hexagonal structures with $K_1 < 0$. The real part of the susceptibility turns out to be, at very low frequencies.

$$\chi_o \approx \frac{2\omega_1^1}{3\omega_o^1} \,, \tag{33}$$

an equation similar to (32) except that in this case ω_o^1 is the resonant frequency within the Basal plane and is independent of the value of K_1 of equation (26). On the other hand, the resonant frequency is:

$$\omega_r \approx \sqrt{(\omega_2 - \omega_o^1)\omega_o^1} \approx \sqrt{\omega_2 \omega_o^1} \tag{34}$$

where ω_2 is proportional to the anisotropy constant K_1 and :

$$\chi_o \omega_o^2 = \frac{2\omega_1 \omega_2}{3} \tag{35}$$

determines the limiting values of χ_o for a fixed value of ω_r.

A good material exhibiting these anisotropy characteristics is Co_2Z (see Tables II and IV). Using Co_2Z, an initial permeability of about 50 and a resonant frequency of 800 Mc results at room temperature.

4.2.3 Permittivity Spectrum

The polarizability of all electron clouds within the material gives rise to a relative permittivity of about 10 to 15 for ferrites. This value is essentially constant and extends at least down through the millimeter wavelengths. The loss associated with this permittivity is, in general, very low.

In addition, the multivalent atoms can produce a finite conductivity (and thus imaginary permittivity) through the relation:

$$\epsilon = \epsilon' - j\frac{\sigma}{\omega} \,. \tag{36}$$

This is particularly relevant for the cases where either Fe^{+2} and Fe^{+3} or Mn^{+2} and Mn^{+3} are present in the same sample. A slight excess of iron in a sample will produce an increase of up to 8 orders of magnitude in conductivity. It follows that the d-c conductivity is a strong function of the oxygen pressure present during the firing of the sample.

sample will produce an increase of up to 8 orders of magnitude in conductivity. It follows that the d-c conductivity is a strong function of the oxygen pressure present during the firing of the sample.

Another source of permittivity separate from a d-c conductivity is due to a difference in conductivity between the interior of a single grain of material and the surface layer. In many cases an insulating surface layer separates conducting grains. This produces a permittivity with a relaxation frequency equal to the mean transport time of the conducting charge across a grain. A typical relaxation frequency is from 100 Kc to 1 Mc. Below the relaxation frequency, permittivities on the order of 10^5 exist. Above 10 Mc the permittivity is between 10 and 20. These effects are particularly evident in the $MnFe_2O_4$ compounds, but exist in all ferrites.

4.2.4 Complex Susceptibilities

It is clear from the form of equation (30) that the real and imaginary parts of the susceptibility are related. Although the equation describing the dielectric susceptibility differs slightly from that for the magnetic susceptibility, the real and imaginary parts are also related. It is also clear that

$$U = \frac{1}{2} (\mu' - j\mu'') H^2 + \frac{1}{2} (\epsilon' - j\epsilon'') E^2 \tag{37}$$

where U is the energy density in the system. The real part of (37) is the energy density stored in the system while the imaginary part is the energy lost. The functional relationship between real and imaginary parts has the result that one cannot arbitrarily increase the real part without an increase in the imaginary part. For a single oscillating system the relationship is:

$$\chi'(\omega) = \frac{2}{\pi} \int_0^\infty \frac{\omega \chi''(\omega_1)\, d\omega_1}{\omega_1^2 - \omega^2}$$

(38)

$$\chi''(\omega) = -\frac{2}{\pi} \int_0^\infty \frac{\omega \chi'(\omega_1)}{\omega_1^2 - \omega^2}\, d\omega_1$$

From the first of equations (38) putting $\chi''(\omega_1) = \delta(\omega_0 - \omega_1)$ where the δ represents the Dirac delta function, then $\chi''(\omega)$ becomes:

$$\chi'(\omega) \approx \frac{2}{\pi} \frac{\omega_0}{\omega_0^2 - \omega^2} \qquad \text{(compare with (30) for } \lambda = 0 \text{).} \qquad (39)$$

Equations (38) are for single oscillators only. They must be applied with caution to a solid where the separate oscillators are dependent and the resonant frequencies are not uniquely determined but averaged over the sample. Nonetheless, the relations (38) above, the Kramers-Kronig relations, are useful even when used for the average values.

The result is that loss must always exist. Its magnitude is proportional to λ and the form of the spectrum can be controlled but the loss can never be eliminated without, at the same time, eliminating the real part as well.

The dielectric loss is due predominately to conduction effects, usually local currents. The magnetic loss is due to (1) magnetostrictive coupling, (2) spin wave effects, (3) eddy current losses, and (4) electron level changes.

All usable antenna materials have a sufficiently high resistivity so that item (3) is negligible. Item (1) is determined by the magnitude of the magnetostrictive constants. It is subject to optimization through the original choice of material but is only a slowly varying function of composition of the sample and is in the class of structure insensitive properties. Item (2), on the other hand, is structure sensitive with an irreducible minimum.

Item (2) can be understood as follows. Referring to equation (30), a resonant frequency ω_0 exists with a particular value of wave number ℓ . The

exchange field that produced the magnetic alignment can also be put into an equation of the form of (30). The result is a separate resonance in the exchange field at the same frequency! There is, however, a very much shorter wavelength This represents a magnetic wave traveling through the medium at a lower velocity than that of electromagnetic propagation.

Thus there is always the possibility of energy transfer from the electromagnetic to the spin wave modes and the transfer can only be prevented by the elimination of coupling mechansims and this is a structure sensitive property of the material. The coupling centers, on the other hand, occur whenever $\nabla \cdot \underline{M}$ is large within the sample; i.e. abrupt changes in the local magnetic fields. Thus impurity grains, rough surfaces, etc., must be eliminated insofar as possible.

Item (4) involves a shift in the energy level of an electron due to the electromagnetic field. After the field maximum passes, the electron decays to its original energy level. (It is interesting to note that the spontaneous magnetic moment, in general, decreases with increasing temperature. This is due to thermally generated spin waves.)

4.2.5 Temperature Effects

The anisotropy, in most cases, is very strongly temperature dependent and decreases with increasing temperature. So it follows that ω_o of equation (30) decreases rapidly and therefore the maximum operating frequency of a given material decreases with increasing temperature. The anisotropy constant K_1 for the case of Co_2Z decreases until it passes through zero at about $280^{\circ}C$. A factor of importance in antenna material is the magnetic $Q = \chi' \chi''$, by definition. From Eq. (30)

$$\frac{1}{Q} \frac{dQ}{d\omega_o} = \frac{4\omega^2 \omega_o}{\omega_o^4 - \omega^4} , \tag{40}$$

and in the usable frequency range the denominator is greater than zero and the Q decreases with decreasing ω_o. Thus results can only become worse as the temperature goes up. It then appears that the temperature should be lowered for better results. However, the factor $\chi'Q$ is also important, and

$$\frac{1}{\chi'Q} \frac{d}{d\omega_o} (\chi'Q) \approx - \frac{\omega_o^2 - \omega^2}{\omega_o(\omega_o^2 + \omega^2)} \tag{41}$$

The left side of Eq. (41) increases with decreasing ω_o. The possible range of operation is limited to a certain temperature range by Eqs. (40) and (41).

4.2.6 Conclusions

Antenna material could probably be made that would be usable to about 700 Mc, using the hexagonal compounds. At present the lower Q at higher frequencies is the governing limitation. There is now an effort being made in Europe (but none in the United States) to better control the loss and improve the Q. An operating temperature over a broad frequency band in excess of $225^\circ C$ seems improbable. A lower frequency (200 Mc) material could probably be made operable to a temperature up to $350^\circ C$.

V

FUTURE WORK [+]

The future program of the ferrite antenna project should include:

1. An extension of the frequency coverage down to 50 Mc. New materials will have to be acquired and measured, and then employed.

2. Consideration will be given to different types of antennas, particularly the continuously excited traveling wave antennas with and without taper.

3. Additional efficiency measurements on loaded antennas vs frequency of operation will be made allowing more accurate comparisons to conventional antennas. This will include antennas studied in the past as well as the new antennas to be studied.

4. An increase will be made in maximum rf power used in ferrite-heating tests from 10 - 50 watts if possible.

5. Studies of the near fields of broadband ferrite-loaded antennas will be made to determine the phenomenon causing the miniaturization and to compare with theoretical predictions. Particularly important is a determination of current densities and phase velocities.

[+] The study of UHF-VHF antennas loaded with ferrite and dielectric materials is continuing at The University of Michigan Radiation Laboratory under Contract Nr. AF33(615)-2102.

ACKNOWLEDGMENT

REFERENCES

Adams, A. T. (March 1964), "The Rectangular Cavity Slot Antenna with Homogeneous Isotropic Loading," The University of Michigan Cooley Electronics Laboratory Report No. 05549-7-T.

Dyson, J. D. (October 1959), "The Unidirectional Equiangular Spiral Antenna," IRE Trans. PGAP, Vol. AP-7, pp. 329-341.

Kraus, J. D. (1950) Antennas, McGraw-Hill Book Company, New York.

Lax, B. and K. J. Button (1962), Microwave Ferrites and Ferrimagnetics, McGraw-Hill Book Company, New York, p. 442.

Maclean, T. S. M. and R. J. Kouyoumjian (December 1959), "The Bandwidth of Helical Antennas," IRE Trans. PGAP, Vol. AP-7, pp. 379-386.

Rado, G. T. (1953), "Magnetic Spectra of Ferrites," Rev. Modern Phys., Vol. 25, No. 1, p. 81.

Tang, C. H. and O. L. McClelland (June 1962), "Polygonal Spiral Antennas," University of Illinois Technical Report No. 57.

DOCUMENT CONTROL DATA - R&D

(Security classification of title, body of abstract and indexing annotation must be entered when the overall report is classified)

1. ORIGINATING ACTIVITY *(Corporate author)*	2a. REPORT SECURITY CLASSIFICATION
The University of Michigan	Unclassified
	2b. GROUP

3. REPORT TITLE

STUDY AND INVESTIGATION OF A UHF-VHF ANTENNA

4. DESCRIPTIVE NOTES *(Type of report and inclusive dates)*

Final Report January 1963 through January 1965

5. AUTHOR(S) *(Last name, first name, initial)*

Lyon, J. A. M.; Rassweiler, G. G.; Grimes, D. M.; Rhee, S. B.; Herman, J. E.; Simanyi, A. I.

6. REPORT DATE	7a. TOTAL NO. OF PAGES	7b. NO. OF REFS
February 1965	100	7

8a. CONTRACT OR GRANT NO. AF33(657)-10608	9a. ORIGINATOR'S REPORT NUMBER(S) 5549-1-F
b. PROJECT NO. 6278	
c. 627801	9b. OTHER REPORT NO(S) *(Any other numbers that may be assigned this report)*
d.	

10. AVAILABILITY/LIMITATION NOTICES

Agencies of the Department of Defense and other Government agencies may obtain copies of this report from DDC. Other persons and organizations should apply to U. S. Department of Commerce Office of Technical Services.

11. SUPPLEMENTARY NOTES	12. SPONSORING MILITARY ACTIVITY
	Air Force Avionics Laboratory AVWE Research and Technology Division, AFSC Wright-Patterson Air Force Base, Ohio

13. ABSTRACT

The results of a program for the miniaturization of antennas through the use of ferrite materials is described. The antennas include the log conical spirals, both within and outside a cavity, the cavity-backed log spiral, a helix, a zigzag, and the cavity-backed slot antenna are described. Generally speaking, linear reductions of the order of 2 or 3:1 were achieved for the wideband antennas, and above 6:1 for the slot antenna. An experimental study of ferrite material vs temperature and frequency is included as well as a theoretical review of the current status and basic limitations of ferrite materials.

DD FORM 1473 1 JAN 64

14. KEY WORDS	LINK A		LINK B		LINK C	
	ROLE	WT	ROLE	WT	ROLE	WT
Antennas						
Ferrite loading of antenna						
UHF-VHF frequency						
Miniaturized Antennas						
Log-conical Antennas, ferrite loaded						
Slot cavity-backed antennas, ferrite loaded						

INSTRUCTIONS

1. ORIGINATING ACTIVITY: Enter the name and address of the contractor, subcontractor, grantee, Department of Defense activity or other organization (corporate author) issuing the report.

2a. REPORT SECURITY CLASSIFICATION: Enter the overall security classification of the report. Indicate whether "Restricted Data" is included. Marking is to be in accordance with appropriate security regulations.

2b. GROUP: Automatic downgrading is specified in DoD Directive 5200.10 and Armed Forces Industrial Manual. Enter the group number. Also, when applicable, show that optional markings have been used for Group 3 and Group 4 as authorized.

3. REPORT TITLE: Enter the complete report title in all capital letters. Titles in all cases should be unclassified. If a meaningful title cannot be selected without classification, show title classification in all capitals in parenthesis immediately following the title.

4. DESCRIPTIVE NOTES: If appropriate, enter the type of report, e.g., interim, progress, summary, annual, or final. Give the inclusive dates when a specific reporting period is covered.

5. AUTHOR(S): Enter the name(s) of author(s) as shown on or in the report. Enter last name, first name, middle initial. If military, show rank and branch of service. The name of the principal author is an absolute minimum requirement.

6. REPORT DATE: Enter the date of the report as day, month, year; or month, year. If more than one date appears on the report, use date of publication.

7a. TOTAL NUMBER OF PAGES: The total page count should follow normal pagination procedures, i.e., enter the number of pages containing information.

7b. NUMBER OF REFERENCES: Enter the total number of references cited in the report.

8a. CONTRACT OR GRANT NUMBER: If appropriate, enter the applicable number of the contract or grant under which the report was written.

8b, 8c, & 8d. PROJECT NUMBER: Enter the appropriate military department identification, such as project number, subproject number, system numbers, task number, etc.

9a. ORIGINATOR'S REPORT NUMBER(S): Enter the official report number by which the document will be identified and controlled by the originating activity. This number must be unique to this report.

9b. OTHER REPORT NUMBER(S): If the report has been assigned any other report numbers (either by the originator or by the sponsor), also enter this number(s).

10. AVAILABILITY/LIMITATION NOTICES: Enter any limitations on further dissemination of the report, other than those

imposed by security classification, using standard statements such as:

(1) "Qualified requesters may obtain copies of this report from DDC."

(2) "Foreign announcement and dissemination of this report by DDC is not authorized."

(3) "U. S. Government agencies may obtain copies of this report directly from DDC. Other qualified DDC users shall request through
_____ ."

(4) "U. S. military agencies may obtain copies of this report directly from DDC. Other qualified users shall request through
_____ ."

(5) "All distribution of this report is controlled. Qualified DDC users shall request through
_____ ."

If the report has been furnished to the Office of Technical Services, Department of Commerce, for sale to the public, indicate this fact and enter the price, if known.

11. SUPPLEMENTARY NOTES: Use for additional explanatory notes.

12. SPONSORING MILITARY ACTIVITY: Enter the name of the departmental project office or laboratory sponsoring (paying for) the research and development. Include address.

13. ABSTRACT: Enter an abstract giving a brief and factual summary of the document indicative of the report, even though it may also appear elsewhere in the body of the technical report. If additional space is required, a continuation sheet shall be attached.

It is highly desirable that the abstract of classified reports be unclassified. Each paragraph of the abstract shall end with an indication of the military security classification of the information in the paragraph, represented as (TS), (S), (C), or (U).

There is no limitation on the length of the abstract. However, the suggested length is from 150 to 225 words.

14. KEY WORDS: Key words are technically meaningful terms or short phrases that characterize a report and may be used as index entries for cataloging the report. Key words must be selected so that no security classification is required. Identifiers, such as equipment model designation, trade name, military project code name, geographic location, may be used as key words but will be followed by an indication of technical context. The assignment of links, rules, and weights is optional.